DOCTORAL THESIS

Role of hypoxia and PARP1 in the regulation of vasculogenic mimicry

MÓNICA FERNÁNDEZ CORTÉS

INSTITUTE FOR PARASITOLOGY AND BIOMEDICINE LÓPEZ-NEYRA

CONSEJO SUPERIOR DE INVESTIGACIONES CIENTÍFICAS

PhD Program in Biomedicine (B11.56.1)

University of Granada

May 2021

**UNIVERSIDAD
DE GRANADA**

ipbln

CSIC

CONSEJO SUPERIOR DE INVESTIGACIONES CIENTÍFICAS

TABLE OF CONTENTS

TABLE OF CONTENTS

TABLE OF CONTENTS

ABSTRACT

ABSTRACT

Melanomas represent a variety of neoplastic diseases that derive from the malignant transformation of melanocytic cells. Cutaneous and uveal melanoma are the most common presentations of this cancer type. Unfortunately, current therapies have proved insufficient in the management of melanoma, highlighting the need for further research.

Solid tumors usually present a state of low oxygenation known as hypoxia. Hypoxic microenvironments trigger adaptive responses that contribute to the malignization of tumors. For instance, the hypoxia response plays a key role in tumor neovascularization. Angiogenesis consists in the sprouting of new blood vessels from pre-existing vasculature and it is the best known form of tumor neovascularization. However, alternative neovascularization mechanisms, such as vasculogenic mimicry, have been gaining attention in recent years. Vasculogenic mimicry describes the ability of highly aggressive tumor cells to acquire endothelial traits and develop vessel-like structures capable of carrying blood without the participation of endothelial cells. It is correlated with metastasis, shorter survival and poor prognosis in cancer patients. Unfortunately, there are currently no available drugs to target vasculogenic mimicry in clinical settings, and its treatment remains a major biomedical challenge.

Poly-(ADP-ribose) polymerase (PARP) 1 catalyzes the synthesis and transfer of poly-(ADP-ribose) to target proteins. PARP inhibitors cause synthetic lethality in cells with genetic deficiencies in the homologous recombination DNA repair pathway, inducing the selective elimination of cancer cells with these defects. As a result, four PARP inhibitors have been approved so far for their clinical use against tumors displaying characteristics of "BRCAness". Furthermore, PARP1 has been implicated in multiple physiological and pathological processes. For instance, PARP1 can promote the stability and function of hypoxia-inducible factors, which raises PARP1 as an attractive druggable target for the control of hypoxia-derived tumor processes, like vasculogenic mimicry.

The purpose of the present thesis was to explore the consequences of PARP inhibition in the context of melanoma vasculogenic mimicry, which could

expand the therapeutic benefit of PARP inhibitors while potentially targeting a malignant trait which so far remains untreatable.

Our study shows that PARP inhibition and hypoxia can modulate the expression of hundreds of genes during melanoma tube formation on matrigel. The profound impact of PARP inhibition was partly due to the modulation of long non-coding RNA, a class of RNA transcripts that do not encode any protein products but can regulate gene expression in a variety of ways. PARP inhibition during hypoxia significantly modulated the expression of numerous genes implicated in vascular biology, resulting in the global modulation of a number of vasculature-related signaling pathways and seemingly enhancing the endothelial-like characteristics of melanoma cells.

Consistent with previous results, PARP1 chemical inhibition or genetic knockdown could reduce the phosphorylation of vascular endothelial cadherin on tyrosine 658 in normoxia and hypoxia. Previous publications have proved the crucial role of this cadherin and this specific phosphorylation in vasculogenic mimicry. Moreover, this phosphorylation is reportedly correlated with increased endothelial vessel permeability, which can favor metastatic spread. Our study also found that PARP inhibition can upregulate the expression and secretion of the platelet-derived growth factor β in vasculogenic melanoma cells. This cytokine is involved in the recruitment of pericytes to blood vessels. In endothelial vessels, low permeability and high pericyte coverage are markers of vascular normalization, which is considered a sign of good prognosis in tumors. In addition, melanoma tubular networks on matrigel seemed to undergo a structural normalization after treatment with PARP inhibitors.

Finally, studies with human uveal melanoma xenografts showed that treatment with PARP inhibitor olaparib improved pericyte coverage specifically of vasculogenic mimicry pseudovessels *in vivo*, which was concomitant with a decrease in metastasis in tumors with the ability to develop vasculogenic mimicry.

In conclusion, the results of this thesis indicate that PARP inhibitors may reduce the metastatic spread of melanoma tumors capable of vasculogenic mimicry by normalizing vasculogenic mimicry pseudovessels.

INTRODUCTION

INTRODUCTION

CANCER

The word "cancer" is frequently used as a generic term that seems to describe a specific disease. However, the term "cancer" actually comprises a large group of over 200 different diseases, each of these with particular causes, characteristics and treatments. The common feature to all of these different diseases or cancer types is the uncontrolled growth of a group of abnormal cells, which give rise to a neoplasm. These malignant cells have the ability to invade adjacent tissues and to even metastasize, that is, the ability to migrate to and grow in distant organs. Metastases are the most usual cause of death by cancer.

According to the World Health Organization (WHO), cancer is the second leading cause of death globally, accounting for almost one out of every six deaths in the world. The WHO estimates that over 18 million new cases of cancer were diagnosed in 2018, and that approximately 9.6 million people died of cancer that year. In Spain, 282,421 people were diagnosed with cancer in 2020, according to data gathered by the Global Cancer Observatory in the Globocan database. Taking into account all diagnoses made in previous years, this number adds up to a 5-year prevalence of 858,220 patients, that is, 1,836 cancer patients per 100,000 people. Lastly, Globocan reported 113,054 deaths by cancer in Spain in 2020.

In general terms, the causes of cancer can be ascribed to individual genetic susceptibility plus the exposure to external agents that may increase cancer risk, known as carcinogens. Furthermore, the WHO claims that nearly one third of all cancer deaths are ultimately due to a small group of behavioral patterns, in particular high body mass index, scarce physical activity, insufficient fruit and vegetable consumption, and alcohol and tobacco use. In fact, the WHO calculates that tobacco use alone could be responsible for up to 22% of all deaths from cancer. Another major risk factor for cancer is ageing, with virtually all cancer types having a higher incidence in older individuals.

At the molecular level, the process of carcinogenesis starts with an imbalance in proliferation signals within the cell. Normally, cell proliferation is controlled by a number of strict signaling pathways, with several checkpoints that must be overcome before the cell engages in effective division. However, mutations in key genes involved in these pathways may disrupt the whole mechanism of control and lead to disproportionate cell growth and eventually cancer.

Genes that promote cell proliferation are known as oncogenes. In a physiological context, oncogenes need to be activated by specific stimuli in order to trigger cell growth. Therefore, any mutation that will render an oncogene as constitutively active, increase its expression or otherwise make it more active than usual in any way, can potentially contribute to abnormal cell proliferation. On the contrary, the role of tumor suppressor genes is to hinder cell growth. In this case, inactivating mutations that interfere with the normal expression or function of tumor suppressor genes may favor cell proliferation and hence carcinogenesis. It is important to note that isolated mutations can rarely cause cancer by themselves; usually, a number of concomitant genetic defects are required to initiate cancer[1].

In their prestigious review, Hanahan and Weinberg originally highlighted six hallmarks of cancer[2], to which they added four more in the revised version published in later years[3]. That makes a total of ten defining molecular traits whose progressive acquisition by incipient cancer cells will enable malignant transformation: genomic instability, sustained proliferative signaling, insensitivity to growth suppressors, resistance to programmed cell death, replicative immortality, metabolic reprogramming, induction of angiogenesis, inflammation, immune escape and tissue invasion and metastasis. The updated review also emphasized the important role that intratumor heterogeneity and tumor microenvironment may play in cancer progression. The simplistic idea that a tumor is no more than a group of cancer cells is nowadays obsolete, and more and more research groups are focusing their attention in components of the tumor stroma, such as endothelial cells, pericytes, cancer-associated fibroblasts, tumor-associated macrophages and other immune inflammatory cells. The interactive signaling between all of these cell

types and cancer cells is crucial in the definition of the tumor microenvironment, and in the acquisition of an invasive, malignant phenotype.

The treatment of cancer is highly dependent on a number of parameters, such as location and stage of the neoplasia, as well as the age of the patient and their medical history, among others. Normally, several different treatments are combined in order to increase the chances of recovery. The main therapeutic approaches are surgery, radiotherapy and chemotherapy, although other more specific treatments can be used in the case of certain patients and tumors.

Surgical removal of the primary tumor is most useful in the absence of metastatic spread. In order to ensure that all tumor tissue is eliminated, part of the surrounding healthy tissue must be removed too. In many cases, lymph nodes near the tumor will be removed as well, to avoid the risk of future metastasis due to the undetected presence of tumor cells. Radiation therapy, commonly known as radiotherapy, is another form of local treatment, which uses ionizing radiation to kill cancer cells. There are two main kinds of radiotherapy: external beam and brachytherapy, where radioactive materials are implanted next to or within the tumor tissue. On the other hand, chemotherapy is a systemic treatment which can affect tumor cells anywhere in the body, so it is indicated for metastatic disease. Chemotherapeutic agents include a wide variety of cytotoxic drugs which interfere with cell proliferation and ultimately cause cell death. Although any proliferating cell can be potentially affected, the abnormally high growth rate of cancer cells make them especially sensitive to chemotherapy[4,5].

In the past few decades, the deeper understanding of cancer biology has encouraged the search for more specific treatments which may reduce the unwanted side effects of conventional therapies. The aim is to find drugs that kill tumor cells exclusively, while leaving healthy cells unharmed. Therefore, ideal drugs must target signaling pathways or molecules which are specifically deregulated in cancer cells. In fact, most targeted therapies developed so far act upon molecular targets which somehow enable the previously mentioned hallmarks of cancer. For instance, the monoclonal

antibody bevacizumab interferes with angiogenesis signaling, and poly-(ADP-ribose) polymerase inhibitors target genomic instability.

Unfortunately, all ten hallmarks of cancer are regulated by several, partly redundant signaling pathways. In consequence, targeting a particular pathway does not often block a malignant feature permanently; some cancer cells can evade targeted therapies by favoring alternative pathways that rescue the lost ability, leading to acquired resistance and clinical relapse. Moreover, tumors can potentiate other hallmarks in order to compensate for those that have been temporarily inhibited. For this reason, combined therapies should be applied whenever possible, in order to target several different hallmarks at the same time and hence improve the curative potential[3].

MELANOMA

The term melanoma refers to a variety of cancer types all of which derive from the malignant transformation of melanocytic cells or melanocytes.

Melanocytes are a distinct cell type whose best known function is the synthesis of melanin, the pigment that gives color to skin, hair and eyes. In the skin, melanin has protective properties against ultraviolet (UV) radiation from the sun, which can cause deoxyribonucleic acid (DNA) damage in cells. Actually, one of the triggers for melanin production is UV light-induced DNA damage to keratinocytes[6]. In the eyes, melanocytes are present in the conjunctiva and in the uveal tract. The purpose of melanocytes in the conjunctiva remains elusive, but uveal melanocytes seem to be associated with photoprotection as well. Uveal pigmentation is believed to protect against several diseases, including age-related macular degeneration and senile cataract[7].

Apart from skin and eyes, melanocytes can be found in several other organs where their role is not fully understood, such as the meninges, the anogenital tract, the heart and the cochlea. The fact that melanocytes are present in organs that are not subjected to UV radiation indicates that their function cannot be limited to solar protection. Several syndromes affecting melanocytes, like Vogt-Koyanagi-Harada, Tietz or Waardenberg syndromes, show a correlation between hypopigmentation and hearing impairment[8–10], suggesting a role for otic melanocytes in sound perception.

Malignant transformation of melanocytes in any location can give rise to a wide variety of melanoma types. The more common cutaneous and uveal melanomas will be discussed in detail further on. Some other rarer types of melanoma include the following:

- Primary melanomas of the central nervous system derived from meningeal melanocytes. They are extremely rare, with only very few cases ever reported[11].

- Conjunctival melanoma is very infrequent too, with an incidence of barely 0.2-0.8 cases per million people, though it shows a rising trend[12–14].

- Mucosal melanoma is a particularly aggressive melanoma subtype. It arises from melanocytes in mucosal surfaces of the body, such as the nasal and oral cavities, the urogenital tracts and the anorectal mucosa[15]. Among these, vulvovaginal melanoma is especially frequent, so much so that the global incidence of mucosal melanoma is significantly higher in women than in men[16]. It is also much more prevalent in Asian (22-27% of all melanoma cases), compared to Western populations (1-5% of all melanomas)[17,18]. The overall incidence in the United States was calculated at 2.2 cases per million people per year[16]. While UV radiation is a clear risk factor for other melanomas, it does not seem to influence mucosal melanoma[15].

CUTANEOUS MELANOMA

Cutaneous melanoma (CM) arises from skin melanocytes and it is the most common type of melanoma. According to Globocan, 324,635 new cases of CM were diagnosed worldwide in 2020, and 57,043 people died of this disease. The global 5-year prevalence that same year was estimated at 1,092,818 patients. Almost 80% of incident cases in the world took place in Europe and North America, due to the fact that fair skin is a prominent risk factor for CM[19]. Importantly, the global incidence of CM shows a clear rising trend, having increased almost fourfold in thirty years in populations of European descent[20]. In Spain, Globocan registered 5,728 new CM diagnoses, 1,097 deaths and a 5-year prevalence of 19,616 CM patients in 2020.

The chief risk factor for CM is exposure to UV radiation. Initially, solar exposure induces the formation of melanocytic nevi (commonly known as moles or birthmarks), which are chronic but benign hyperplasias of melanocytes. However, these pigmented skin lesions may progress to CM[6]. Individual nevi have a very low risk of giving rise to malignant melanoma, but numerous studies show that at least ≈20% of all CM are associated to a pre-existing nevus[21]. Furthermore, the risk of CM proved significantly higher in people with a high number of nevi[22].

As a strategy to promote early detection and hence improve patient prognosis, public efforts have been made to educate the general population

on how to distinguish a common mole from CM. The most popular method is the "ABCDE rule", an easy, mnemonic acronym for the warning signs of malignant CM: Asymmetry, Border irregularity, Color variegation, Diameter larger than 6 mm and Evolution over time[23]. Unfortunately, not all CMs display these visual features, so non-ABCD CMs may go unnoticed even after careful examination. Secondly, in certain individuals most nevi show ABCD signs, a condition known as "atypical nevus syndrome". A complementary tool to overcome these limitations is the "ugly duckling sign". This rule is based on the observation that, within a given individual, all common nevi share similar characteristics of color, shape and size. Thus, the ugly duckling nevus, one which does not resemble the other nevi in that same individual, should be regarded as suspicious for malignancy[24].

Attending to anatomical and histological parameters, cutaneous melanoma can be further classified into four types of CM:

- Superficial spreading melanoma (SSM). It is the most common in white populations. In the United States, the overall incidence by 2007 was calculated at 6.63 cases per 100,000 people per year, though this rate was shown to be steadily rising[25]. It usually affects intermittently sun-exposed skin so it often appears on the torso, the back and the extremities. It starts growing radially on the skin and then proceeds into a vertical growth phase[20,26]. As a result, the vast majority of SSMs are diagnosed as thin tumors of less than 1 mm thickness[27], which is a classic sign of good prognosis[19].

- Nodular melanoma (NM). It grows as nodules, that is, it does not go through a radial growth phase but rather grows vertically from the start[26]. NM often lacks the ABCD criteria, so it can easily escape early identification[28]. For these reasons, a great number of nodular melanomas are already thicker than 2 mm at the time of diagnosis[27]. Moreover, NM has been shown to grow faster than other melanomas[29]. All these qualities make NM a very aggressive tumor, with higher fatality and shorter survival than other CM subtypes[25,30,31].

- Lentigo maligna melanoma. It is less frequent than SSM and NM, though its incidence is rising faster than any other CM subtype. It presents on patients with the highest median age, usually in the form

of a large, flat macule with irregular borders and pigmentation[26,32]. It is strongly correlated to UV-induced DNA damage so it mainly affects chronically sun-damaged areas of the skin, such as the head and neck[20].

- Acral melanoma (AM). It is specific of acral skin, that is, palms, soles and nailbeds[33]. In the United States, overall incidence has been estimated at 1.8-2.1 cases per million people per year (around 2% of all melanomas)[25,34]. However, similarly to mucosal melanoma, the relative incidence of AM is much higher in Asian countries, where it accounts for ≈42% of all cases of melanoma[17,18]. The vast majority of AMs arise on the feet[35]. Interestingly, in AM with a plantar location, it seems that most of them occur in weight-bearing areas of the sole, which suggests a role for mechanical stress in the induction of this melanoma subtype[36].

In recent years, though, this classification has been deemed as irrelevant. Histopathological classification of CM is not always obvious, due to similarities among the different subtypes; but most importantly, it does not provide much useful prognostic information to help direct clinical management[37]. A new molecular classification has been proposed, based on the driver mutation signature of CM. This system enables the application of rational, targeted therapies against the signalling pathways that are deregulated in each genomic subtype, ensuring optimal treatment for every patient.

The four CM genomic subtypes, in order of incidence, are listed below:

- **BRAF subtype**.
  BRAF belongs to the RAF family of serine/threonine kinases. RAF activity triggers the mitogen-activated protein kinase (MAPK) pathway. RAF first phosphorylates MEK1/2, which in turn are rendered active and phosphorylate ERK1/2. Active phospho-ERK1/2 go on with a signalling cascade that eventually promotes cell proliferation, differentiation, migration and survival[38]. The high abundance of BRAF mutations in human cancer, especially melanoma, was first reported in 2002[39]. BRAF is reportedly mutated in over 50% of human CM. Around 80% of BRAF mutations come

down to the substitution of the residue of valine (V) 600 for glutamic acid (E)[39,40]. This residue is located in the kinase domain and the V600E mutation increases BRAF basal kinase activity, therefore enhancing MAPK signalling[39].

This discovery opened a seemingly clear therapeutic window for CM in the form of BRAF inhibitors (BRAFi). However, monotherapy with BRAFi did not give as good results as expected. There was a high rate of intrinsic resistance and even in responsive patients the treatment was only effective for a short time. In addition, BRAFi promoted other skin neoplasias, such as squamous cell carcinoma. A common mechanism of resistance was the presence of downstream activating mutations in the MAPK pathway, which compensated for the inhibition of BRAF. Fortunately, combination therapies with MEK inhibitors (MEKi) have addressed this issue, improving CM survival and reducing unwanted side effects. These results have led to the approval by both the American Food and Drug Administration (FDA) and the European Medicines Agency (EMA) of three different BRAFi + MEKi combination treatments for CM so far[41].

Interestingly, BRAF-mutated CMs often present genomic amplifications for BRAF, microphthalmia-associated transcription factor (MITF) and programmed death-ligand 1 (PDL1)[40]. PDL1 alterations hold a particular interest, due to its repercussions in PD1-targeted immunotherapy.

- **RAS subtype**.
The RAS family comprises the three small GTPases HRAS, KRAS and NRAS. In their active guanosine triphosphate (GTP)-bound state, RAS can bind and activate a number of effector proteins, like the aforementioned RAF kinases, but also phosphoinositide 3-kinase (PI3K)[42]. PI3K triggers a proliferation pathway that acts parallel to the BRAF-MAPK pathway, so the RAS-PI3K axis can override the effect of BRAFi[41].

In CM, the most frequently mutated RAS member is NRAS. NRAS mutations are present in around 30% of CMs, which makes it the second most common driver mutation in this cancer type after BRAF, although RAS and BRAF mutations are mutually exclusive. Almost all NRAS mutations affect the residue of glutamine (Q) 61, which usually

changes to arginine (R) or lysine (K)[40]. These mutations abrogate NRAS GTPase activity, so NRAS locks into a GTP-bound active state which constitutively stimulates all downstream effectors[42].

The direct targeting of RAS proteins is a longstanding challenge in cancer research, and no specific treatment for NRAS-mutant CM is available to this day. Most therapeutic approaches have focused on using MEKi as a way to inhibit NRAS downstream pathway, but results have not been very promising[43].

- **NF1 subtype**.

   Neurofibromin 1 (NF1) is a RAS GTPase activating protein (GAP), that is, NF1 induces RAS GTPase activity, so that bound GTP hydrolyzes to guanosine diphosphate (GDP) and RAS goes back to an inactive state. Therefore, NF1 is a negative regulator of the RAS-RAF-MAPK and RAS-PI3K pathways, and hence a tumor suppressor[44]. NF1 is mutated in ≈15% of all CMs, mainly in the form of loss of function mutations that trigger RAS signaling[40].

   Mutations in the retinoblastoma protein RB1 are especially abundant in NF1-mutant CM compared to other subtypes. Disturbances in the cyclin-dependent kinase (CDK) inhibitor 2A (CDKN2A)/CDK4/RB1 pathway are frequent in CM, particularly in cases of familial CM, stressing the relevance of RB1 mutations.

- **Triple wildtype subtype**.

   This subtype comprises a heterogenous group of CMs which are not driven by any of the previous mutations. It is characterized for having a low UV-induced mutation signature compared to other subtypes[40]. On the other hand, it is enriched for copy number amplifications of known oncogenes, such as KIT, PDGFRA, KDR, CDK4, CCND1, MDM2 and TERT.

   Of all these, activating mutations and amplifications of the receptor tyrosine kinase KIT, which can be targeted by a number of KIT inhibitors, are particularly frequent in melanoma and enriched in this subtype. In addition, as previously mentioned, CDK4 can play an important role in the onset of familial melanoma.

Overall, the RAS-RAF-MAPK pathway is altered in over 90% of CMs (Figure 1), which highlights the importance of this route in CM initiation,

and its potential in targeted therapeutic approaches. The second most frequently mutated pathway appears to be the CDKN2A/CDK4/RB1 pathway[40]. In fact, germline mutations on any of those three genes are strongly associated with familial CM, which represents around 10% of all cases of CM[7].
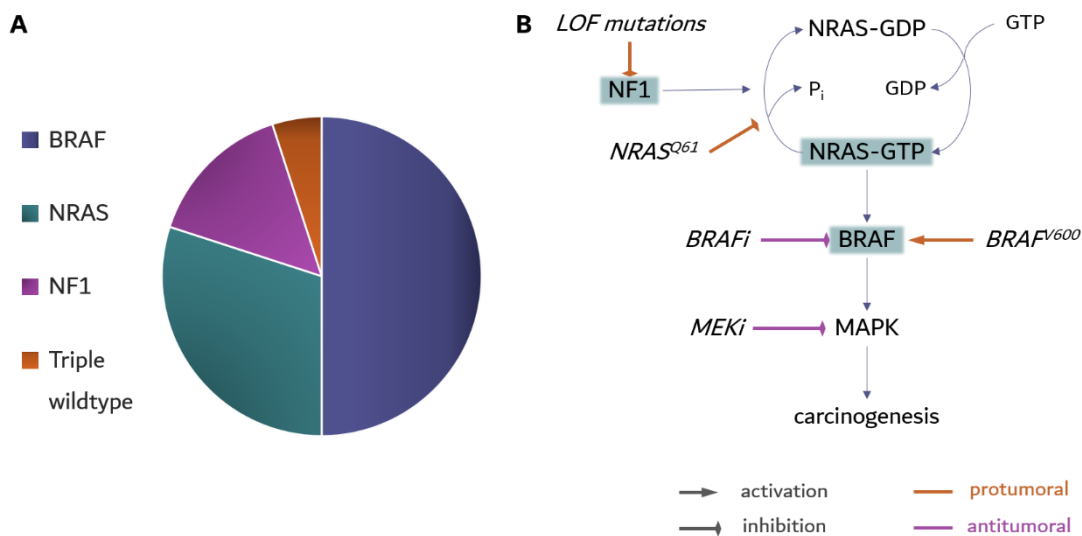
Figure 1. Driver mutations in CM. **A** Relative abundance of the different CM genomic subtypes. **B** BRAF, NRAS and NF1 can potentially induce carcinogenesis through the activation of the MAPK pathway, which is constitutively active in CM due to BRAF, NRAS and NF1 mutations. Selective targeting with BRAFi and MEKi aims to reduce CM progression. LOF: loss-of-function.

Nevertheless, most of the alterations mentioned so far are often found in common nevi. CM initiation seems to require additional loss of function mutations in well-known tumor suppressors, like TP53 or the phosphatase and tensin homolog (PTEN), mutated in ≈20% and ≈10% of CMs, respectively; or gain of function mutations in oncogenes such as the telomerase reverse transcriptase (TERT), whose promoter is mutated in a high number of CMs, leading to an overexpression of TERT[7,40].

UVEAL MELANOMA

Uveal melanoma (UM) is an eye malignancy derived from melanocytes in the uveal tract of the eye, which comprises the iris, the ciliary body and the choroid. Around 90% of UMs occur in the choroid[7].

UM is the most prevalent eye cancer in adults, though it is still a rare disease. In the United States, UM has a yearly incidence of 5 cases per million, accounting for 3% of all melanoma cases, yet unlike CM, UM incidence does not seem to be rising. It is slightly more common in men than women, and much more frequent in white populations than other races[16,45]. Similarly to CM, fair skin and eye color are important risk factors for UM development[46]. In fact, a study comparing UM incidence across Europe found significant geographical differences: southern countries like Spain and Italy reported an incidence below 2 cases per million, as opposed to Denmark or Norway with over 8 cases per million[47]. This north-to-south variation could be attributed to differences in pigmentation.

Overall 5-year survival in UM patients is in the region of 70%[45,48,49]. However, UM is a highly metastatic cancer. Around 30% of UM patients develop metastasis within 10 years of diagnosis[50,51], and risk of metastasis persists after as long as 20 years, even after successful eradication of the primary tumor[52]. This suggests that micrometastasis must take place early in disease progression. Once metastasis occurs, mortality is very high; the 1–year survival rate drops to hardly 20%. In around 90% cases of metastatic disease, liver metastases are present[51,53], and in many cases there are extra-hepatic metastasis too.

Unlike CM, UM does not usually show external signs. The exception is UM of the iris, where the appearance of pigmented areas or changes in the shape of the pupil are visible signs of UM. Other than that, and bearing in mind that only 5% of UMs involve the iris[7], the only noticeable symptoms of UM are usually blurred or distorted vision (metamorphopsia) and seeing flickering lights (photopsia). In many cases, UM is completely asymptomatic and is only detected during routine eye examination[54]. That means that UM is often diagnosed at a late stage.

The molecular etiology of UM is very different from CM too. BRAF or NRAS mutations are not involved in UM development. Instead, driver mutations in guanine nucleotide-binding protein (G protein) α-subunits q (GNAQ) or 11 (GNA11) can be found in over 40% of primary UMs each[55].

G proteins function as signal transducers between membrane G-protein-coupled receptors (GPCR) and a wide variety of downstream effectors. G proteins are heterotrimeric, that is, they consist of three different subunits, Gα, Gβ and Gγ, each of whom comprises a number of isoforms. Gα subunits are the actual GTPase component of G proteins; their binding to GTP activates the full G protein, and subsequent hydrolysis returns it to an inactive state. GNAQ and GNA11 belong in the Gα family, specifically the $G\alpha_q$ subfamily, which leads to the activation of phospholipase C (PLC) β. They are close homologues, with 90% of protein sequence identity[56]. Driver mutations in GNAQ and GNA11 are mutually exclusive in UM, and nearly always (>90%) involve the residue Q209. This residue is critical for GNAQ/11 GTPase activity, which is entirely abolished by Q209 mutations. Thus, mutant GNAQ/11 remain permanently bound to GTP, resulting in constitutively active G protein signaling. Another, much less common GNAQ/11 mutation that hinders GTPase activity affects the residue R183. Again, Q209 and R183 mutations take place in a mutually exclusive pattern[55].

Interestingly, in spite of GNAQ and GNA11 homology, their mutation pattern is different in primary versus metastatic UM tumors. GNAQ mutations are more frequent in primary uveal melanoma (45%) and even in benign blue nevi, compared to GNA11 mutations (32%). On the contrary, metastatic uveal melanomas are more frequently mutated for GNA11 (57%) than GNAQ (22%). The reason for these different metastatic potentials remains unknown[55].

On the other hand, mutations in Q209 or R183 have a different significance as well. Firstly, while R183 mutations seem to be caused by UV-induced DNA damage, that is not the case for Q209. That means that UV exposure plays a role in only a small part of UMs (circa 5%)[55]. In addition, R183 mutations do not inhibit GNAQ/11 GTPase activity completely, so GNAQ/11-mediated signaling activation is weaker in R183

than in Q209 mutants. Also, R183 and Q209 may respond differently to Gα_q-targeted drugs, which usually give better results in R183 mutant cells[57,58].

In total, around 90% of UMs harbor a mutation in GNAQ or GNA11[55,59,60]. Furthermore, activating mutations in the GPCR cysteinyl leukotriene receptor 2 (CYSLTR2), which is directly upstream of GNAQ/11, and in PLCB4, which is directly downstream of GNAQ/11, have been reported in UM as well. Each of them is present in ≈4% of UM tumors, and they are mutually exclusive with each other and with GNAQ and GNA11 mutations[59,60]. In consequence, the total fraction of GNAQ/11-dependent UMs rises to over 95% (Figure 2). This mutation landscape visibly highlights the relevance of GNAQ/11 signaling in UM development. Interestingly, GNAQ/11 driver mutations occasionally occur in triple wildtype CM too[40].
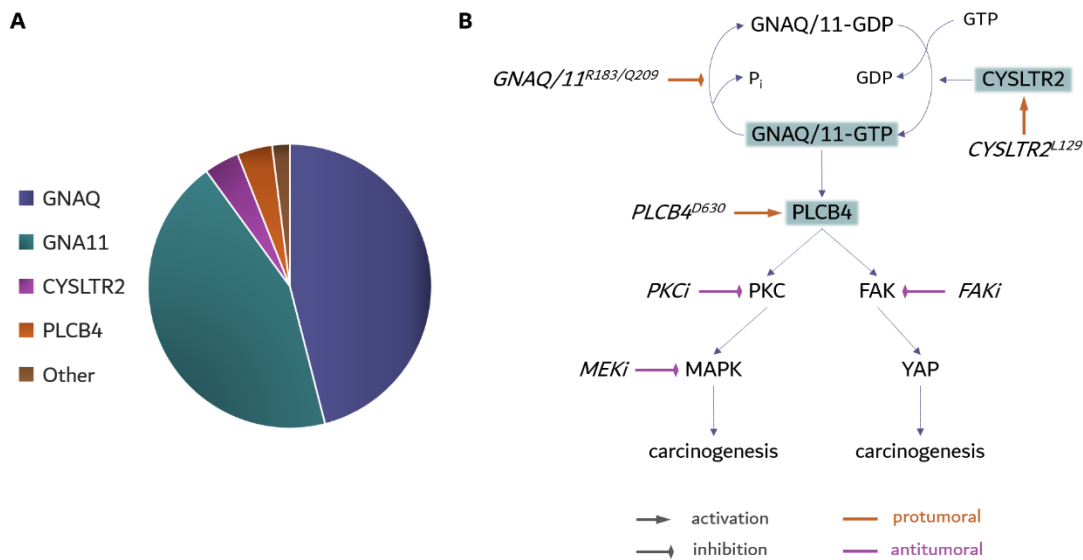
Figure 2. Driver mutations in UM. **A** Relative mutation frequency of genes involved in the GNAQ/11 pathway in UM. **B** GNAQ/11 signaling, which is constitutively active in almost all UMs due to mutations in GNAQ, GNA11, CYSLTR2 or PLCB4, can induce carcinogenesis through the activation of the MAPK and YAP pathways. MEK, PKC and FAK inhibitors have been proposed as targeted therapies for the treatment of UM.

As mentioned above, GNAQ/11 activate PLCβ, which induces the formation of inositol-1,4,5-trisphosphate (IP₃) and diacylglycerol (DAG). Both of these trigger a variety of signaling pathways, such as protein kinase C (PKC) signaling, that modulate many aspects of cell physiology[56]. Both IP₃ and DAG can potentially activate the MAPK signaling pathway through different mechanisms that lead to RAF or RAS activation[61]. Indeed, MAPK pathway is upregulated in GNAQ-mutant UM cells[62].

GNAQ/11 can also stimulate yes-associated protein (YAP) signaling[63]. YAP is a transcriptional coactivator that promotes cell proliferation and survival in growing tissues. Once appropriate cell density or organ size are achieved, YAP is inactivated by other components of the Hippo pathway, inhibiting further growth. Malfunctions in this signaling pathway can thus lead to tumor development[64]. In that line, mutant GNAQ/11 lead to the activation of YAP, which is basally active in UM cell lines. Moreover, YAP activation was demonstrated necessary for mutant GNAQ/11-dependent tumorigenesis[65], and it was sufficient to drive UM initiation[66].

Apart from the activation of GNAQ/11 signaling, another recurrent molecular event in UM is the loss of chromosome 3, which can be found in about 50% of patients. Monosomy 3 was reported as the most significant sign of metastatic risk and poor prognosis in UM[67]. Other chromosomal aberrations typically found in UM include partial or total 6p and 8q gains[59].

Inactivating mutations in BRCA1-associated protein 1 (BAP1) occur in over 80% of monosomy 3 UMs[59,68]. Since this gene is located in chromosome 3, BAP1 mutations have a major impact due to loss of heterozygosity. Despite the fact that germline mutations in BAP1 are rare, they have been associated with familial melanoma, both CM and UM. Moreover, germline mutations in BAP1 are correlated with larger tumor size and increased risk of metastasis in UM patients[69]. BAP1 is a deubiquitinating enzyme with crucial roles in DNA replication and repair, as well as apoptosis. Therefore, loss of function mutations induce genomic instability and resistance to cell death, making BAP1 an important tumor suppressor[70].

Other frequently mutated genes in UM are the eukaryotic translation initiation factor 1A X-linked (EIF1AX) and the splicing factor 3B subunit

1 (SF3B1). These mutations are almost specific to disomy 3 UMs[71], and they are mutually exclusive[59]. 77% of disomy 3 UMs have a mutation in either EIF1AX or SF3B1[71]. Mutations in SF3B1 usually affect the residue R625, and they are correlated with good prognostic factors and low metastasis rate[72]. Mutations in EIF1AX happen on its N-terminal region, and are correlated with good prognosis too[71].

Current therapies against UM are very effective in the control of primary tumors. The preferred treatment for tumors under 10 mm is radiotherapy, specifically eye plaque brachytherapy, where radioactive seeds (usually iodine-125 or ruthenium-106) are implanted in the affected eye for a period of a few days. This method has the advantage of preserving the vision, as well as the cosmetic benefit of preserving the eye. In patients with larger tumors or severe ocular complications, the treatment must resort to enucleation, in other words, complete removal of the globe. Uvectomy, that is, selective resection of the uveal tumor may be a conservative alternative to enucleation in iris melanomas[54].

Unfortunately, as previously mentioned, a great number of patients (up to 59%) develop metastasis even after successful treatment of the primary tumor. At this point, none of the current therapeutic options have shown satisfactory results. Liver-directed therapies have many limitations and high relapse, and UM has proved strongly resistant to systemic chemotherapy, with response rates under 1%[54]. For this reason, targeted therapies arise as a promising alternative and lots of clinical trials are currently in progress.

Due to GNAQ/11-dependent increase in MAPK signaling, a variety of MEKi have been proposed for the treatment of UM. Though preclinical results were encouraging, clinical trials showed marginal if any improvement in overall and progression-free survival. A few ongoing clinical trials are testing the efficacy of MEKi in combination with other drugs.

Preclinical studies showed that MEK and PKC co-targeting had a potent synergistic effect repressing MAPK signaling and inducing apoptosis in GNAQ/11-mutant UM cell lines. Moreover, the combined inhibition led to significant tumor regression in UM xenografts[73]. MEK and PKC

inhibitor combination treatments have only entered a dose escalation clinical trial (NCT01801358), so their therapeutic effect in UM patients remains to be evaluated.

Another potential combination is MEKi plus focal adhesion kinase (FAK) inhibitors, since FAK was found to mediate GNAQ/11-dependent YAP activation[74]. Therefore, co-targeting of MEK and FAK can accomplish the inhibition of both MAPK and YAP signaling pathways, the two most prominent routes to proliferation in UM. Indeed, combination of MEK and FAK inhibitors resulted in reduced cell growth and increased apoptosis in UM cell lines, as well as tumor regression in mouse and xenograft models, including a liver metastasis model[75]. This report was published earlier this year, so this combination has not been registered for any clinical trials in UM yet. Nevertheless, several MEK and FAK inhibitors have been or are being clinically tested individually in cancer patients for other purposes[76].

Finally, direct targeting of GNAQ/11 has been attempted too. FR900359 (FR) is a plant-derived peptide that traps GDP in $G\alpha_q$ proteins, preventing its exchange for GTP and therefore maintaining $G\alpha_q$ in a permanently inactive state. FR reportedly induced cell cycle arrest, melanocytic differentiation and apoptosis in GNAQ/11-mutant UM cell lines[58,77,78]. In addition, it suppressed tumor growth in GNAQ/11-mutant UM xenograft models[79]. However, FR has not been tested in any clinical trials so far.

POLY-(ADP-RIBOSE) POLYMERASE

Poly-(ADP-ribose) polymerases (PARP), also known as diphtheria toxin-like ADP-ribosyl transferases (ARTD), are a family of enzymes whose role is the posttranslational modification of target proteins via the synthesis and transfer of groups of adenosine diphosphate (ADP)-ribose. If only one monomer of ADP-ribose is transferred, the reaction will be classed as mono-(ADP-ribosyl)ation or marylation. Alternatively, some PARPs can produce long polymers of ADP-ribose, in which case the reaction is called poly-(ADP-ribosyl)ation or parylation[80].

The presence of poly-(ADP-ribose) (PAR) was discovered for the first time in 1963, when it was wrongly identified as poly-adenosine monophosphate (poly-A). This "poly-A" was synthesized by a DNA-dependent nuclear enzyme which was unknown at the time, and which did not behave like any previously described poly-A polymerase or ribonucleic acid (RNA) polymerase[81]. In a second article published in 1966, Chambon et al reported that the product they had described was not actually poly-A, but a polymer of ADP-ribose[82].

From that moment and all throughout the 1970s, both PAR and PARP activity were thoroughly described and characterized in a wide variety of animal tissues and species[83–85], including human cells[86]. The ubiquity of parylation certainly encouraged further research, since it was an indication that PARP must have a very relevant role in cell biology.

PAR STRUCTURE, SYNTHESIS AND HYDROLYSIS

PAR is synthesized from nicotinamide adenine dinucleotide (NAD+), which provides the necessary ADP-ribose units, with the concomitant release of nicotinamide (Figure 3A)[83,87]. The first ADP-ribose unit is covalently linked to an acceptor amino acid residue in the target protein. Many different amino acids can function as acceptors of ADP-ribose: aspartate, glutamate, phosphoserine, serine, threonine, tyrosine, cysteine, asparagine, lysine and arginine[88,89]. Remarkably, PARP1 can be the target of its own parylation, which different reports have ascribed to many different residues, mostly E. In particular, E488 and E491 have been

identified as PAR acceptor sites in the highest number of independent investigations[88].
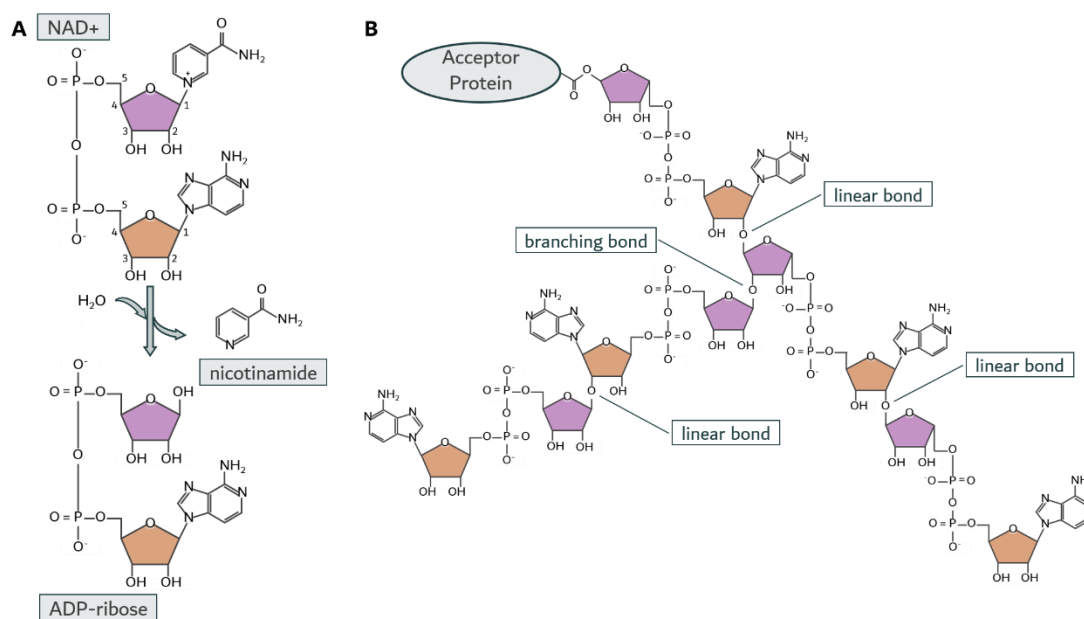
Figure 3. PAR synthesis and structure. **A** ADP-ribose units are obtained from the hydrolysis of NAD+, with the release of nicotinamide. Carbon positions in ribose rings are numbered as indicated in the NAD+ molecule. Every NAD+ molecule has two ribose rings: one of them (shown in purple) is linked to nicotinamide and the other (shown in orange) is linked to adenosine. Both ribose rings remain in the ADP-ribose structure (and so does the color code, for easier understanding). **B** During parylation initiation, the first ADP-ribose is attached to an acceptor protein. PAR is then elongated via the addition of subsequent ADP-ribose units through a linear 2,1-O-glycosidic bond between an adenosine-ribose (orange) and the following nicotinamide-ribose (purple); or else PAR is branched through a 2,1-O-glycosidic bond between two nicotinamide-riboses (purple).

During elongation of PAR, consecutive units of ADP-ribose are linked primarily through an O-glycosidic bond between the 2'-OH of the first adenosine-ribose and the 1'-OH of the following nicotinamide-ribose (Figure 3B)[82,90]. Subsequent addition of ADP-ribose units in this way produces a linear chain of PAR. Moreover, PAR can have ramifications that occur once every ≈30 units of ADP-ribose. Branching O-glycosidic bonds involve the 2'-OH of a nicotinamide-ribose and the 1'-OH of another nicotinamide-ribose (Figure 3B)[91,92]. PAR has been found to be as large as 200-mers, and have up to six points of branching[93].

Physiological degradation of PAR requires a number of different enzymes. The first one to be discovered was PAR glycohydrolase (PARG), which can cleave the ribose-ribose bonds to release ADP-ribose[94]. However, PARG is not capable of removing the first ADP-ribose unit from the acceptor protein so, essentially, it just turns parylated substrates into marylated substrates. Due to the wide variety of chemical bonds which can link ADP-ribose to the chemically different acceptor amino acids, the hydrolysis of each type of bond is carried out by different enzymes, such as MacroD1, MacroD2, terminal ADP-ribose protein glycohydrolase 1 (TARG1) and ADP-ribosyl hydrolases 1 and 3[89].

PARP FAMILY: FOCUS ON PARP1

Early research in the 1970s focused on purifying the enzyme that produced PAR and on characterizing parylation[95–98]. Presumably, most of the first descriptions of PARP activity and properties correspond to the member we know today as PARP1, which back then was referred to simply as PARP or PAR synthetase. PARP1 is a nuclear protein of 113 kDa and 1,014 amino acids, and upon discovery it was considered the only enzyme with parylation activity in eukaryotes.

It was not until the late 1990s, over 30 years after the first descriptions of parylation, that the idea of a PARP family of proteins took shape. Shieh et al inferred the existence of more than one PARP enzyme, based on the observation that PARP-knockout (KO) cells could still produce PAR[99]. In parallel investigations published within a few months, Smith et al described tankyrase and its parylation-mediated role in human telomeres[100], Johansson identified the PARP2 and PARP3 genes and messenger RNA (mRNA)[101], and Amé et al characterized the PARP2 protein[102].

As of today, the PARP family comprises 17 members in humans (Table 1; Figure 4), all of which share the "PARP signature", a ≈50 aminoacid motif that contains the catalytic core required for (ADP-ribosyl)ation[103]. Nevertheless, the presence of the PARP signature does not guarantee parylation ability. In fact, only four members of the PARP family (PARP1, PARP2, tankyrase 1 and tankyrase 2) are true PAR polymerases. Most

other members (PARP3, PARP4, PARP6, PARP10, PARP14, PARP15 and PARP16) are actually mono-(ADP-ribosyl) (MAR) transferases, while PARP9 and PARP13 seem to have no enzymatic activity whatsoever[80].

ARTD nomenclature	PARP nomenclature	Other names	(ADP-ribosyl)ation	Class
ARTD1	PARP1		P	DNA-dep
ARTD2	PARP2		P	DNA-dep
ARTD3	PARP3		M	DNA-dep
ARTD4	PARP4	vaultPARP	M	
ARTD5	PARP5a	tankyrase 1	P	tankyrase
ARTD6	PARP5b	tankyrase 2	P	tankyrase
ARTD7	PARP15	BAL3	M	macro
ARTD8	PARP14	BAL2	M	macro
ARTD9	PARP9	BAL1	-	macro
ARTD10	PARP10		M	
ARTD11	PARP11		M	
ARTD12	PARP12		M	CCCH
ARTD13	PARP13	ZAP1	-	CCCH
ARTD14	PARP7	TiPARP	M	CCCH
ARTD15	PARP16		M	
ARTD16	PARP8		M	
ARTD17	PARP6		M	

Table 1. PARP family of proteins.
P: parylation; M: marylation; DNA-dep: DNA-dependent; BAL: B-aggressive lymphoma; ZAP: zinc-finger antiviral protein; TiPARP: TCDD-inducible PARP.

Thus, it soon became evident that referring to all family members as "polymerases" is patently inaccurate, which is why the new ARTD nomenclature was proposed in 2010[103]. However, as usually happens in all fields of science, most researchers continue using the original nomenclature. For example, only 5 results come up under the search for "ARTD9" in PubMed between 2013 and 2020, while 45 results come up in

the same period of time if the search is for "PARP9", even if that enzyme is not a polymerase.
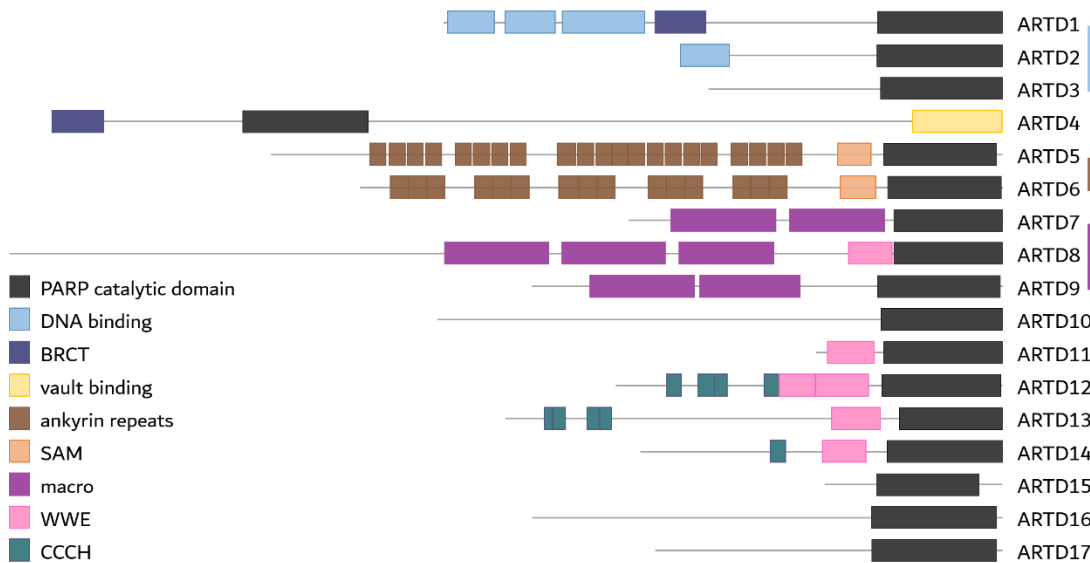
Figure 4. Structure of PARPs.
— DNA-dependent; — tankyrases; — macro PARPs; — CCCH.

According to their domain composition, PARPs are usually classified as follows[104]:

- DNA-dependent PARPs (PARP1, PARP2, PARP3) contain DNA-binding domains. Binding to DNA triggers their catalytic activity, although they can also be activated independently of DNA.
- Tankyrases (PARP5a, PARP5b) have ankyrin repeats that mediate protein-protein interactions.
- Macro PARPs (PARP9, PARP14, PARP15) harbor large macrodomains that can bind to PAR and MAR.
- Cys–Cys–Cys–His (CCCH) PARPs (PARP7, PARP12, PARP13) contain CCCH zinc finger domains that facilitate RNA-binding. They also have tryptophan (W)-W-E domains that are involved in binding to PAR.
- Other PARPs remain unclassified, since they do not fit any of the previous categories.

INTRODUCTION

As mentioned above, PARP1 was the founding member of the family. It is the most abundant and active member of the PARP family, which is why it concealed the existence of every other PARP for so long. It is also the best known PARP and the one that the present thesis will focus on.

The structure of PARP1 is comprised of three main domains: the DNA-binding domain, the automodification domain and the catalytic domain[105]. The DNA-binding region is located on the N-terminus, and it is composed of three distinct zinc finger motifs (ZnF). ZnF1 and ZnF2 are homologous, and they seem to recognize altered DNA structure, rather than specific sequences[106]. ZnF3 is different from the others, and it seems to mediate interdomain contacts which are necessary for PARP activation upon DNA binding[107]. The automodification domain is in the central region of the protein. It contains most acceptor sites of parylation, hence its name. It also harbors a BRCA C-terminus (BRCT) motif, which is present in a number of proteins involved in the regulation of cell cycle in response to DNA damage, and mediates their interaction with phosphorylated proteins[106,108]. Finally, the carboxy-terminal catalytic domain contains the PARP signature, which is highly conserved across all PARPs and eukaryotic species. The catalytic core contains a histidine-tyrosine-glutamate (H-Y-E) triad that is present in all PAR transferases. The H and Y are responsible for the binding and orientation of substrate NAD+, and the E performs the actual catalysis of parylation. The H and Y are present in MAR transferases too, since they use NAD+ as a substrate as well, but the E is often substituted for isoleucine, leucine or another Y. Nevertheless, a few MAR transferases contain a HYE motif yet are still incapable of parylation, which shows that the HYE triad is necessary but not sufficient to enable parylation[80].

Over the years, PARP1 has been implicated in a plethora of physiological and pathological processes, such as the DNA damage response (DDR), gene expression, cell death, cell differentiation, autophagy, inflammation, circadian rhythms or cancer. Some of these functions of PARP1 will be discussed in detail below.

PARP1 AND GENE EXPRESSION

As early as the 1960s, the groups of Hayaishi and Sugimura already showed that PAR could be covalently linked to histones[109,110] and other nuclear proteins[111], altering their structure, activity and interactions. As a result, PARP can influence many nuclear activities, such as gene expression.

PARP1 can affect gene expression through several different mechanisms. Indirect, non-specific regulation of gene expression can take place via modulation of chromatin structure, DNA methylation or the basal transcription machinery. On the other hand, interactions with sequence-specific transcription factors mediate a more precise control of certain signaling pathways.

PARP1 binding and activity have been repeatedly associated with a relaxed chromatin structure[112–114]. This could be partly due to an antagonism between PARP1 and histone H1, which seem to bind nucleosomes in a competitive pattern. H1 is a linker histone, responsible for compacting the nucleosomes into transcriptionally inactive heterochromatin. PARP1 appears to displace histone H1, hence promoting chromatin decondensation and transcription[115]. Furthermore, PARP1 was shown to parylate and thus inhibit the histone K demethylase 5B (KDM5B), leading to an enrichment of histone H3 K4 trimethylation (H3K4me3)[116]. This methylation mark is classically associated with open, transcriptionally active chromatin. On the contrary, PARP1, in cooperation with ubiquitin-like containing PHD and RING finger domains 1 (UHRF1), may also increase the repressive methylation mark H4K20me3 at pericentric heterochromatin, favoring transcriptional repression[117].

PARP1 has been associated with chromatin insulator function too, since it parylates the CCCTC-binding factor (CTCF), contributing to its insulator properties[118]. The interaction between PARP1 and CTCF have been implicated in circadian regulation of transcription. In particular, PARP-CTCF complexes promoted the cyclic migration of circadian loci towards the nuclear periphery, where they acquire repressive methylation marks that reduce gene expression[119].

Interestingly, it has been suggested that PARP1 may participate in chromatin remodeling indirectly, serving as an energy supply for adenosine triphosphate (ATP)-consuming chromatin remodelers. Apparently, ADP-ribose obtained from the hydrolysis of PAR can be used by the nucleoside diphosphate–linked moiety X (NUDIX) 5 to produce ATP in the presence of pyrophosphate[120]. This makes for a rapid and abundant source of nuclear ATP, meeting the high energetic demands of chromatin remodeling in response to certain signals, such as hormones, enabling hormone-induced transcription changes.

PARP1 can also modulate the transcriptional machinery. For example, the negative elongation factor (NELF), which interrupts the elongation step of RNA polymerase II-dependent transcription, can be parylated by PARP1. Parylated NELF is incapable of binding RNA, so RNA polymerase II is released and productive elongation enabled[121].

As for more targeted gene regulation, PARP1 is involved in the regulation of several sequence-specific transcription factors of great biological importance. For instance, PARP1 is a coactivator of NFκB, so much so that PARP1-KO can strongly abrogate the inflammatory response[122]. The impact of PARP1 on NFκB transcriptional activity does not require parylation, but rather the collaborative interaction with a number of coactivators that synergistically enhance NFκB-dependent transcription[123–125]. PARP1 can also activate sex determining region Y-box 2 (SOX2)-mediated transcription, with important implications in the maintenance of pluripotency in stem cells[126–128]. The role of parylation in the regulation of SOX2 is not clear, with some authors reporting that SOX2 is parylated by PARP1[126], while others state that it is PARP1 automodification what enhances SOX2 activity[127]. Other major transcription factors whose activity is promoted by PARP1 are the hypoxia-inducible factors (HIF) 1α[129–131] and 2α[132]. At the post-transcriptional level, PARP1 seems to contribute to the stability and function of both transcription factors in a parylation-dependent manner. Furthermore, PARP1 can also increase the expression of HIF2α at the transcriptional level. This denotes a relevant role for PARP1 in the hypoxia response, which may have a great significance in the progression of solid tumors.

On the other hand, PARP1-mediated parylation of CCAAT/enhancer-binding protein (C/EBP) β was shown to repress its transcriptional activity, since it prevented C/EBPβ from binding DNA. C/EBPβ is crucial in the differentiation of mature adipocytes, so the inhibition or depletion of PARP1 may increase adipogenesis[133].

All these examples illustrate how PARP1 may influence important physiological processes through the modulation of the cell transcriptional program.

PARP1, DNA REPAIR AND CANCER

In 1975 Miller anticipated that PARP could be involved in DNA repair, after noticing increased parylation in the presence of endonucleases[134]. Indeed, several DNA-damaging agents, such as UV light, bleomycin or gamma irradiation, were shown to increase parylation too[135,136]. Several reports in the early 1980s proved that parylation had a role in DNA strand break repair, with double strand breaks causing the highest PARP1 activation[137,138]. PARP inhibitors were shown to delay DNA repair and consequently enhance cytotoxicity in the presence of DNA-damaging agents[137,139,140]. PARP1 was further associated with maintenance of chromosome stability. PARP inhibition or KO result in increased sister chromatid exchanges (SCE), chromatid breaks, and sensitivity to DNA-damaging agents[141–143]. On the contrary, PARP1 overexpression in wildtype cells was correlated to low genomic instability[144], and the rescue of PARP1 expression in PARP1-KO mice restored genomic stability as well[145].

All these effects are mediated by the contribution of PARP1 to the repair of both single and double strand breaks (SSB, DSB), as well as global genome nucleotide excision repair (ggNER). In a nutshell, PARP1 acts as a DNA strand break sensor and binds to sites of DNA damage. This binding activates PARP1, triggering its automodification, which in turn promotes the recruitment and/or parylation of other participants of the DDR[105].

During spontaneous SSB repair, SSB-bound PARP1 recruits X-ray repair cross-complementing protein (XRCC) 1, a scaffold protein that further recruits essential repair enzymes, such as DNA ligase 3 and DNA

polymerase β. Furthermore, PARP1 is involved in the repair of single-stranded DNA nicks caused by malfunctions of topoisomerase 1 (TOP1). The recruitment and parylation-mediated stabilization of tyrosyl-DNA phosphodiesterase 1 (TDP1) by PARP1 enhance the removal of TOP1 cleavage complexes from DNA to allow its re-ligation[105].

Appropriate repair of DSBs is key for the perpetuation of genomic integrity. The two main pathways that repair DSBs are homologous recombination (HR) and non-homologous end-joining (NHEJ). HR is restricted to the S and G2 phases of the cell cycle due to the requirement for the sister chromatid as a template, while NHEJ is active throughout the cell cycle and does not rely on a template. PARP1 has been implicated in both pathways. To begin with, PARP1 may recruit meiotic recombination 11 (MRE11), which interacts with RAD50 and Nijmegen breakage syndrome protein 1 (NBS1) in what is known as the MRN complex, a crucial player in the initiation of DSB repair through the appropriate pathway. In the case of HR, PARP1 also recruits breast cancer susceptibility protein (BRCA) 1, which in turn mobilizes RAD51 to form filaments on single-stranded DNA, an essential step in strand invasion of the homologous DNA template. As for NHEJ, PARP1 can bind and parylate DNA-dependent protein kinase catalytic subunit (DNA-PKcs), enhancing its kinase activity. DNA-PKcs then phosphorylates itself and other DDR components to promote NHEJ. Moreover, PARP1 helps recruit the chromodomain helicase DNA-binding protein 2 (CHD2) via XRCC4. Finally, PARP1 also promotes the recruitment of DNA polymerase θ which can be crucial in end joining[105].

Thus, the importance of PARP1 in DNA repair is undeniable, and even more so in the context of cancer. Alterations in many of the proteins mentioned in this section have been reported in cancer, since defects in DNA repair may lead to genomic instability, one of the hallmarks of cancer. The most relevant alterations in relation to PARP1 are germline loss-of-function mutations in BRCA1 and BRCA2. BRCA mutations are present in about 15% of ovarian cancer patients[146] and 2-3% of breast cancer patients[147], and may increase the lifetime risk for other cancer types such as prostate.

BRCA-deficient cells are incapable of HR, meaning that DSB repair is heavily compromised. In this context, further disruption of SSB and DSB repair by PARP inhibition results in extreme genomic instability and the subsequent induction of cell cycle arrest and apoptosis, as shown independently by the groups of Helleday and Ashworth in 2005[148,149]. The isolated perturbation of either BRCA1/2 or PARP1 does not affect cell viability, but the combination of both defects results in cell death, a cytotoxic mechanism known as synthetic lethality.

In the case of BRCA-deficient cancers, the synthetic lethality of PARP inhibition will be highly specific for tumor cells, since healthy cells do not have aberrant HR or innate genomic instability. Furthermore, later investigations proved that other cancer susceptibility mutations involving HR genes, like mutations on RAD51 or NBS1, can sensitize to PARP inhibition as well[150]. This condition is commonly referred to as "BRCAness", since these mutations induce a phenotype that is similar to BRCA mutations. In consequence, PARP1 emerged as a druggable target with promising therapeutic potential in the treatment of HR-deficient cancer patients.

PARP INHIBITORS

Several PARP inhibitors (PARPi) have been developed by different companies in the last decades. All of them are analogs of NAD+, so they compete with NAD+ for binding the catalytic core of PARP, interfering with the production of ADP-ribose[151]. Due to the similar sequence and structure of PARP1 and PARP2 catalytic domains, PARPi can usually inhibit both enzymes. Apart from the catalytic inhibition, modern PARPi have the ability to trap PARP1/2 at sites of DNA damage, which increases their cytotoxic potential. The reason is that DNA-trapped PARP can be an extra source of genomic instability, since it blocks the progression of DNA-related enzymes, like DNA polymerase, inducing the accumulation of stalled replication forks[152].

The first few clinical trials for PARPi were carried out in the 2000s with the idea that PARP inhibition could sensitize to conventional DNA-damaging chemotherapeutic agents[153], like temozolomide[154].

Nevertheless, the preclinical studies from 2005 reporting a synthetic lethal interaction with BRCA deficiencies changed the course of all investigations regarding PARPi. The first great success came with a clinical trial in 2009 for PARPi olaparib, which was orally administered as a single agent to cancer patients with or without BRCA1/2 mutations (NCT00516373)[155]. Though mild side effects were reported, it showed fewer adverse effects than conventional chemotherapy, and it exerted significant antitumor activity in BRCA-deficient ovarian, breast and prostate cancer patients. These results were confirmed in subsequent clinical trials[156,157], which also showed that ovarian cancer usually had a higher response rate.

Further trials found a correlation between response to PARPi and response to platinum-based chemotherapy[158]. The mechanism of action of platinum salts is the induction of crosslinks in DNA that would be normally resolved by HR, which makes HR-deficient cells especially sensitive[159]. Therefore, platinum-based drugs and PARPi share the same tumor targets, and platinum sensitivity can be used as a predictor for response to PARPi.

Numerous clinical trials for PARPi as single agents or in combination with other antitumor drugs have led to the FDA and EMA approvals of four different PARP inhibitors so far: olaparib, rucaparib, niraparib and talazoparib, each of them with specific indications (Table 2).

In agreement with the findings described above, eligibility for treatment with any PARPi usually requires suspected BRCA mutation and/or response to platinum-based chemotherapy. PARPi are mostly indicated in the treatment of ovarian cancer, except talazoparib which is used in breast cancer patients. Olaparib, the best known PARPi, has the wider target population, being approved in the treatment of epithelial ovarian, fallopian tube and primary peritoneal cancers, breast cancer, pancreatic adenocarcinoma and castration-resistant prostate cancer.

Unfortunately, as often happens with targeted therapies, acquired resistance to PARPi may arise. For instance, revertant mutations in BRCA1/2, or any mutations that restore HR function will abrogate the synthetic lethality of PARPi[151]. Also, mutations in PARP1 itself that interfere with its binding to DNA were found to generate resistance, since

they reduce the DNA-trapping potential of PARPi[160]. Alternatively, loss-of-function mutations in PARG lead to the accumulation of parylated PARP1, compensating for the presence of PARPi and causing resistance[161].

PARPi	Brand name	FDA first approval	As a single agent	In combination
Olaparib	Lynparza	2014	Ovarian cancer: BRCA-mutated or recurrent platinum-sensitive Breast cancer: metastatic, HER2-negative and BRCA-mutated Pancreatic adenocarcinoma: metastatic, BRCA-mutated and platinum-sensitive Prostate cancer: metastatic, castration-resistant and non-responsive to enzalutamide nor abiraterone	With *bevacizumab* in platinum-sensitive, HR-deficient ovarian cancer
Rucaparib	Rubraca	2016	Ovarian cancer: BRCA-mutated, after 2+ chemotherapy regimens	
Niraparib	Zejula	2017	Ovarian cancer: platinum-sensitive; HR-deficient after 3+ chemotherapy regimens	
Talazoparib	Talzenna	2018	Breast cancer: HER2-negative, BRCA-mutated	

Table 2. PARP inhibitors that are officially approved for clinical use.
"Ovarian cancer" includes epithelial ovarian, fallopian tube and primary peritoneal cancers.

In conclusion, and despite resistance-related limitations, PARPi have proved to be safe, reliable drugs in the treatment of several cancer types in different contexts. However, their clinical application is currently very restricted to the HR status of tumor cells. Further research should be carried out regarding the other, ever-expanding roles of PARP1 in cell physiology, which may provide new therapeutic opportunities for the use of PARPi.

LONG NON-CODING RNA

For a long time, the field of genetics has traditionally focused on protein-coding genes, and even referred to non-coding DNA as "junk DNA". However, the development of the Human Genome Project in the early 2000s, the in-depth knowledge of the genome organization provided by next-generation sequencing and the advances in the -omics sciences have readjusted this vision. In fact, most of the actively transcribed regions of the human genome produce non-coding RNA, rather than protein-coding mRNA. In addition, more and more investigations point to a crucial role of non-coding RNAs in pathological settings[162]. As a result, recent decades have seen a growing interest in understanding the regulation and functions of non-coding RNA.

Depending on their location, function and size, non-coding transcripts can be classified into circular RNA, extracellular RNA, microRNA (miRNA), small nuclear RNA, small nucleolar RNA, piwi-interacting RNA and long non-coding RNA (lncRNA), which will be the subject of this section. A genome-wide study determined that lncRNA represent over 68% of the human transcriptome, and highlighted that about 7% of all lncRNA contain some disease-associated single-nucleotide polymorphism[163]. This evidence underlines the relevance of lncRNA in cell biology.

LncRNA are transcripts longer than 200 nucleotides that do not encode any protein products. There are four classes of lncRNA, according to their location in the genome relative to protein-coding loci: intergenic, intronic, overlapping and antisense lncRNA[164]. All of them can regulate gene expression in a wide variety of ways, both pre- and post-transcriptionally. Moreover, lncRNA expression and distribution seem to be extremely tissue-specific, so they may play a part in the acquisition of different gene expression profiles in the different cell types[163].

LONG NON-CODING RNA AND GENE EXPRESSION

The first level of lncRNA-mediated modulation of gene expression is the regulation of chromatin structure. LncRNA can bind, recruit or repel chromatin-remodeling enzymes as well as DNA methyltransferases[165]. For instance, the lncRNA X-inactive specific transcript (Xist) mediates X-

chromosome inactivation in female mammalian cells via the sequential interaction with SHARP, SMRT, HDAC3 and eventually the recruitment of the polycomb repressive complex 2 (PRC2). PRC2 then represses gene expression by trimethylating histone H3K27 (H3K27me3) across the X chromosome in a Xist-dependent manner, ultimately leading to complete chromosome silencing[166].

LncRNA can also regulate transcription directly both in *cis* and in *trans*, interacting with the transcriptional machinery and with sequence-specific transcription factors. On the one hand, lncRNA can recruit transcription factors to the promoters of target genes, acting as scaffolds between DNA and DNA-binding proteins. This is the case of the rhabdomyosarcoma 2-associated transcript (RMST), which is necessary for the binding of SOX2 to promoter regions during neurogenesis[167]. On the other hand, the mere binding of lncRNA to transcription factors often modulates their activity. Some lncRNA can enhance the activity of transcription factors, while others can block their DNA-binding region and hence inhibit transcriptional activity[164]. For example, lnc-DC can affect dendritic cell differentiation by enhancing the activity of signal transducer and activator of transcription (STAT) 3. The binding of lnc-DC to STAT3 interferes with STAT3 recognition by the phosphatase SHP1, leading to increased phosphorylation and activity of STAT3[168].

Finally, lncRNA can regulate gene expression at the post-transcriptional level, affecting splicing, mRNA stability and/or initiation of translation.

Regarding splicing, lncRNA can promote the binding of nuclear ribonucleoproteins to splicing silencer elements and induce alternative splicing[164]. For instance, in pancreatic glucagon-producing α cells the lncRNA Paupar interacts with serine- and arginine-rich splicing factors (SRSF) to promote alternative splicing of Pax6, favoring the α cell-specific isoform[169]. As a result, Paupar can be an important modulator of α cell function, affecting glucose homeostasis through glucagon production.

LncRNA can modulate mRNA stability by directly interacting with miRNA, acting as competing endogenous RNA (ceRNA) or miRNA "sponges" which prevent miRNA-dependent degradation of target mRNA[170]. Otherwise, lncRNA can modulate the degradation of mRNA

that harbor AU-rich elements (ARE). AREs are targeted by a number of proteins to control mRNA turnover, but some lncRNA can interfere with the activity of ARE-binding proteins. One such case is Linc-RoR, which can hinder ARE-mediated degradation of c-Myc mRNA, therefore increasing c-Myc expression[171].

As for translation, some lncRNA can facilitate the interaction of target mRNA with ribosomes[164]. That is how lncRNA antisense to ubiquitin carboxy-terminal hydrolase L1 (AS-Uchl1) can promote the translation of Uchl1[172].

All these different mechanisms of control turn lncRNA into master regulators of gene expression, with the potential to influence a large number of physiological and pathological processes. For instance, lncRNA have been associated with cancer, where some of them display tumor suppressor properties while others function as oncogenes[170].

LONG NON-CODING RNA AND CANCER

The best-known lncRNAs in the context of cancer are HOX transcript antisense RNA (HOTAIR) and metastasis-associated lung adenocarcinoma transcript 1 (MALAT1), both of which have been associated with tumor progression[170]. HOTAIR is overexpressed in a variety of human cancers. In breast cancer, HOTAIR expression is correlated with poor survival and metastasis. This lncRNA has been shown to interact with several histone modifying enzymes, mainly PRC2. HOTAIR appeared to reprogram PRC2 targeting, changing the genomic pattern of the repressive histone mark H3K27me3 to favor a more invasive gene expression profile[173].

MALAT1 is one of the most expressed lncRNA in normal tissues. What is more, it is highly conserved across mammals, a very unusual characteristic in lncRNA. Upon discovery, it was regarded as a marker of lung cancer metastasis, but later research has associated MALAT1 to many other cancer types, like hepatocellular and colorectal carcinomas[174]. MALAT1 has been reported to modulate mRNA splicing by interacting with SRSFs and regulating their level of phosphorylation[175]. In addition, several studies have shown that MALAT1 can promote tumor progression via sponging various miRNA[176–178]. However, MALAT1 has been recently identified as

a tumor suppressor in breast cancer, so the role of MALAT1 in cancer has turned controversial[179].

On the contrary, a number of lncRNA can hinder tumorigenesis. Many of them have been identified as up- and downstream mediators of the renowned tumor suppressor p53. For example, the lncRNA damage-induced non-coding (DINO) is a transcriptional target of p53. Once transcribed, DINO binds and stabilizes p53, and it is necessary for p53-dependent signaling in response to DNA damage[180]. Also induced by p53, lincRNA-p21 mediates p53-dependent gene repression and apoptosis[181]. The promoter of the lncRNA p53 target 1 (TP53TG1) was found to be hypermethylated in tumor cells, leading to tumor-specific TP53TG1 silencing. TP53TG1 epigenetic silencing promoted tumor growth and chemoresistance, and was correlated with poor outcome[182].

These are only a few examples to present lncRNA as an emerging area in the research of tumor biology. Further studies may provide a more in-depth understanding of the molecular events underlying cancer.

Every human tissue requires the presence of oxygen and nutrients to support cell metabolism and growth. Their availability is determined by the balance between delivery and consumption. In the case of tumor tissue, both the supply and demand of oxygen and nutrients are markedly altered. On the one hand, the abnormally elevated proliferation rate of tumor cells makes for an exceptionally high metabolic intake. On the other hand, tumor perfusion is usually compromised due to insufficient and/or aberrant vascularization. As a result of this imbalance, most solid tumors present large areas of low oxygenation, a condition known as hypoxia[183,184].

Within a solid tumor above a certain size, oxygen is typically dispersed in a gradient demarcated by blood vessels. Tumor cells surrounding functional vessels are well-oxygenated, since those regions are in normoxia. On the opposite end, the regions that are farthest away from blood vessels can end up subjected to complete oxygen deprivation, also known as anoxia, which triggers cell death by necrosis. In between the normoxic and anoxic regions lies the hypoxic tumor microenvironment, where tumor cells are not only viable, but actually more aggressive, since hypoxia induces an adaptive cellular response that promotes a number of pro-malignant features. For example, hypoxia enhances cell motility and angiogenesis, which in turn favor invasion and metastasis. Moreover, conventional radio- and chemotherapy require the presence of oxygen to achieve their optimal antitumor activity, which depends on oxidative stress-mediated DNA damage and cytotoxicity. In consequence, hypoxic tumor cells may resist conventional therapies[185,186]. For all these reasons, tumor hypoxia constitutes a sign of poor prognosis.

ACTIVATION OF THE HYPOXIA RESPONSE

The hypoxia response is mediated by the activation of the hypoxia-inducible factors (HIF) (Figure 5). HIFs are heterodimeric transcription factors made of one α- and one β-subunit. There is only one β-subunit in humans (HIF1β) but three different α-subunits (HIF1α, HIF2α and HIF3α) that will determine the formation of HIF1, HIF2 or HIF3. All HIF subunits are constitutively transcribed and translated, but the formation of active

HIFs depends on the presence of the oxygen-labile α-subunits, whose stability and function are regulated in a post-translational manner[184].
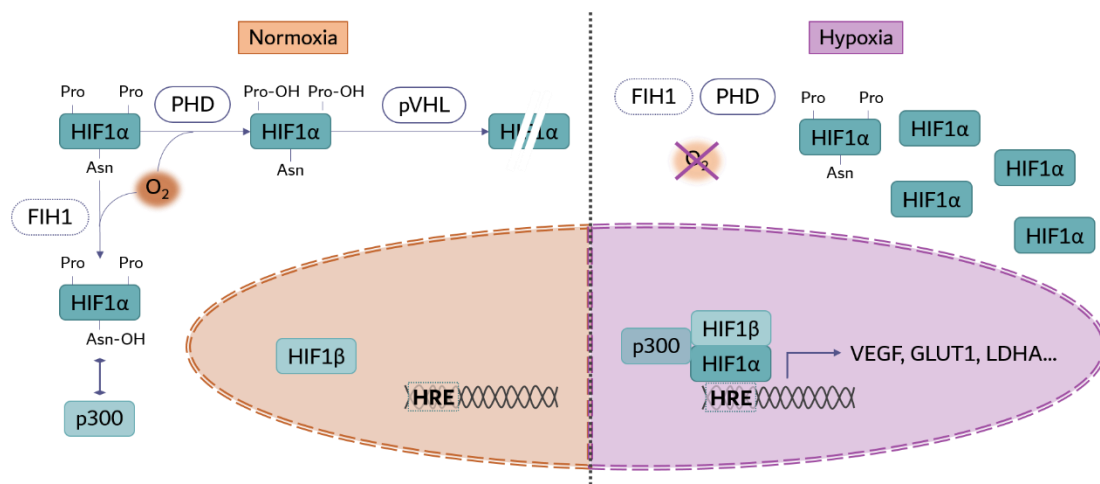
Figure 5. Activation of the hypoxia response. During normoxia, PHD and FIH1 use oxygen to hydroxylate HIFα on proline and asparagine residues, respectively. These hydroxylations trigger the VHL-mediated ubiquitination and degradation of HIFα and prevent the interaction with co-activator p300. During hypoxia, oxygen-dependent hydroxylations are not possible, so HIF α-subunits remain stable and translocate to the nucleus, where they form a complex with HIF1β and p300. This transcriptional complex can bind HRE and regulate the expression of HIF target genes to initiate the hypoxia response.

In particular, the abundance and activity of HIFs depend on the oxygen-dependent hydroxylation of HIF α-subunits, carried out by prolyl hydroxylase domain-containing enzymes (PHD) 1–3 (also known as EGLN1–3) and factor inhibiting HIF 1 (FIH1), collectively known as HIF hydroxylases. PHDs catalyze the hydroxylation of one or both of two proline residues in the oxygen-dependent degradation region of HIFα[187,188]. FIH1 catalyzes the hydroxylation of an asparagine residue in the HIFα C-terminal transactivation domain, hindering the interaction of HIF with the transcriptional co-activator proteins CBP/p300 (CREB-binding protein/p300)[189,190]. PHDs and FIH1 are proposed to act as oxygen sensors in cells, providing a direct link between cellular oxygen concentrations and the hypoxia response.

The different hydroxylations of HIFα allow the binding of the von Hippel-Lindau tumor suppressor (pVHL)[187,188], which is part of a E3 ubiquitin

ligase complex. Recognition by pVHL induces HIFα ubiquitination and subsequent proteasomal degradation[191–193].

However, none of these hydroxylations can take place during hypoxia due to the lack of oxygen as a substrate. As a result, HIFα do not undergo proteasomal degradation. Instead, HIFα translocate to the nucleus, where they can bind HIF1β and p300 to promote the transcription of a large number of genes that initiate the hypoxia response. In particular, HIF bind specific sequences in the promoters of target genes, commonly referred to as hypoxia response elements (HRE)[184].

This mechanism allows for a rapid adaptation to the hypoxic microenvironment as soon as oxygen availability starts to decrease. HIF transcriptional activity triggers a distinct gene expression program aimed at compensating the lack of oxygen in the short term, and ultimately restoring physiological oxygen levels in the longer term.

Notably, the hypoxia response is highly conserved in animals. Though the present thesis will focus on the implications of hypoxia in the context of cancer, hypoxia plays a central role in a number of physiological processes. During embryonic development, the hypoxia response is essential for erythropoiesis[194], vasculogenesis and cardiac morphogenesis[195], among others. In fact, the KO of HIF1β, HIF1α, HIF2α or PHD2 cause embryonic lethality[195–198].

HYPOXIA AND METABOLISM

The first and foremost consequence of cellular hypoxia is the disruption of oxidative phosphorylation, which is the major source of energy in the cell. In order to overcome this challenge, hypoxic adaptation must induce a metabolic shift, averting oxygen-dependent pathways and boosting glycolytic metabolism instead.

In that line, some of the most prominent targets of HIF are glucose transporters (GLUT) 1 and 3, as well as glycolytic enzymes like hexokinases 1 and 2, phosphoglycerate kinase 1, enolase 1 and pyruvate kinase M2. Moreover, pyruvate dehydrogenase (PDH) kinase 1 (PDK1) is also upregulated by hypoxia, promoting the phosphorylation-mediated

inhibition of PDH. PDH produces acetyl-CoA from pyruvate, so PDK1 deprives the Krebs cycle of acetyl-CoA. As a result, the progression of glycolysis towards oxidative phosphorylation decreases, and instead pyruvate is channeled to anaerobic fermentation. Indeed, lactate dehydrogenase A (LDHA), which converts pyruvate to lactate, is another major target of HIF, and so is the lactate transporter monocarboxylate transporter 4. Altogether, the hypoxia response increases glucose uptake, anaerobic glycolysis from glucose to lactate and lactate removal, while simultaneously downregulating the preliminary steps of oxidative phosphorylation[184].

Amino acid metabolism is modified under hypoxia too. The main effects of hypoxia affect glutamine metabolism. In particular, glutamine reductive carboxylation is used during hypoxia as the main source of citrate for the synthesis of fatty acids, therefore avoiding the oxidative pathway to citrate via the Krebs cycle[199,200]. Fatty acid and subsequent lipid synthesis are essential for the sustained proliferation of tumor cells, since they are indispensable elements of the plasma membrane. However, fatty acid catabolism through the β-oxidation pathway must be necessarily avoided during hypoxia. Surely, HIF1 can inhibit fatty acid oxidation by downregulating medium- and long-chain acyl-CoA dehydrogenases[201].

As previously mentioned, the reprogramming of energy metabolism is considered a hallmark of cancer[3], which highlights the importance of the hypoxia response in supporting tumor progression.

HYPOXIA AND THE QUEST FOR OXYGEN

Apart from adapting cell metabolism to low oxygen conditions, the other cornerstone of the hypoxia response is the attempt to restore oxygen availability.

Firstly, hypoxia is notorious for promoting erythropoiesis[186]. In fact, the first ever report of HIF1α described its ability to upregulate erythropoietin expression in response to hypoxia[202]. Moreover, hypoxia can also increase iron absorption and transport[186]. These two processes can potentially enhance oxygen delivery, since they elevate the number of circulating red blood cells as well as the hemoglobin required for their function.

Most importantly for the subject of this thesis, hypoxia triggers the formation of new blood vessels with the purpose of increasing tissue oxygenation. Hypoxia is a master regulator of neovascularization in all kinds of contexts. As previously mentioned, HIFs are essential for vasculogenesis and angiogenesis during embryonic development[195], but also during pathological settings such as pulmonary hypertension, ischemia, diabetes or cancer[203].

Specifically, HIFs have been shown to directly modulate the expression of numerous genes involved in endothelial cell metabolism, proliferation and migration, all of which mediate the growth and recruitment of new blood vessels to hypoxic tissues. The paramount regulator of angiogenesis vascular endothelial growth factor is strongly upregulated by hypoxia[204], and so are other important pro-angiogenic signal mediators[185]. This has crucial implications in the progression of solid tumors, since angiogenesis is a hallmark of cancer[3]. The molecular mechanisms underlying tumor neovascularization and their regulation by hypoxia and other stimuli will be discussed in more detail in the following section.

Hypoxia can also improve tissue oxygenation by increasing vasodilation of existing blood vessels. To this end, hypoxia has been shown to promote the synthesis and release of nitric oxide (NO), namely via the upregulation of the endothelial NO synthase[203].

Alternatively, instead of attempting to restore tissue oxygenation, hypoxia can promote the migration of cells towards better oxygenated areas. Hypoxic cells undergo an epithelial–mesenchymal transition (EMT) that facilitates motility and invasion. Moreover, hypoxia enables extracellular matrix remodeling, further enhancing the invasive potential of hypoxic cells[185]. In cancer, increased invasiveness is closely associated with metastasis, both of which are yet another hallmark of cancer[3].

That makes for a total of three hallmarks of cancer that can be directly influenced by tumor hypoxia, stressing its relevance in cancer research.

TUMOR VASCULATURE

As previously mentioned, solid tumors have high metabolic demands and concomitantly generate great amounts of metabolic waste. In these conditions, tumors can only grow above a certain size ($\approx$1 mm) if it is with the assistance of new blood vessels that can provide oxygen and nutrients, and evacuate carbon dioxide and other waste products.

Adult vasculature is largely quiescent, that is, the endothelial cells (EC) that line blood vessels rarely proliferate. A few physiological exceptions are wound healing and the female reproductive cycle. In these instances, the growth of new blood vessels is required for tissue repair, in the first case, or to support the growth of a potential embryo, in the second. New blood vessels sprout from pre-existing vasculature in a process termed angiogenesis, which is carefully regulated in physiological contexts. However, even this neovasculature quickly returns to a latent state as soon as its physiological purpose is fulfilled[3].

On the contrary, cancer is known to trigger an "angiogenic switch", which is characterized by the continual predominance of pro-angiogenic signals and a downregulation of anti-angiogenic regulatory steps[3]. Furthermore, tumors can increase blood supply through a variety of mechanisms, other than angiogenesis, like intussusception, vessel co-option or vasculogenic mimicry[205] (Figure 6). Angiogenesis is by far the best known form of tumor neovascularization. It has been one of the main fields of cancer research for decades and the target of many clinical studies. However, the limitations encountered by antiangiogenic therapies have led to a growing interest in the understanding of alternative neovascularization mechanisms.

The molecular aspects of angiogenesis will be detailed below, as well as the therapeutic approaches adopted for cancer treatment. The final section will focus on vasculogenic mimicry, a form of tumor neovascularization that overrides antiangiogenic therapies and has been repeatedly associated with poor prognosis in cancer patients, and constitutes the main issue of the study presented in the current memory.
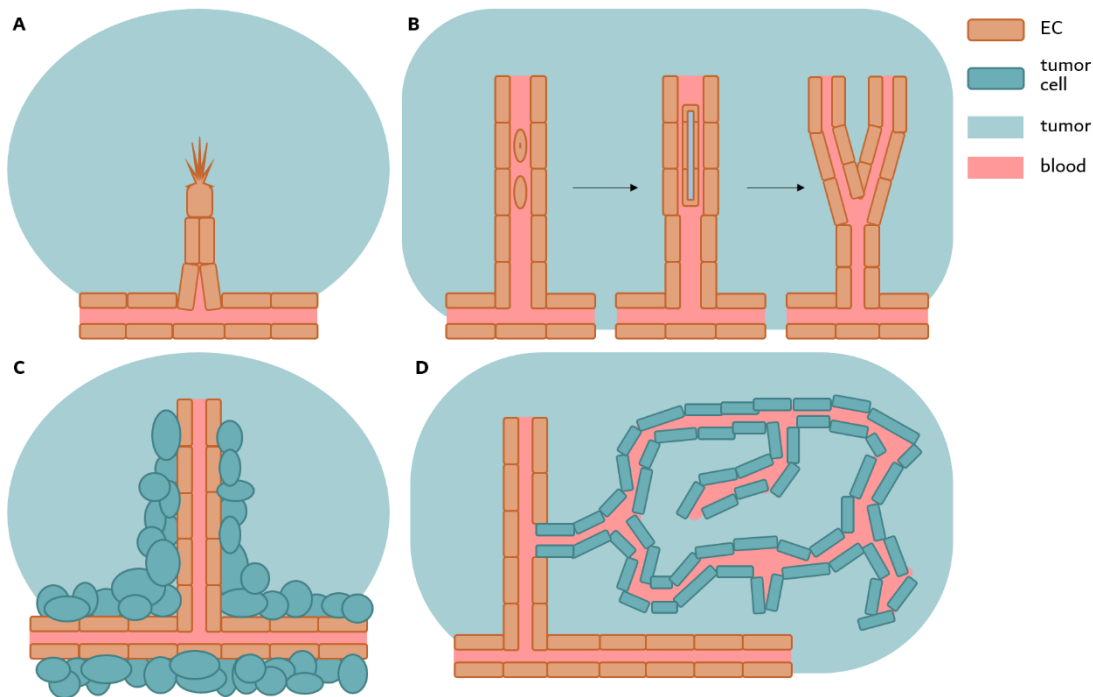
Figure 6. Mechanisms of tumor neovascularization. **A** Sprouting angiogenesis, where new vessels grow from pre-existing vasculature. **B** Intussusception, also known as intussusceptive angiogenesis, where a certain vessel splits into two separate vessels due to invagination of ECs into the vessel lumen. **C** Vessel co-option, where tumor cells migrate towards and grow around tumor vessels. **D** Vasculogenic mimicry, where tumor cells acquire an endothelial-like phenotype and create aberrant pseudovascular channels.

ANGIOGENESIS

The term angiogenesis refers to the sprouting and subsequent growth of new vessel branches from pre-existing blood vessels. The process of angiogenesis starts with the activation of pro-angiogenic signals, which is triggered by oxygen and/or nutrient deprivation in poorly perfused tissues.

In particular, hypoxic cells have an increased expression and secretion of vascular endothelial growth factors (VEGF)[204], which bind VEGF receptors (VEGFR) expressed on the surface of ECs[206]. VEGF signaling is the core of the angiogenic process. It initiates a signaling cascade that regulates multiple signaling pathways implicated in EC specification, migration, proliferation and apoptosis, and that will shape the different stages of angiogenesis (Figure 7)[207].
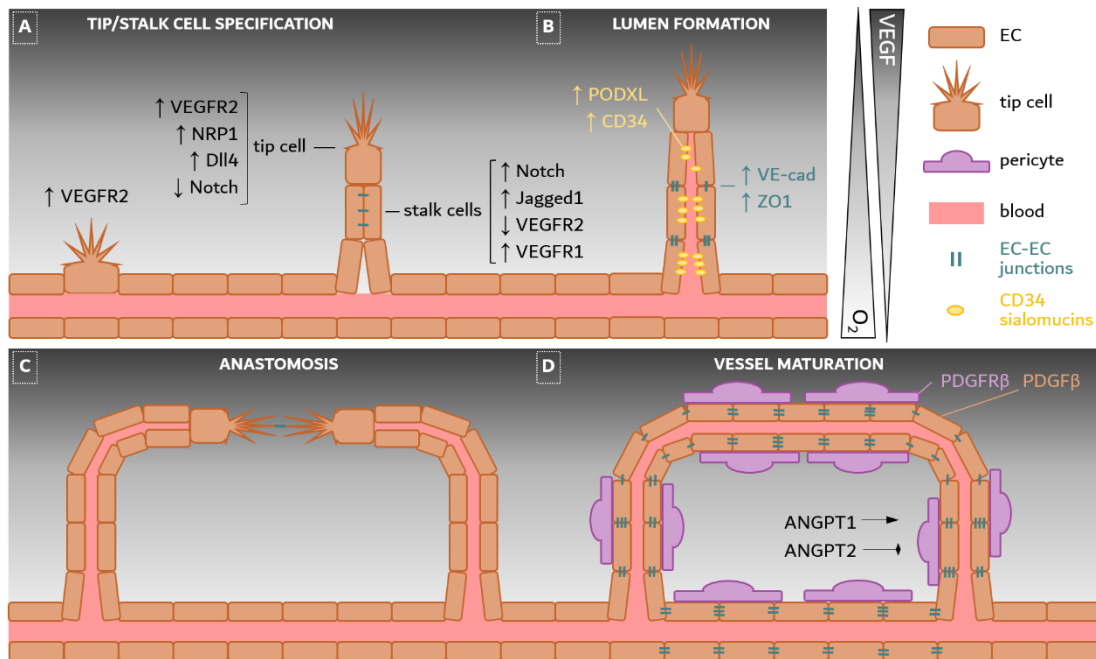
Figure 7. Stages of sprouting angiogenesis. **A** Hypoxia establishes a gradient of VEGF, which binds VEGFR2 on ECs to promote a tip cell phenotype. VEGFR2 signaling induces Dll4 expression on tip cells, which activates Notch signaling in neighboring highly proliferative stalk cells. The Notch pathway upregulates Jagged1, which represses Notch in tip cells to ensure differential VEGFR2/Notch signaling in tip vs stalk ECs. **B** Lumen formation is driven by negatively-charged CD34-sialomucins, which locate to EC cord contacts, causing electrostatic repulsion between ECs. EC junctions are pushed to a lateral position, reinforcing EC polarity. **C** Tip cells from different sprouts eventually contact with each other and initiate anastomosis, that is, the fusion of both sprouts into one vessel. **D** Vessel maturation requires the stabilization of the vessel wall with mural cells and strong EC junctions. ECs secrete PDGFβ to recruit PDGFRβ⁺ pericytes towards new vessels. ANGPT1/Tie2 signaling reinforces EC junctions and contributes to pericyte recruitment, while ANGPT2 antagonizes these effects.

Tip/Stalk EC Specification

The starting point of angiogenic sprouting is tip cell formation. Tip cells are specialized ECs located at the very end of vascular sprouts. They present a large number of filopodial extensions which guide the migration of tip cells and hence of the newly formed endothelial sprouts. The tip cell phenotype is induced upon binding of secreted VEGF-A to EC-bound VEGFR2. In fact, the gradient of VEGF-A along hypoxic tissues determines the direction of tip cell migration[208], meaning that hypoxia-induced VEGF

can direct the growth of new blood vessels towards severely hypoxic regions within a certain tissue. However, tip cells do not show an active proliferation. Instead, highly proliferative ECs located right after the tip cell in a vascular sprout, also known as stalk cells, are responsible for the actual elongation of the nascent blood vessel. As expected, stalk cell proliferation is also stimulated by VEGF[208]. The different phenotypes displayed by migratory tip ECs and proliferative stalk ECs are due to the acquisition of distinct gene expression profiles[208]. This suggest that there must be some regulatory mechanism implicated in EC specification.

Presumably, only ECs with the highest VEGFR2 signaling (due to higher exposure to VEGF and/or higher expression of VEGFR2) switch to a tip cell phenotype. VEGFR2 signaling in established tip cells upregulates the expression of delta-like ligand 4 (Dll4)[209], which binds the receptor Notch1 expressed in neighboring ECs. This interaction activates Notch signaling, which in turn restricts further tip cell formation and instead favors the stalk cell phenotype[210,211]. On the contrary, stalk cells have a strong expression of the Notch antagonist Jagged 1. Jagged 1 on stalk cells binds Notch receptors on tip cells, downregulating Notch signaling in the latter phenotype and so maintaining the tip cell phenotype[212].

Therefore, the patterned expression of Notch ligands in different ECs in response to VEGFR2 signaling will determine EC specification, with low Notch signaling promoting tip cell formation while high Notch signaling leads to a stalk cell phenotype. This is accompanied by differential VEGFR expression: VEGFR1 has been associated with stalk cell specification, but tip cells predominantly express VEGFR2 as well as its co-receptor neuropilin (NRP) 1[213,214]. Interestingly, NRP1 was reported to activate CDC42, which is essential for filopodia formation[215].

However, neither VEGFR/Notch signaling nor EC phenotype are static within a vascular sprout. In fact, the adoption of a tip or stalk cell phenotype has proved to be a highly dynamic process, where ECs move along the growing sprout competing for the tip cell position[213].

EC Migration and Sprout Elongation

Sprout elongation relies on the migration of tip cells that guide the growth of the new vessel and the simultaneous proliferation of adjacent stalk cells. The direction of migration and growth are not arbitrary; there are several attractive and repulsive signals that guide the direction of angiogenesis.

A prime requirement for effective sprout elongation is the interaction with extracellular matrix components. Stalk cell proliferation requires the disruption of EC intercellular contacts, meaning that the extracellular matrix is the only support of proliferating stalk cells. ECs anchor to the surrounding extracellular matrix through surface expression of various integrins that bind to extracellular laminins and fibronectin[216]. Adhesion to extracellular matrix through $\alpha_1\beta_1$- and $\alpha_2\beta_1$- integrins was shown to support stalk cell proliferation by activating the MAPK pathway[217]. Moreover, the retention of VEGF by fibronectin and heparan-sulfate is essential for the establishment of VEGF gradients and directional tip cell migration[218], which also depends on $\alpha_1\beta_1$- and $\alpha_2\beta_1$- integrin contacts[217]. Moreover, the interaction between α_5-integrin and fibronectin contributes to the adhesion of tip cell filopodia to the extracellular matrix during migration[218].

As previously mentioned, VEGF gradients are the primary cue to direct tip cell migration towards hypoxic areas[208]. Another way in which hypoxia can control tip cell migration is through the production of reactive oxygen species (ROS), which activate the mammalian sterile 20-like kinase 1 (MST1). In turn, MST1 induces the nuclear translocation of FOXO1, whose transcriptional activity promotes cell polarity and migration. MST1/FOXO1 activation proved essential for perpendicular vascular branching[219]. A similar role has been attributed to NRP1, which was found to be crucial for vessel sprout turning and perpendicular vascular expansion[220]. Some other proteins that have been shown to sustain EC migration are eNOS[221], angiomotin[222,223], and endophilin-A2[224].

On the contrary, some signals can repel EC migration and growth. For example, the binding of netrin-1 to the receptor uncoordinated (UNC)5B, expressed by tip cells, causes filopodial retraction and reduces tip cell migration[225,226]. Alternatively, UNC5B can be activated by Roundabout4

(Robo4), resulting in decreased VEGF-dependent intracellular signaling and decreased angiogenesis[227].

Notably, the collective migration and elongation of a nascent vascular sprout requires the precise coordination of all the ECs involved. Continual EC division necessarily disrupts all EC-EC contacts, which might lead to the loss of intercellular VEGFR and Notch regulation, with a concomitant loss of EC and sprout polarity. However, appropriate VEGFR and Notch signaling can be maintained during vessel growth thanks to asymmetric cell division, which generates daughter cells of different size and different content of pro-angiogenic signals, facilitating correct EC specification and polarity[228].

Lumen Formation

Vascular sprouts are not created with a proper tubular structure from the start. Initially, nascent vessels sprout as "cords" with no lumen, and then an actual lumen progressively opens from the pre-existing blood vessel towards the expanding vascular front in order to establish blood flow.

In early sprouts tight and adherens junctions are present all around the EC surface, keeping all ECs together in the cord structure. An indispensable step in lumen formation is the polarization of EC-EC contacts, which must be restricted to a lateral position and entirely disappear from the luminal side[229]. The main component of homotypic EC-EC adherens junctions is the vascular endothelial cadherin (VE-cadherin; also known as cadherin-5 or CD144), which was shown to recruit sialomucins CD34 and podocalyxin (PODXL) to EC adherens contacts prior to lumen formation[230]. These negatively charged glycoproteins generate electrostatic repulsions within the vessel cord, triggering the separation of adjacent ECs and the formation of an extracellular space between them[231], which eventually grows into a functional lumen. In parallel, VE-cadherin and zonula occludens-1 (ZO1), responsible for tight junctions, migrate to their final lateral position[229].

Correct lumen formation additionally requires the involvement of the cytoskeleton. CD34 and PODXL are linked to cytoskeletal F-actin via adaptor proteins such as moesin[230]. Formin-like 3, which is involved in the

assembly of actin filaments, was shown to locate at EC junctions too, where it polymerized F-actin to ensure F-actin availability. Reduced F-actin polymerization reportedly hindered lumen formation[232]. Moreover, the dedicator of cytokinesis 4 (DOCK4) was shown to induce cytoskeletal rearrangements that resulted in the formation of Cdc42-dependent abluminal lateral filopodia. This process appeared to be essential for effective lumen formation as well[233]. Interferon-induced transmembrane protein 1 (IFITM1) has been implicated in lumen formation too. Reportedly, IFITM1 interacts with occludin and is essential for the stability of EC junctions during lumen formation[234].

Another modulator of lumen formation is blood flow, whose pressure induces spherical invaginations (blebbing) of the luminal membrane of ECs, triggering the recruitment and contraction of myosin fibers necessary for lumen expansion[235].

Anastomosis

At some point, growing sprouts must fuse together to form new vascular circuits. The fusion process is known as anastomosis. Tip cell filopodia from different sprout make an initial contact, where new VE-cadherin adherens junctions are established in the shape of a ring. The membrane region inside this circle becomes an apical membrane, where PODXL is deposited. The lumen of the original sprout then extends through the tip cell to reach the newly created apical membrane. This results in the fusion of both sprouts through a short stretch of unicellular tube where the tip cells used to be. Subsequent cell rearrangements turn it into a normal multicellular tube structured vessel[236,237].

Vessel Maturation

Once the new vascular network is established, all the pro-migratory and proliferative features of tip and stalk cells must disappear. Instead, mature blood vessels are characterized by strong intercellular contacts and endothelial quiescence. A crucial part of vessel maturation is the coverage by mural cells such as pericytes, which stabilize blood vessels, consolidate the endothelial barrier, contribute to extracellular matrix and basement membrane deposition and decrease EC proliferation[238,239]. In fact, many of the signals involved in vessel maturation are correlated with pericyte

recruitment. For example, the platelet-derived growth factor β (PDGFβ), actively secreted by tip cells, binds PDGF receptor β (PDGFRβ) on the surface of pericytes and thereby recruits pericytes towards the nascent sprout[208,240].

Angiopoietin (ANGPT) signaling is the major signaling pathway in blood vessel maturation. ANGPT1 has been correlated with decreased vascular leakage and permeability[241,242]. It has been shown to reduce the phosphorylation-mediated internalization of cell junction proteins such as VE-cadherin and platelet endothelial cell adhesion molecule 1 (PECAM1, also known as CD31), therefore reinforcing intercellular contacts and vessel integrity[242]. Moreover, ANGPT1 stimulates the production of sphingosine-1-phosphate (S1P) by sphingosine kinase-1[243]. SP1 plays important roles in vascular maturation as well, increasing adherens junctions and mural cell recruitment[244,245], so it adds up to the stabilizing effect of ANGPT1.

ANGPT1 signals through the endothelial receptor Tie2, although it triggers different responses depending on the cellular context. In mobile ECs, ANGPT1 translocates Tie-2 to cell-matrix contacts and induces EC polarization and migration. However, in contacting ECs, ANGPT1-activated Tie-2 moves to intercellular contacts and interacts in *trans* with Tie2 expressed on neighboring ECs, leading to the *trans*-activation of a different signaling cascade. In this case, ANGPT1/Tie2 enhance cell-cell adhesion and survival[246,247]. When located at cell-cell contacts, Tie2 activity can be regulated by the vascular endothelial-protein tyrosine phosphatase (VE-PTP), which dephosphorylates and hence inhibits Tie2[246,248]. Moreover, Tie2 signaling can be repressed by its antagonist ligand ANGPT2[249].

Vascular Remodeling

In order to optimize blood flow, new vascular networks are thoroughly remodeled, increasing the lumen diameter of highly perfused blood vessels, and decreasing or even eliminating ("pruning") poorly perfused vessels[239].

Not surprisingly, vascular remodeling is largely regulated by fluid shear stress exerted by blood flow on the vessel wall. Shear stress induces several morphological changes in ECs, like the redistribution of focal adhesions and the alignment of the cytoskeleton in the direction of blood flow[250,251]. It can also trigger the activation of several signaling pathways, like VEGFR2, PI3K, ERK or Akt[252–254]. All these responses are initiated by EC-EC and EC-extracellular matrix adhesion complexes, which behave as cellular sensors and signal transducers of mechanical tension. VE-cadherin and PECAM1 are the main mechanosensory components of intercellular contacts[252,253], while laminin α5 and integrin β1 are important mechanosensory complex in extracellular matrix adhesions[255].

In any case, ECs seem to morphologically adapt to high blood flow, which also contributes to the activation of pro-survival signaling. On the contrary, low and fluctuating blood flow prompts vessel regression[256], which in this context follows very similar steps to anastomosis, only in reverse: morphological rearrangement, lumen constriction and EC migration away from the regressing vessel and into adjacent, higher-flow blood vessels[257].

Due to the importance of extracellular matrix in the structural and functional support of blood vessels, matrix alterations can induce vessel remodeling. For example, the activation of MMP1, MMP9 and MMP10 results in collagen proteolysis, which subsequently triggers vessel regression[258,259]. Extracellular matrix remodeling by MMPs can also modulate vessel morphology. For instance, overexpression of MMP9 was shown to increase vessel diameter but reduce the thickness of the vessel wall[260]. The role of MMPs in vascular remodeling has proved particularly relevant in a number of cardiovascular diseases, such as atherosclerosis or hypertension[261].

In addition, Notch signaling has proved vital for this aspect of vascular homeostasis as well, in this case complemented by Wnt signaling. Inhibition of Dll4/Notch signaling was shown to hinder vessel pruning. Conversely, KO of the Notch-regulated ankyrin repeat protein (Nrarp), a feedback suppressor of Notch intracellular signaling, resulted in excessive vessel regression[262]. Reportedly, Nrarp acts as a common link between

Notch and Wnt/β-catenin pathways in ECs. In particular, Notch-induced Nrarp downregulates Notch signaling while upregulating Wnt/β-catenin signaling, with important implications in vessel remodeling. In that line, β-catenin deletion produced excessive vessel regression as well[263]. Moreover, the inhibition of Wnt non-canonical signaling can increase vessel pruning too, reducing EC survival and proliferation[264]. Therefore, the role of Wnt in vessel remodeling is mediated by both β-catenin-dependent and -independent pathways.

TARGETING ANGIOGENESIS IN CANCER

Antiangiogenesis

Angiogenesis was first proposed as a potential therapeutic target in cancer treatment 50 years ago, when Dr Judah Folkman (sometimes referred to as "The Father of Angiogenesis") published his then revolutionary hypothesis that neovascularization was indispensable for the growth of solid tumors[265]. Later research certainly proved him right; angiogenesis is now considered a hallmark of cancer[3], and it has been on the focus of cancer research for decades.

The signaling pathways detailed in the previous section provide many potentially druggable targets for cancer therapy, though most studies have focused on inhibiting the VEGF pathway. The reason is that VEGF signaling is reportedly upregulated in most human cancers, and it is correlated with increased microvessel density and poor prognosis in patients[266]. So far, over ten different drugs that interfere with VEGF signaling have been approved by the FDA and EMA for the clinical treatment of a number of cancers[266]. Most of them (sorafenib, sunitinib, etc.) are actually unspecific tyrosine kinase inhibitors (TKI) whose multiple targets include VEGFR. A few drugs, however, are specific repressors of VEGF signaling. Bevacizumab and ramucirumab are monoclonal antibodies that target VEGF-A and VEGFR2, respectively, and hence prevent VEGF-VEGFR binding[266]. In addition, aflibercept is a fusion protein that contains VEGFR extracellular domains and works as a VEGF trap, preventing VEGF binding to actual VEGFR[267].

INTRODUCTION

Anti-VEGF therapies (hereafter referred to as antiangiogenic therapies) created a great expectation and hope in the 1990s and 2000s, but their actual curative effect in cancer was overestimated. First of all, a few cancer types, like pancreatic and prostate, are completely non-responsive to anti-VEGF drugs. Secondly, even in responsive cancer types, antiangiogenic therapy merely delays tumor growth, and rarely promotes tumor regression. In consequence, although it is true that antiangiogenic drugs can significantly increase the survival of cancer patients, this increase is usually in the order of months or even weeks[205,266]. The relative failure of antiangiogenic therapies is due to several reasons, as discussed below.

To begin with, the major argument in favor of antiangiogenesis as a concept is that the disruption of angiogenesis can decrease tumor perfusion, leading to oxygen and nutrient starvation and tumor cell death by necrosis. In addition, this effect is supposed to affect tumor tissues exclusively, since normal adult vasculature is quiescent so it will not suffer the consequences of VEGF blockade. Even more, the initial belief was that antiangiogenic therapies would not encounter any kind of resistance, since they target "healthy" ECs instead of aberrant tumor cells. With this information, one would certainly believe that antiangiogenesis meets all the criteria for an ideal therapy. Indeed, these hypotheses were correct to some extent, accounting for the short-term benefits of antiangiogenic therapies.

Unfortunately, low tumor perfusion goes hand in hand with tumor hypoxia. As previously discussed, hypoxia can trigger tumor malignancy in a variety of ways, like enhanced invasion, metabolic reprogramming and resistance to radio- and chemotherapy[185]. More importantly, hypoxia can promote angiogenesis through the upregulation of several genes other than VEGF, like fibroblast growth factors (FGF)[268] or ANGPT2[269], which means that there can be intrinsic and acquired resistance to anti-VEGF drugs. In addition, hypoxia can stimulate the recruitment of endothelial progenitor cells from the bone marrow via the upregulation of stromal cell–derived factor-1 (SDF1), supporting *de novo* vasculogenesis within tumors[270,271]. In summary, antiangiogenesis-induced hypoxia leads to acquired resistance to antiangiogenic therapy, malignant transformation and relapse.

Furthermore, tumor neovascularization is far more complex than just angiogenesis. Alternative forms of neovascularization, like vessel co-option and vasculogenic mimicry, are often VEGF-independent, so they represent another source of intrinsic and acquired resistance to antiangiogenic therapy[272,273]. Vessel co-option describes the ability of tumor cells to migrate towards and grow along pre-existing blood vessels in order to obtain nutrients and oxygen. This way, tumor growth does not strictly require the formation of new blood vessels, meaning that it is independent of angiogenesis and therefore is not susceptible to antiangiogenic therapies[274]. Vasculogenic mimicry will be discussed in detail in later sections.

Tumor Vessel Normalization

In response to the limitations of anti-angiogenic therapy, a new approach to angiogenic targeting has been gaining attention in recent years: normalizing tumor blood vessels in order to minimize tumor hypoxia and maximize drug delivery[238].

The basis for this approach is the observation that tumor vasculature tends to be morphologically and functionally abnormal, due to excessive pro-angiogenic signaling. ECs in tumor vessels do not have proper cell polarity nor stable intercellular junctions. Moreover, continual angiogenesis leads to pericyte detachment. All these issues compromise the integrity of the vessel wall and contribute to vessel permeability and leakiness. In turn, leakiness can reduce blood flow and increase interstitial fluid pressure. Fluid and solid pressure within the tumor tissue subsequently compress structurally deficient blood vessels, further jeopardizing blood flow. Of course, flow alterations at a certain vessel will affect all downstream capillaries, meaning that poor blood flow can affect large areas within a tumor. Altogether, abnormal vasculature results in poor perfusion, high acidity, inflammation and hypoxia, a tumor microenvironment that will definitely support tumor malignancy. Adding in that faulty tumor vessels cannot offer much resistance to tumor cell intravasation, we could conclude that abnormal tumor vasculature is an unquestionable gateway to metastasis[238,275].

INTRODUCTION

In this unfavorable scenario, the idea of "normalizing" tumor blood vessels to try and make them more similar to functional, physiological blood vessels raises as a powerful strategy to curb metastatic spread.

In fact, the first notions regarding tumor vessel normalization as a way to prevent tumor cell dissemination and metastasis emerged a long time ago, even before Folkman's initial hypothesis of antiangiogenesis. In the early 1970s, the group of Dr Kurt Hellmann reported that the drug razoxane completely inhibited the occurrence of metastasis in mice, and proposed the normalization of tumor vasculature as the mechanism of action[276,277]. Indeed, they observed a different morphology of the tumor vascular networks, a more defined structure of blood vessels, a decrease in tumor hemorrhage and a complete eradication of circulating tumor cells after treatment with razoxane[276]. Although studies with razoxane progressed and gave rise to dexrazoxane, an FDA- and EMA-approved cardioprotective drug[278], the initial reports regarding tumor vascularization were largely ignored and forgotten for decades.

However, the idea of vascular normalization reappeared in 2001 thanks to Dr Rakesh Jain[279]. He noticed that in some preclinical studies VEGF-targeted drugs improved the efficacy of irradiation and chemotherapy, and he claimed that this effect must be due to an increase in drug delivery and tumor oxygenation. Therefore, he suggested that, at certain doses and times, anti-VEGF drugs provide a "window of normalization" during which the benefit of conventional therapies is enhanced. A few years later, his research group published a few articles showing how DC101, an antibody against VEGFR2, could normalize tumor vasculature (improved vessel architecture and increased coverage by mural cells), increasing tumor oxygenation and enhancing the perfusion of large molecules, which in turn might improve radiotherapy and chemotherapeutic delivery[280,281]. Furthermore, a few clinical studies proved a correlation between tumor vessel normalization induced by anti-VEGF drugs and increased survival in glioblastoma patients[282–284].

Apart from VEGF, preclinical research has found a few other pathways that can potentially regulate vascular normalization.

The ANGPT pathway is attracting more and more interest in this field. Due to their opposed effect on Tie2, inhibiting ANGPT1 or ANGPT2 can render very different results. As previously explained, ANGPT1 is correlated with vessel maturation, while ANGPT2 is usually an antagonist of ANGPT1/Tie2. In tumor models, ANGPT2 inhibition was reported to reinforce VE-cadherin- and PECAM1-mediated EC junctions in tumor vessels, increase pericyte coverage and decrease angiogenic sprouting, overall reducing tumor growth. However, additional inhibition of ANGPT1 abrogated the normalizing effect of the ANGPT2 inhibitor, suggesting that ANGPT2 inhibition can induce tumor vessel normalization by potentiating ANGPT1 signaling[285]. In that line, an antibody that inhibits ANGPT2 and simultaneously activates Tie2 was shown to induce tumor vessel normalization, improve drug delivery and reduce tumor growth and metastasis[286]. Moreover, the VE-PTP inhibitor AKB-9778, by preventing Tie2 dephosphorylation and so triggering basal activation of Tie2, could also promote tumor vessel normalization. It delayed tumor growth, decreased tumor cell intravasation and improved the effect of radiotherapy[287]. Overexpression of ANGPT2 is a potential mechanism of resistance to anti-VEGF drugs, but co-targeting the VEGF pathway and ANGPT2 improved tumor vessel normalization, delayed tumor growth and increased survival, compared to individual treatments[288,289].

On the other hand, Tie1 is an endothelial receptor analogous to Tie2 but to which ANGPTs cannot bind. However, Tie1 has been shown to dimerize with Tie2 and modulate its activity[290]. Tie1 EC-specific KO normalized tumor vasculature, increasing tumor vessel coverage by mural cells as well as tumor perfusion, and reduced circulating tumor cells and metastasis[291].

As previously mentioned, NRP can act as co-receptors of VEGFR for VEGF binding. Apart from this, NRP can also be co-receptors of plexins for binding to semaphorins (Sema)[292]. In particular, Sema-3A, a ligand of NRP1, has been implicated in tumor vascular normalization, increasing pericyte coverage and decreasing tumor hypoxia[293]. However, NRP1 does not seem to be strictly necessary for Sema-3A-mediated normalization[294].

INTRODUCTION

Seeing as pericyte coverage is a clear determinant of vessel normalization in most studies, it is not surprising to find a role for PDGFβ in this process. Indeed, Wnt canonical signaling through β-catenin was reported to normalize tumor vasculature by upregulating PDGFβ[295]. Wnt/β-catenin concomitantly activated Notch signaling, which was also implicated in vascular normalization in independent studies[296].

Interfering with the hypoxia response should be expected to affect tumor vasculature as well. Haplodeficiency of PHD2 leads to increased HIF stabilization and thus a cellular "pre-adaptation" to hypoxia, even in non-hypoxic conditions. Surprisingly, this situation significantly reduced the metastatic burden in PHD2-haplodeficient mice. High HIF2α levels in ECs triggered a shift in gene expression, upregulating genes like VE-cadherin and VEGFR1 that favor a more quiescent phenotype. Therefore, haplodeficiency of PHD2 in ECs promoted vascular normalization, increased tumor perfusion, oxygenation, and pericyte coverage of tumor blood vessels, and prevented tumor cell intravasation and metastasis[297].

A much more unfamiliar protein with the ability to regulate vascular normalization is hornerin. Hornerin is a S100 fused-type protein, mostly studied in epidermal contexts. However, hornerin was found to be overexpressed in ECs in pancreatic tumors, where hornerin knockdown reduced tumor vessel tortuosity and leakiness, and increased tumor oxygenation. Furthermore, hornerin expression was independent of VEGF, and VEGFR inhibition combined with hornerin knockdown resulted in enhanced therapeutic effect[298].

In conclusion, the last few decades have seen a growing body of evidence supporting the potential of tumor vessel normalization in cancer treatment. A wide variety of signaling pathways and molecules have been associated with vascular normalization, but in all cases the normalization of tumor vessels has been correlated with reduced tumor growth and metastasis, and improved efficacy of additional therapies for the control of primary tumors.

VASCULOGENIC MIMICRY

Unlike angiogenesis, vasculogenic mimicry (VM), also known as vascular mimicry, is a form of tumor neovascularization that does not involve ECs. Instead, VM channels are lined up by the tumor cells themselves, which is why they are not considered true blood vessels. However, VM pseudovessels are capable of carrying blood and blood cells, and therefore they can supply the tumor with nutrients and oxygen independently of endothelial angiogenesis[299].

VM was first described by Maniotis et al in 1999[300], when they were studying tumor microcirculation using periodic acid-Schiff (PAS) stainings. This procedure can reveal the extracellular matrix depositions that make up the basement membrane around blood capillaries. Maniotis et al reported the presence of matrix-rich networks in sections of human uveal and cutaneous melanoma. These PAS[+] networks were hollow in some places and even contained red blood cells, although ECs were not detected (the channels were negative for PECAM1 and CD34, among others). Therefore, the channels appeared to be lined by melanoma cells, which prompted the authors to grow several CM and UM cell lines in type I collagen or matrigel 3D cultures. They found that highly invasive, but not poorly invasive melanoma cell lines could recapitulate matrix-rich network formation, and that the resulting structures could distribute microinjected dyes. This suggested that those channels could actually distribute blood *in vivo* without the assistance of any other cell type. Due to the similarities with *de novo* vasculogenesis, the formation of tumor cell-lined channels was termed vasculogenic mimicry.

This was only the first of a series of reports that the group of Dr Mary J. C. Hendrix published during the 2000s unravelling the molecular basis of vasculogenic mimicry and reshaping the paradigm of tumor vascularization. Although the concept of VM faced some degree of controversy and opposition at first[301], other research groups soon reported the presence of VM in many tumor types, like breast cancer, Ewing sarcoma, multiple myeloma, hepatocellular carcinoma and glioblastoma[302–306], among others. Remarkably, VM is correlated with metastatic spread

and shorter survival in cancer patients, constituting an independent predictor of poor prognosis[307].

An early approach to understanding the causes of VM involved microarrays of gene expression comparing VM$^+$ highly aggressive with VM$^-$ poorly aggressive melanoma cell lines. The results showed that VM$^+$ tumor cells expressed a variety of genes typical of epithelial, endothelial and hematopoietic cell types[300,308]. This suggested that the ability to engage in VM is determined by the reversion to a pluripotent state.

One of the first genes to be associated with the VM phenotype was VE-cadherin[308]. In spite of being a classic marker of endothelial cells, VE-cadherin aberrant expression was found in several VM$^+$ melanoma cell lines, where its downregulation interfered with VM formation. Following this report, VE-cadherin was repeatedly detected in a variety of VM$^+$ tumors and tumor cell lines, always playing a crucial role in the acquisition of the VM phenotype[305,309–312].

Several different proteins and pathways have been shown to induce VE-cadherin expression in tumor cells, like zinc finger E-box binding homeobox 1 (ZEB1)[309], human epidermal growth factor receptor 2 (HER2)[310] or Nodal[313]. The transcription factors Twist1, HIF1α, HIF2α and SP1 have been directly implicated in VE-cadherin expression during VM. All four have been reported to bind VE-cadherin promoter and upregulate its transcription[305,311,314]. HIFs and Twist1 are activated by hypoxia[315], while SP1 activity seemed to be induced by insulin-like growth factor–binding protein 2 (IGFBP2), which is frequently upregulated in cancer. In melanoma, VE-cadherin expression has been associated with ABCB5$^+$ and CD133$^+$ cancer stem cell subpopulations, in both cases contributing to VM[316–318]. In turn, the metalloproteinase ADAMTS1 has been shown to promote stemness and VE-cadherin expression in various melanoma cell lines[319].

Notably, the role of VE-cadherin in VM formation is more complicated than mere expression. Our research group has found that the phosphorylation of VE-cadherin on the residue Y658 can be crucial for VM.

In an endothelial context, VE-cadherin can be phosphorylated in a number of tyrosines and serines in order to regulate its location and stability. When VE-cadherin is phosphorylated on Y658, serine (S) 665 or Y685, it is internalized and marked for degradation, resulting in a destabilization of EC adherens junctions[320,321]. This effect is necessary for some physiological events, such as vessel growth and leukocyte transmigration[322]. However, excessive internalization of VE-cadherin can disrupt the endothelial cell barrier (as seen in tumor abnormal angiogenesis), so VE-cadherin phosphorylation must be carefully regulated. Normally, VE-cadherin is only phosphorylated upon specific stimuli, like VEGF, and then it is dephosphorylated by phosphatases like VE-PTP[323].

However, in human VM+ UM and CM cell lines, VE-cadherin is constitutively phosphorylated on Y658 by FAK[324], which appeared to be permanently active too[324,325]. As mentioned in previous sections, FAK has been identified as a downstream effector of the GNAQ/11 signaling pathway[74], which could explain FAK hyperactivity in highly aggressive melanoma cell lines. In ECs, FAK has been shown to phosphorylate VE-cadherin on Y658 in response to VEGF during tumor angiogenesis, promoting vessel permeability, tumor cell intravasation and metastasis[326]. In VM+ cell lines, phospho-Y658 (pY658)-VE-cadherin was internalized but it did not undergo ubiquitination and degradation. Instead, it translocated to the nucleus in complex with p120-catenin, where they sequestered the transcriptional repressor kaiso, resulting in the upregulation of kaiso target genes. The inhibition of FAK or the knockdown of kaiso target genes abrogated tube formation on matrigel, indicating that pY658-VE-cadherin and its effect on kaiso are important signaling mediators of VM[324] (Figure 8, blue). In a preliminary report, our group showed that PARP inhibition increased VE-cadherin expression in ECs, but it could reduce pY658-VE-cadherin in a mouse melanoma cell line, which could have a relevant implication in VM signaling[327].

In addition, Delgado-Bellido et al showed that VE-PTP is co-expressed with VE-cadherin during VM. In particular, VE-PTP seemed to contribute to VM by protecting VE-cadherin from degradation. VE-PTP knockdown resulted in increased phosphorylation of p120, destabilization of p120—

VE-cadherin complexes, autophagic degradation of VE-cadherin and hence reduced tube formation on matrigel[328].

pY658 is not the only phosphorylation of VE-cadherin that has proved relevant in VM. Sphingosine-1-phosphate receptor 1 (S1PR1) can induce the phosphorylation of VE-cadherin on Y731[329]. Unlike Y658 or Y685, whose phosphorylation occurs in response to certain stimuli, Y731 of VE-cadherin is constitutively phosphorylated, and it is a dephosphorylation of this residue what can trigger VE-cadherin internalization[330]. Therefore, S1PR1-induced phosphorylation of Y731-VE-cadherin reduced VM formation in breast cancer cells[329].

Another protein which has been associated with VM is the ephrin type-A receptor 2 (EphA2), also known as epithelial cell kinase (Eck), which was found in highly aggressive but not poorly aggressive melanoma cells[300]. EphA2 was constitutively phosphorylated on tyrosine residues in VM+ cells, and EphA2 knockdown hindered VM formation[331].

Apart from its role in the phosphorylation of VE-cadherin, FAK can promote VM by increasing ERK1/2 signaling, which in turn enhances the activity of the extracellular matrix proteases urokinase and MMP14[325]. MMP14 can also be activated by PI3K[332]. MMP14 then activates MMP2, which subsequently cleaves the basement membrane component laminin 5γ2 to produce the pro-migratory fragments γ2' and γ2x. Moreover, MMP2, MMP14 and laminin 5γ2 are upregulated in highly aggressive VM+ melanoma, compared to poorly aggressive VM- melanoma[333]. In summary, VM is enabled via the promotion of extracellular matrix degradation and remodeling (Figure 8, red-pink). On the contrary, interfering with this pathway using FAK or PI3K inhibitors could disrupt VM *in vitro*[325,332]. Moreover, extracellular matrix composition and architecture can affect VM. Collagen I was shown to hinder, while the non-collagenous 11-domain of collagen XVI seemed to favor VEGFR-mediated VM formation *in vitro*[334,335]. In addition, high-density collagen matrix promotes β1-integrin upregulation, which triggers a pro-migratory and pro-VM transcriptional response[336].

Similarly, hypoxia can promote VM independently of HIF-mediated upregulation of VE-cadherin. For example, HIF1α can also upregulate

lysyl oxidase like 2 (LOXL2), another extracellular matrix remodeler which reportedly favored VM[337]. BNIP3, a well-known target of HIF1, could enhance VM by modulating the actin cytoskeleton. Notably, BNIP3 knockdown abrogated melanoma tube formation on matrigel despite increasing the activation of FAK[338].

Notch has also been implicated in VM (Figure 8, yellow). In particular, Notch4 was reported to induce the expression of the transforming growth factor (TGF) β family member Nodal. As previously mentioned, Nodal can increase VE-cadherin expression, but blocking Notch4 or Nodal reduces VE-cadherin and VM formation[339].

Wnt/β-catenin signaling can promote VM as well (Figure 8, green). The expression of Wnt3a was correlated with VM in colon cancer patients. *In vitro*, Wnt3a upregulated VE-cadherin and VEGFR2, and increased tube formation by colon cancer cells, while Wnt antagonist dickkopf-1 reverted these effects[340].

Interestingly, VM has been reported to occur without VE-cadherin. Since the initial reports made by Hendrix's research group, VM is usually detected *in vivo* as PAS$^+$/PECAM1$^-$ or PAS$^+$/CD34$^-$ channels. However, Dunleavey et al showed that subpopulations of mouse melanoma cells could spontaneously express PECAM1 and promote VM formation *in vitro* and *in vivo*, independently of VE-cadherin and VEGFR[341].

A recent report by Thijssen et al revealed that, similarly to endothelial angiogenesis, VM does not rely exclusively on tumor cells. They demonstrated that pericytes can associate to VM pseudovessels in human melanoma samples and in human melanoma cell line-derived xenografts. Resembling endothelial vessels, pericyte recruitment to VM channels was mediated by tumor cell secretion of PDGFβ. The presence of pericytes increased melanoma sprouting and pseudovessel network stability *in vitro*[342]. Therefore, pericytes may play an important role in VM-dependent tumor vascularization.

Several lncRNAs have been shown to influence VM. The expression of MALAT1 correlated with VM in gastric cancer patients. Reportedly, MALAT1 could upregulate VE-cadherin and promote the activity of FAK,

ERK, MMP14 and MMP2[343]. In non-small cell lung cancer cell lines, MALAT1 was directly upregulated by estrogen receptor β, and it enhanced NEDD9-mediated VM formation *in vitro*[344]. A recent publication showed that the lncRNA TANAR affected VM in clear cell renal cell carcinoma. Androgen receptor directly induced the expression of TANAR, which subsequently stabilized Twist1 mRNA, increasing Twist1 expression and hence VM formation *in vitro*[345]. The lncRNA actin filament-associated protein 1-antisense RNA 1 (AFAP1-AS1) could also promote Twist1-dependent VM formation in osteosarcoma cell lines[346].
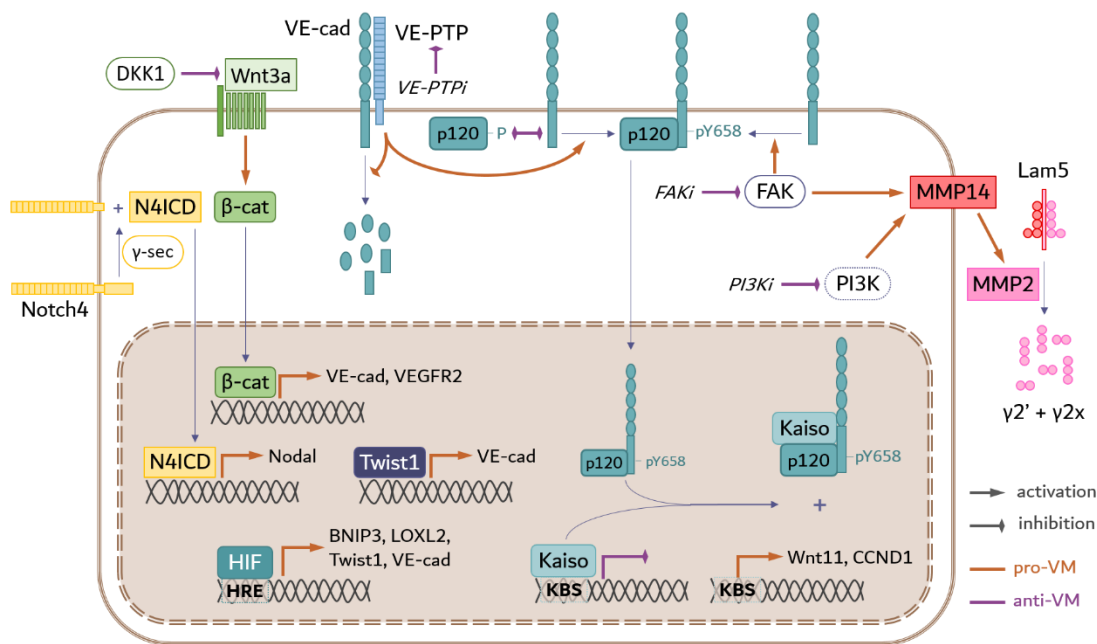
Figure 8. Molecular mechanisms underlying the VM phenotype. A number of pathways can upregulate VE-cadherin, whose expression is instrumental in VM. Among these, HIF1/2 and Twist1 can directly induce VE-cadherin transcription. Notch4 can favor VE-cadherin expression and VM via Nodal. Wnt/β-catenin signaling can increase VE-cadherin and VM as well. VE-PTP can promote VM by dephosphorylating p120, hence stabilizing VE-cadherin+p120 complexes and preventing VE-cadherin degradation. VE-cadherin can be phosphorylated by FAK on Y658, triggering VE-cadherin+p120 translocation to the nucleus, where they sequester the transcriptional repressor kaiso therefore inducing the expression of kaiso target genes. FAK, as well as PI3K, can further contribute to VM by increasing MMP14 activation, which leads to MMP2-mediated extracellular matrix remodeling. β-cat: β-catenin; γ-sec: γ-secretase; CCND1: cyclin D1; DKK1: dickkopf-1; N4ICD: Notch4 intracellular domain; VE-cad: VE-cadherin.

VM represents an obstacle in cancer treatment. As discussed above, VM is a marker of poor prognosis in patients[307]. Furthermore, it often arises in response to antiangiogenic therapies, leading to resistance and relapse[273]. The previous paragraphs have mentioned a few potential targets with promising results in preclinical studies, such as FAK inhibition[324,325]. However, only one drug with the specific purpose of targeting VM development has reached clinical trials in humans so far. It is the case of CVM-1118, a chemical compound obtained from plant-derived phenyl-quinoline. CVM-1118 produced a potent inhibition of VM *in vitro*, mediated by a downregulation of Nodal, Notch4 and VEGFA, among others[347]. In 2018, CVM-1118 entered two different phase 2 clinical trials for the treatment of hepatocellular carcinoma (NCT03582618) and neuroendocrine tumors (NCT03600233), with estimated completion in 2021 and 2022.

In conclusion, although preclinical studies are slowly unveiling the molecular mechanism underlying VM, the clinical application of the proposed targets still remains unknown. Hopefully, the upcoming years will see new useful targets and positive results in the control of VM in different cancer types.

AIMS

AIMS

VM was first described based on the histologic observation of samples from UM and CM patients. In subsequent years, this neovascularization mechanism was extensively characterized in these tumor types, turning them into the best known model of VM. Certainly, VM provides a basis for the rapid and high metastatic incidence that characterizes UM. The discouraging mortality rates of UM in its metastatic presentation and the high resistance to current therapies highlight the urgency to find new therapeutic options.

PARPi have consolidated as a safe and effective therapy in the treatment of HR-deficient tumors. However, multiple investigations have described a role for PARP1 in other aspects of tumor biology, such as the modulation of cell death pathways and the regulation of transcriptional networks. For instance, PARP1 can regulate the hypoxia response, which in turn is the main trigger of tumor neovascularization.

Therefore, the **general aim** of the present thesis is to evaluate the effect of PARP inhibitors and hypoxia on VM development in melanoma. With this purpose, the have pursued the following **specific aims**:

1. Examine the impact of PARP inhibition and hypoxia on melanoma VM signaling, specifically the phosphorylation of VE-cadherin.
2. Analyze the influence of PARP inhibition and hypoxia on the modulation of global gene expression in VM⁺ melanoma cells, using a whole transcriptomic approach and focusing our attention on the lncRNA expression landscape and on vasculogenic signaling.
3. Assess the effect of PARP inhibition and hypoxia on *in vitro* VM⁺ melanoma tube formation.
4. Evaluate the impact of the treatment with PARPi on *in vivo* VM formation, tumor progression and metastasis in VM⁺ and VM⁻ human UM xenografts.

MATERIALS
&
METHODS

MATERIALS AND METHODS

Cell culture

As a model of human UM we used the cell lines Mum2B and Mum2C. They are syngeneic cell lines obtained from a liver metastasis of the same patient. However, Mum2B are characterized as highly aggressive and VM$^+$, while Mum2C are poorly aggressive and VM$^-$. These cell lines were kindly provided by Dr Juan Carlos Rodríguez Manzaneque (Centro Pfizer-Universidad de Granada- Junta de Andalucía de Genómica e Investigación Oncológica). They were cultured in RPMI 1640 medium supplemented with 2 mM of L-glutamine, 10% fetal bovine serum and 1% penicillin/streptomycin (everything from Gibco).

As models of human CM we tested the cell lines A375, C8161 and G361. A375 (ATCC CRL-1619) were cultured in low-glucose (1.5 g/L) DMEM medium supplemented with 4 mM L-glutamine, 1% minimum essential medium non-essential amino acids, 10% fetal bovine serum and 1% penicillin/streptomycin (everything from Gibco). G361 (ATCC CRL-1424) were cultured in high-glucose (4.5 g/L) DMEM medium supplemented with 10% fetal bovine serum and 1% penicillin/streptomycin (everything from Gibco). C8161, originally obtained from a liver metastasis of a CM patient and kindly provided by Dr Benilde Jiménez Cuenca (Instituto de Investigaciones Biomédicas CSIC-UAM), were cultured in RPMI 1640 medium supplemented with 2 mM of L-glutamine, 10% fetal bovine serum and 1% penicillin/streptomycin (everything from Gibco).

The cell line HEK293T (ATCC CRL-3216), that we used as packaging cells during lentiviral production, was cultured in low-glucose (1.5 g/L) DMEM medium supplemented with 4 mM of L-glutamine, 1% minimum essential medium non-essential amino acids,10% fetal bovine serum and 1% penicillin/streptomycin (everything from Gibco).

Human brain vascular pericytes (ScienCell, USA) were cultured in pericyte medium supplemented with 1% pericyte growth supplement, 2% fetal bovine serum and 1% penicillin/streptomycin (everything from ScienCell, USA).

For co-culture experiments, Mum2B and pericytes were counted independently and mixed at a proportion of 20:1 (Mum2B: pericytes).

All cell lines were kept in a cell incubator at 37°C and 5% CO_2. When hypoxic conditions where required, cells were placed in a sealed hypoxic workstation (InvivO$_2$ 200, Ruskinn, UK) with an atmosphere of 1% O_2 and 5% CO_2, at 37°C. Unless stated otherwise, hypoxic incubation took place for 24 hours. In short-term hypoxia experiments, cells spent the first 20 hours in normoxia and were only incubated in hypoxia during the last 4 hours of the experiment.

All cell lines were regularly passaged, applying a trypsinization step with trypsin/EDTA 0.25% (Gibco). All cell lines were periodically analyzed to rule out mycoplasmal contamination.

PARP inhibitors

Two different PARPi were used during the course of the present thesis. For *in vitro* experiments, olaparib (Selleckchem), also known as AZD2281 and commercialized as lynparza for clinical applications, was used at 5 μM. BMN673 (Selleckchem), also known as talazoparib and commercialized as talzenna for clinical applications, was used at 1 μM. *In vitro* treatment with PARPi always had a duration of 24 hours. Dimethyl sulfoxide (DMSO), which is the diluent of both PARPi, was used as a negative control.

For *in vivo* experiments, olaparib was purchased from Quimigen, dissolved in minimal necessary DMSO, according to the manufacturer's instructions, and further diluted in 10% (2-hydroxypropyl)-β-cyclodextrin (Sigma Aldrich) in phosphate-buffered saline (PBS). The same vehicle solution of DMSO + 10% (2-hydroxypropyl)-β-cyclodextrin in PBS was used as negative control for *in vivo* treatments. Olaparib was used at a dose of 50 mg/kg, and treatments took place three times a week for three weeks.

Small interfering RNA (siRNA)-mediated knockdown

For PARP1 and HIF1α knockdown experiments, we used siRNA purchased from Sigma Aldrich. The sequences and concentrations are

detailed in Table 3. Appropriate siRNA was transfected using the transfection reagent jetPRIME (Polyplus, USA).

120,000 cells were seeded on each well of a 6-well plate and incubated overnight. The transfection mix was then prepared according to the instructions provided by the manufacturer: for every well in a 6-well plate 200 µL of jetPRIME buffer + siRNA + 4 µL of jetPRIME reagent. After 15 min of incubation at room temperature, the transfection mix was added drop by drop to the cell cultures with fresh growth medium. Growth medium was replaced the following day and the cells were incubated in normoxia or hypoxia for another 24 hours.

Target gene		Nucleotide sequence	Concentration (nM)
PARP1	sense	5'-GAAGAUGGUGGACCCGGAG[dT]-3'	75
	antisense	5'-CUCCGGGUCCACCAUCUUC[dT]-3'	
HIF1α	sense	5'-CUGAUGACCAGCAACUUGA[dT]-3'	50
	antisense	5'-UCAAGUUGCUGGUCAUCAG[dT]-3'	
sima	sense	5'-CCUACAUCCCGAUCGAUGAUG[dT]-3'	75
	antisense	5'-CAUCAUCGAUCGGGAUGUAGG[dT]-3'	

Table 3. siRNA used for knockdown experiments. Sima, a gene from *Drosophila melanogaster*, was used as a negative control. All siRNA were purchased from Sigma Aldrich.

Western blot

In order to obtain protein extracts and assess protein expression, 200,000 cells were seeded on each well of a 6-well plate and incubated overnight. Cells were then treated with DMSO or PARPi and incubated in normoxia or hypoxia. After 24h, cell cultures were washed with cold PBS and scraped in 65 µL of TR3 lysis buffer (3% sodium dodecyl sulfate [SDS], 10% glycerol, 10 mM Na_2HPO_4). Cells were then subjected to sonication (Vibra-Cell VC375, Sonics & Materials, USA) for 10 seconds at power output 5 to complete cell lysis.

The protein concentration of our extracts was determined performing the Lowry protein assay with the commercial kit DC protein assay (BioRad), following the instructions provided by the manufacturer. Briefly, 5 μL of each protein extract (and of bovine serum albumin at several known concentrations, as a standard control) were mixed with 100 μL A+S reagent mix, followed by 800 μL of reagent B. After a 15-min incubation at room temperature, color production at 750 nm was measured in a microplate reader (VersaMax, Molecular Devices, USA).

40 μg worth of protein of each protein extract were then mixed with the appropriate volume of 6X loading buffer (375 mM Tris-HCl pH 6.8, 12% SDS, 20% glycerol, 30% β-mercaptoethanol, 0.1% bromophenol blue), and denatured at 95°C for 5 min.

Denatured protein extracts were separated by SDS-polyacrylamide gel electrophoresis (polyacrylamide, electrophoresis chambers and power supplies from BioRad) and subsequently transferred to methanol-activated polyvinylidene difluoride (PVDF) membranes (Amersham). Wet protein transfer was carried out at 100 V for 90 min.

Prior to western blot, membranes were blocked in 5% powdered milk in PBS-Tween 0.1% for 2 hours under agitation. Proteins of interest were then detected with specific primary antibodies diluted in 1% powdered milk in PBS-Tween 0.1% as indicated in Table 4. Incubation with primary antibodies was performed overnight at 4°C under gentle agitation. Membranes were washed in PBS-Tween 0.1% for 5 min three times under agitation and then incubated with the adequate secondary antibody for 90 min. Secondary antibodies, tagged with horseradish peroxidase (HRP), were diluted in 5% powdered milk in PBS-Tween 0.1% as indicated in Table 4. Membranes were washed in PBS-Tween 0.1% three more times under agitation before protein detection.

Chemiluminescent detection of secondary antibodies was carried out using Immobilon Western Chemiluminescent HRP Substrate (Millipore) or ECL Western Blotting Detection Reagents (Amersham) according to the manufacturer's instructions. Signal was captured on medical X-ray films (Agfa, Belgium).

MATERIALS & METHODS

Antibody	Host	Manufacturer	Dilution
VE-cadherin (F-8): sc-9989	Mouse	Santa Cruz Biotechnology	1: 500
pY658 VE-cadherin (ab27775)	Rabbit	Abcam	1: 1,000
HIF1α (A300-286A)	Rabbit	Bethyl Laboratories	1: 1,000
PARP1 (C-2-10)	Mouse	Enzo Life Sciences	1: 2,000
tubulin (B-5-1-2)	Mouse	Sigma Aldrich	1: 10,000
Anti-Rabbit Immunoglobulins/HRP	Goat	Dako	1: 10,000
Anti-Mouse Immunoglobulins/HRP	Goat	Dako	1: 10,000

Table 4. Primary and secondary antibodies used in western blot and their respective dilutions.

Quantitative polymerase chain reaction (qPCR)

In order to obtain RNA extracts and assess gene expression, 500,000 cells were seeded on 60 mm culture dishes and incubated overnight. Cells were then treated with DMSO or PARPi and incubated in normoxia or hypoxia. After 24h, whole RNA was extracted using RNeasy Mini Kit (Qiagen, Germany) following the instructions provided by the manufacturer.

Briefly, cell cultures were washed with cold PBS twice, scraped in 350 μL of RLT lysis buffer containing β-mercaptoethanol and homogenized with syringe and needle to disrupt genomic DNA. 350 μL of 70% ethanol were added and RNA was purified in RNeasy spin columns as indicated by the manufacturer. RNA was eluted in 30 μL of RNAse-free water.

To ensure that there was no contamination with genomic DNA, RNA extracts were subjected to a digestion step with DNAse I (Invitrogen, USA) in the presence of RNasin Plus ribonuclease inhibitor (Promega). Pure RNA extracts were subsequently quantified with a NanoDrop ND-1000 spectrophotometer (NanoDrop Technologies).

1 μg of each RNA extract was retrotranscribed to complementary DNA (cDNA) using iScript Reverse Transcription Supermix (BioRad) according to the manufacturer's instructions.

qPCR of genes of interest was then performed using the primers shown in Table 5. Target sequences were amplified with iTaq Universal SYBR Green Supermix (BioRad) in a CFX96 Real-Time System thermal cycler (BioRad).

Target gene		Nucleotide sequence
CDH5	forward	5'- AACTTCCCCTTCTTCACCC-3'
	reverse	5'- AAAGGCTGCTGGAAAATG-3'
NRP1	forward	5'-AAAACGGTGCCATCCCT-3'
	reverse	5'-AAGAAGCAGAGTGGGTCGTT-3'
Tie1	forward	5'-GTGCCACCATTTTGACACTG-3'
	reverse	5'-CAGGCACAGCAGGTTGTAGA-3'
PDGFB	forward	5'-CATTCCCGAGGAGCTTTATG-3'
	reverse	5'-CTCAGCAATGGTCAGGGAAC-3'
36B4	forward	5'-CAGATTGGCTACCCAACTGTT-3'
	reverse	5'-GGCCAGGACTCGTTTGTACC-3'

Table 5. Primers used for qPCR experiments. 36B4, which codes for a ribosomal subunit, was used as a positive and normalization control.

Enzyme-linked immunosorbent assay (ELISA)

In order to detect and quantify PDGFβ secretion, 200,000 Mum2B cells were seeded on each well of a 6-well plate and incubated overnight. Cells were then treated with DMSO or PARPi and incubated in normoxia or hypoxia. After 24h, all supernatants were recovered for ELISA.

As a preliminary step, supernatants were concentrated using Amicon Ultra-2 centrifugal filter units (Millipore) with a 10 kDa nominal molecular weight cutoff (PDGFβ has a molecular weight of 27 kDa). ELISA ("sandwich" variation) was then performed with the commercial human PDGF-BB Mini ABTS ELISA Development Kit (PeproTech), following the instructions provided by the manufacturer.

Briefly, ELISA microplate wells were pre-treated the previous day with capture antibody overnight. Wells were then washed, blocked for one hour at room temperature and washed again. Mum2B supernatants or

recombinant human PDGF-BB standards of known concentration were added to the microplate wells and incubated at room temperature for 2 hours. After another wash step, the biotinylated detection antibody was added and incubated for 2 hours. Avidin-HRP conjugate was added and incubated for 30 min to label detection antibodies. Finally, warm ABTS liquid substrate was added to each well and color production at 405 nm was measured in a microplate reader (VersaMax, Molecular Devices, USA) according to the manufacturer's instructions.

Tube formation assay

In order to assess melanoma tube formation, wells of a 96-well plate were covered with 50 μL of ice-cold growth factor-reduced matrigel (Corning), which was allowed to warm up and jellify by placing the plates in a cell incubator at 37°C for 30 min. 10,000 cells were then seeded on the matrigel in the presence of DMSO or olaparib. All cells were initially incubated in normoxia for 1 hour to allow their adhesion to matrigel before incubating in normoxia or hypoxia for 24 hours. Images were then taken with the 10X objective of an Olympus CKX41 light microscope coupled to an Olympus E-330 camera (Olympus, Japan).

In the case of tube formation by Mum2B: pericyte co-cultures, a total of 10,000 cells were seeded at a proportion of 20:1. After a 24-hour treatment in the absence or presence of olaparib and hypoxia, images were taken on an Olympus fluorescent microscope at 10x magnification.

Cell recovery from matrigel for RNA extraction

For RNA extraction during tube formation, 35 mm culture dishes were coated with 770 μL of matrigel and 380,000 Mum2B cells were seeded on the matrigel as described in the previous section. After a 24-hour treatment in the absence or presence of olaparib and hypoxia, Mum2B were recovered from matrigel with Cell Recovery Solution (Corning) according to the manufacturer's instructions.

Briefly, each culture dish was gently washed with cold PBS tree times before adding 340 μL of Cell Recovery Solution and scraping the layer of

matrigel and cells into separate conical bottom centrifuge tubes. Each dish was rinsed twice with 340 μL of Cell Recovery Solution, which were transferred to the respective tubes as well, in order to ensure maximal recovery of cells. Tubes were inverted a few times and left on ice for 1 hour to let the matrigel dissolve. Tubes were then centrifuged at 250 g for 5 min at 4oC. The supernatants were discarded and the cell pellets were washed in ice-cold PBS, centrifuged again in the same conditions and supernatants were discarded again.

Whole RNA was extracted from the pelleted cells using RNeasy Mini Kit (Qiagen, Germany). In this case, the RNA extraction protocol started with the addition of RLT lysis buffer containing β-mercaptoethanol to the cell pellet, and went on as described in previous sections. RNA was eluted in 13 μL of RNAse free water instead of 30 μL to ensure an adequate RNA concentration.

RNA sequencing and data analysis

Library preparation and Illumina sequencing were performed at the Genomics Facility of the Institute for Parasitology and Biomedicine López-Neyra (CSIC, Granada, Spain). Data analysis was performed by the Bioinformatics Facility of the same institute. Total RNA quality was verified through Bioanalyzer RNA 6000 Nanochip electrophoresis (Agilent Technologies, USA). All RNA samples showed a RNA integrity number value above 9.6. RNA sequencing (RNAseq) libraries were elaborated from 800 ng of input total RNA using TruSeq stranded mRNA kit (Illumina, USA). A Bioanalyzer high sensitivity DNA assay was performed in order to validate the size and quality distribution of PCR-enriched libraries. Concentration was measured on a Qubit fluorometer (Thermo Scientific, USA). Finally, four types of samples (DMSO+normoxia, olaparib+normoxia, DMSO+hypoxia and olaparib+hypoxia) were sequenced. From each sample type, three biological replicates were made, giving 12 libraries in total. These were pooled in an equimolecular manner and subsequently diluted and denatured following Illumina NextSeq 500 library preparation guide. The 75×2 nt paired-end sequencing was carried out on a NextSeq 500 sequencer, generating an average of 30,059,075 paired reads per sample.

Transcriptomic samples were analyzed using the miARma-Seq pipeline[348]. Firstly, raw sequence data was submitted to evaluation on FastQC software, which provides a thorough report about the quality of the reads[349]. Then, the number of reads per sample was homogenized using the software Seqtk[350]. After sample filtering and trimming, a mean of 28,765,495 fragments per sample were obtained with 49% GC content on average. Secondly, miARma-Seq aligns all processed and quality-filtered sequences using HISAT2[351], giving a result of 95.86% of adequately aligned reads. With that aim, the *Homo sapiens* Gencode version 26, genome-build GRCh38.p10 was used. In order to obtain expression values, the software featureCounts was used to attribute sequence reads to specific genes[352]. The reference gene and lncRNA annotations were obtained from Gencode from the assembly and genome build indicated before.

Differential expression for mRNA and lncRNA

In order to carry out the differential expression analysis, we used the edgeR package[353]. Poorly expressed genes and lncRNAs were eliminated, and the remaining were normalized using the method of trimmed mean of M-values[354]. Counts per million (CPM) and log_2CPM were used for exploratory plots[353] to check the consistency of the replicates. In addition, the number of reads per kilobase per million mapped reads (RPKM), was calculated for every gene on each sample.

Principal component analysis and hierarchical clustering of normalized samples were used to examine the data and get a general outlook of the similarity of RNAseq samples[355,356].

Subsequently, differently expressed genes (DEG) and lncRNAs were calculated between the different samples (false discovery rate (FDR) value< 0.05). In order to analyze the change in expression of a lncRNA or a gene between the different samples, the log_2FC was provided.

Volcano plots were generated to depict the most relevant genes in each comparison. In each volcano plot, upregulated genes fall on the right side of the plot, while downregulated genes are represented on the left side. Moreover, the most significant the expression change was, the higher the genes are represented in the plot.

Gene enrichment analysis

Functional enrichment study was carried out using the clusterProfiler Bioconductor package in order to visualize the effect of altering gene expression more broadly[357]. For this purpose, DEG were compared against all expressed genes in the RNAseq assay.

Gene ontology terms for each gene were obtained from the Bioconductor *Homo sapiens* database and associated to Entrez gene identifiers in an orgDB R object through the AnnotationForge package to be used with clusterProfiler. Thus, Gene Ontology enrichment analysis was obtained for Biological Process, Molecular Function and Cellular Complex terms. KEGG enrichment was also calculated from Homo sapiens gene names previously acquired from Gencode.

Furthermore, a gene set enrichment analysis (GSEA) was also performed between DMSO+normoxia and olaparib+hypoxia samples[358]. Gene sets from the Molecular Signatures database (MSigDB) v6.2 were used for GSEA (KEGG: 186 canonical pathways from the Kyoto Encyclopedia of Genes and Genomes (KEGG) pathway database; C5: 825 gene sets based on gene ontology term). Default parameters were used to identify significantly enriched gene sets (FDR q< 0.25).

LncRNA and mRNA expression integration

LncRNA and mRNA RPKMs were used to assess the correlation between the expression of both types of RNA with MatrixEQTL[359]. This tool enables the study of the correlation in the expression of entities that share close genomic regions, which in our case was 100 kbp. MatrixEQTL was used with the default parameters, and all relationships with a p< 0.01 were considered as significant.

Exploring lncRNA status in cancer

We used the database cBioPortal[360] in order to examine the alteration status in cancer samples of lncRNA that were modulated by olaparib in our VM⁺ UM model. This database collects extensive genomic data from a great variety of cancer patients and samples. We selected the PanCancer Atlas

MATERIALS & METHODS

Studies cohort provided by The Cancer Genome Atlas (TCGA), which has a total of 10,967 cancer samples from a plethora of cancer types. Unfortunately, many of the queried lncRNA were not registered in cBioPortal, since this database is mainly oriented to protein-coding genes. However, we could obtain data about the alteration frequency across cancer types and co-occurring mutations for some of our selected lncRNA. In addition, we investigated the co-expression of olaparib-responsive lncRNA with PARP1 and PARP2 in the UM and the CM TCGA cohorts.

Prediction of transcription factor binding sites

For every lncRNA that was significantly regulated by olaparib, we defined a theoretical promoter region between −1000 bp and +100 bp from the transcription start site. Every promoter was examined for the presence of transcription factor binding sites using the database JASPAR (http://jaspar.genereg.net/)[361], selecting a relative profile score threshold of 95%.

Prediction of lncRNA-mediated transcription changes

We evaluated the potential effect of lncRNA in regulating overall gene expression using the database lncMAP (LncRNA Modulator Atlas in Pancancer; http://www.bio-bigdata.com/LncMAP)[362]. This database contains information about lncRNA-mediated transcription perturbations in multiple cancer types, and provides lists of lncRNA- transcription factor-target gene triplets where the lncRNA can affect the activity of the transcription factor and so trigger a change in the expression of the target gene.

Since there is not a UM cohort in lncMAP, we looked up olaparib-responsive lncRNAs in the CM cohort. Unfortunately, some lncRNAs were not available in lncMAP for this cohort. For those lncRNA that were available, lncMAP offered a list of transcription factors and their target genes that were predicted to be modulated by each lncRNA, sorting lncRNA-transcription factor- gene triplets from highest to lowest FDR. This data was used to make a graphic representation of the 30 most significant triplets predicted for each lncRNA. Every lncRNA (represented

as red squares) was connected to the appropriate transcription factors (orange triangles), and these were further connected to every gene (yellow circles) whose expression was predicted to be affected by the lncRNA-mediated transcription factor modulation. We subsequently looked up all the genes that resulted from this prediction in the RNAseq data, and highlighted with a green outline those genes whose expression was actually changed after treatment with olaparib.

Melanoma spheroid sprouting/invasion assay

In order to evaluate the sprouting potential of VM$^+$ melanoma cells in response to PARPi and hypoxia we decided to perform a sprouting assay similar to what other authors have reported for endothelial cells.

First, we generated melanoma spheroids by seeding 2,000 cells in wells of 96-well plates coated with 100 μL per well of 1.5% agarose in PBS.

After 48 hours, spheroids were recovered, mixed with 50 μL of growth factor reduced matrigel (Corning) plus 20 μL of RPMI and seeded individually in wells of 96-well plates. Matrigel was left to jellify by placing the plates in a cell incubator at 37°C for 30 min. After that, 130 μL of RPMI containing DMSO or olaparib were added to each well, and the plates were incubated in normoxia or hypoxia for 24 hours.

Images were then taken with the 20X objective of an Olympus CKX41 light microscope coupled to an Olympus E-330 camera (Olympus, Japan).

Generation of stably fluorescent cell lines

In order to facilitate the identification of Mum2B and pericytes within co-cultures on matrigel, we decided to transduce each cell line with a different fluorescent protein.

For this purpose, we used HEK293T cells as packaging cells and the following plasmids to produce lentiviral vectors:

–   Plenti-CMV-MCS-RFP-SV-puro, which codes for the red fluorescent protein (RFP) and was a gift from Jonathan Garlick & Behzad Gerami-

Naini (Addgene plasmid #109377; http://n2t.net/addgene:109377; RRID:Addgene_109377); or pLenti-CMV-MCS-GFP-SV-puro, which codes for the green fluorescent protein (GFP) and was a gift from Paul Odgren (Addgene plasmid #73582; http://n2t.net/addgene:73582; RRID:Addgene_73582). These were the plasmids that contained the genes of interest (RFP and GFP) that we wanted to transduce into Mum2B and pericytes, respectively (Figure 9).

– pMD2.G 5824pb, which codes for VSV-G, that is, the envelope glycoprotein protein of the vesicular stomatitis virus (VSV). This plasmid was kindly provided by Dr. Francisco Martín (Centro Pfizer-Universidad de Granada- Junta de Andalucía de Genómica e Investigación Oncológica).

– p8.91delta 12150pb, which codes for other essential genes in the packaging of lentiviral particles, such as Rev and Pol. This plasmid was kindly provided by Dr. Francisco Martín (Centro Pfizer- Universidad de Granada- Junta de Andalucía de Genómica e Investigación Oncológica).
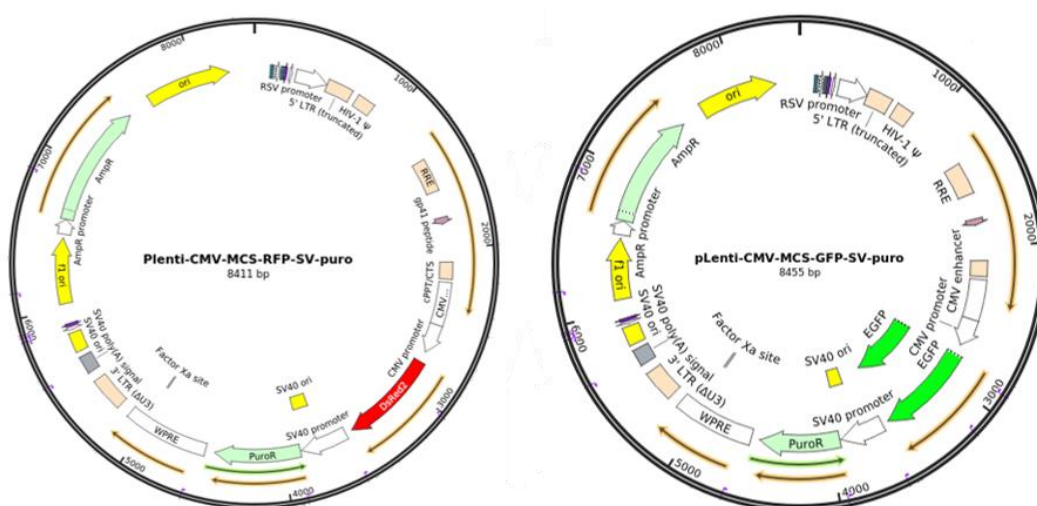
Figure 9. Plasmids containing genes of interest used to generate lentiviral vectors. RFP was used to identify Mum2B while GFP was used to identify pericytes. Diagrams adapted from Addgene.

The first step in the production of lentiviral vectors was seeding 7,000,000 HEK293T cells per dish on multiple amine-coated culture dishes (PureCoat Amine 100 mm Dish, Corning, USA), and incubating overnight.

The following day, plasmids were transfected using LipoD293 In Vitro DNA Transfection Reagent (SignaGen Laboratories, USA). The transfection mix was prepared with 9 μg plasmid of interest + 6 μg p8.91delta + 3 μg pMD2.G diluted in 500 μL of Opti-MEM growth medium (Gibco) per dish. 45 μL LipoD in 500 μL of Opti-MEM per dish were added to the transfection mix, and the complete transfection mix was resuspended and vortexed to facilitate vesicle formation. After a 15-min incubation at room temperature, the transfection mix was added drop by drop to HEK293T dishes with 5 mL of fresh growth medium. After 5 hours, the transfection medium was replaced with 7 mL of Opti-MEM.

Lentiviral particles were collected in two rounds. The first collection took place 48 hours after transfection, taking all the lentiviral medium with a syringe and filtering through 0.22 μm filter units (Whatman). HEK293T dishes were refilled with 7 mL of Opti-MEM. The second collection took place 24 hours after the first, that is, 72 hours after transfection.

Lentiviral particles were then concentrated using Amicon Ultra-15 Centrifugal Filter Units (Millipore), according to the instructions provided by the manufacturer. Briefly, we washed the filters once with 70% ethanol and twice with autoclaved PBS, centrifuging at 1800 g for 15 min at 4ºC. Next, we centrifuged the lentiviral medium at 1800 g and 4ºC until the lentiviral particles were suspended in ≈500 μL.

Concentrated lentiviral particles were added directly to Mum2B or pericytes cultured on 12-well plates. RFP and GFP expression were monitored on an Olympus IX81 microscope (Olympus, Japan).

Human UM melanoma xenografts

In order to study the effect of PARP inhibition on VM *in vivo*, we decided to work with preclinical models of human melanoma xenografts. As host, we chose 5-week-old Swiss nude female mice. As melanoma models, we chose Mum2B as a VM+ UM cell line, and Mum2C as a VM- UM cell line.

MATERIALS & METHODS

The experimental protocols of this study conform to European Union Directive 2010/63 and followed the ethical guidelines for investigations with experimental animals approved by the Ethics Review Committee for Animal Experimentation of Spanish Council of Scientific Research. These procedures were performed at the Animal Facility at the Institute for Parasitology and Biomedicine López-Neyra (CSIC, Granada, Spain).

Each mouse received a subcutaneous injection of 4,000,000 cells in 100 μL PBS. Subcutaneous tumor development was closely monitored in the next few days. Tumor volumes were measured using a caliper and applying the formula: $V = \pi \times [D \times d^2] / 6$, where D is the major tumor axis and d is the minor tumor axis.

Once tumors grew to approximately 100 mm^3 (which took 9-12 days in separate experiments), tumor-bearing mice for each cell line were randomized for further treatment with vehicle or olaparib (50 mg/kg). Treatments took place three times a week for three weeks' time, and they were administered intraperitoneally.

Before sacrifice, final tumor volumes were measured using the same procedure as before. Mice were then anesthetized and perfused with 11 mL of saline followed by 11 mL of 4% paraformaldehyde via intracardiac injection, in order to improve tissue preservation. The internal organs of every mouse were carefully explored to detect the presence of metastasis.

Local and metastatic tumors were harvested and fixed in formalin for 48 hours, and subsequently changed to 70% ethanol for another 24 hours. Tumors were then dehydrated and embedded in paraffin at the Anatomical Pathology Department of the University of Granada, by the team of Dr Francisco O'Valle. Tumor samples were then sectioned at 7 μm thickness by the Histology team of Dr Peter Carmeliet research group.

Detection of *in vivo* tumor hypoxia

In order to assess tumor hypoxia *in vivo*, pimonidazole hydrochloride (Cayman Chemical Company, USA) was dissolved in vehicle solution and injected intraperitoneally into tumor-bearing mice at a dose of 60 mg/kg 60 min before sacrifice.

Hypoxic pimonidazole adducts were detected in tumor sections using the commercial hypoxyprobe kit Hypoxyprobe1-Mab1 (Chemicon), following the instructions provided by the manufacturer. The stainings were performed by the Histology team of Dr Peter Carmeliet research group.

Briefly, tumor sections were heat deparaffinated and rehydrated in aqueous solutions of decreasing ethanol content, until a final wash in PBS. An antigen retrieval step was included at this stage, heating the tumor sections at 95°C for 20 min. After letting all sections cool down for 20 min and washing in Tris-buffered saline (TBS), tumor sections were treated with a solution of methanol plus 0.1% H_2O_2 for 20 min in order to quench native tissue peroxidases, hence avoiding later detection of unspecific signal.

Sections were then washed three times in TBS and subsequently blocked in Tris-NaCl-blocking buffer (TNB; 0,1 M Tris-HCl pH 7.5, 0,15 M NaCl, 0.5% blocking reagent [Akoya Biosciences, USA]) for 45 min. After three washes in Tris-NaCl-Tween (TNT; 0,1 M Tris-HCl pH 7.5, 0,15 M NaCl, 0.05% Tween-20), sections were incubated overnight with mouse hypoxyprobe-FITC antibody diluted 1:200 in TNB. This primary antibody specifically detects pimonidazole adducts. The following day, sections were washed in TNT three times and incubated with rabbit anti-FITC antibody diluted 1:100 in TNB for 45 min. Sections were washed in TNT three times and incubated with a biotin solution for 8 min, in order to label the secondary antibody. After three washes in TNT, sections were incubated with streptavidin-HRP diluted 1:100 in TNB for 30 min. Finally, sections were washed three more times before the addition of the peroxidase substrate 3,3'-diaminobenzidine, which generates a brown reaction product.

Sections were counterstained with Harris hematoxylin and eosin, and mounted with DPX.

Images were acquired on a Leica DMI6000 B microscope (Leica Microsystems, Germany). Leica LAS AF software (Leica Microsystems, Germany) was used to stitch all images of every section together, creating a whole section image, and to quantify hypoxic regions.

Tissue immunofluorescence

In order to examine VM formation *in vivo*, several immunofluorescent stainings were carried out. Firstly, tumor sections were triple stained with CD34, VE-cadherin and S100B antibodies (Table 6). CD34 was used as an EC specific marker, VE-cadherin was used as a dual marker of ECs and VM pseudovessels, and S100B was used as a melanoma cell marker[363]. The purpose of this staining was the general observation of endothelial and VM vessels in VM+ and VM- UM tumors. Secondly, tumor sections were triple stained with CD34, VE-cadherin and α-smooth muscle actin (αSMA) antibodies (Table 6). In this case, αSMA was included as a pericyte marker[364] to detect pericyte coverage of endothelial vessels (CD34+/VE-cadherin+) and VM pseudovessels (CD34-/VE-cadherin+). Stainings were performed by the Histology team of Dr Peter Carmeliet research group.

Antibody	Host	Manufacturer	Dilution	Fluorescent dye
CD34 (BD553731)	Rat	BD Biosciences	1: 25	Tyramide
VE-cadherin (ab205336)	Rabbit	Abcam	1: 500	Cy3 or Cy5
S100B (S2532)	Mouse	Sigma Aldrich	1: 100	Cy5
SMA-Cy3 (C6198)	Mouse	Sigma Aldrich	1: 200	Cy5-labeled
Anti-Rat Immunoglobulins/biotin	Donkey	Jackson Immunoresearch	1: 200	
Anti-Rabbit Immunoglobulins/biotin	Donkey	Jackson Immunoresearch	1: 200	
Anti-Mouse Immunoglobulins/biotin	Horse	Vector Laboratories	1: 100	

Table 6. Primary and secondary antibodies used for immunofluorescent staining of tumor sections and their respective dilutions.

The immunofluorescent staining started with the deparaffination of tumor sections, followed by rehydration in aqueous solutions of decreasing ethanol content, until a final wash in TBS. Antigen retrieval and native peroxidase quenching were carried out as described in the previous section.

Sections were blocked in TNB for 45 min and incubated overnight with CD34 primary antibody diluted in TNB. The following day, sections were washed in TNT three times and incubated with biotinylated secondary antibody diluted in TNB for 45 min. Sections were washed in TNT three times and incubated with streptavidin-HRP diluted 1:100 in TNB for 30 min. After three washes in TNT, sections were incubated with the green fluorescent substrate tyramide (Perkin Elmer, USA) for 8 min, and washed three more times.

The process of peroxidase quenching, blocking, overnight incubation with primary antibody, incubation with secondary antibody, signal amplification and addition of a fluorescent label (Cy3 or Cy5) was repeated two more times with the pertinent antibodies for each staining (VE-cadherin followed by S100B, or αSMA followed by VE-cadherin).

Tumor sections were then counterstained with Hoechst 1:500 in PBS for the detection of cell nuclei, washed three times and mounted with ProLong Gold (Invitrogen, USA).

Images were acquired on a Leica DMI6000 B (Leica Microsystems, Germany) or a Zeiss Axioplan microscope (Zeiss, Germany) at 20x or 40x magnification.

Image analysis

Tube formation images from Mum2B and C8161 (at least three images per condition) were analyzed with the online software Wimtube (Wimasis, Onimagin Technologies, Spain). This software quantifies a number of tubular network parameters, such as covered area, the number of branching points between tubes, the number of closed loops and their average area, and the total length of tubes.

Images from Mum2B and pericyte co-cultures (five images per condition) were analyzed on ImageJ (National Institutes of Health, USA). Pericytes were delineated with the polygon selection tool in order to measure their perimeter and area, which could be indicative of their interaction with Mum2B tubular networks.

Images from hypoxyprobe stainings (at least five whole tumor sections per condition) were acquired and analyzed by the team at the Imaging Facility of Dr Peter Carmeliet research group. A threshold for PIMO$^+$ staining was established, and then PIMO$^+$ areas were quantified as a percentage of total tumor area.

Images from tumor CD34/VE-cadherin/αSMA stainings (10 random optical fields per tumor section, at least 5 tumors per condition) were analyzed on ImageJ. A threshold for CD34$^+$, VE-cadherin$^+$ and αSMA$^+$ staining was established separately. Then, VE-cadherin$^+$ vessels (gray channel) were delineated with the polygon selection tool, and delineated areas were exported to images of the CD34 (green) and αSMA (red) channels. VE-cadherin$^+$ vessels with CD34$^+$ staining were classified as endothelial vessels, whereas VE-cadherin$^+$/CD34$^-$ vessels were classified as VM pseudovessels. Then, pericyte coverage was determined as the percentage of VE-cadherin$^+$ perimeter that was positive for αSMA staining.

Statistical analysis

At least three independent biological replicates were performed for each experiment.

All data from *in vitro* results (qPCR, tube formation parameters, etc; n≥ 3) was subjected to Student's t-test or ANOVA analysis. Results are shown as mean ± standard error of the mean (SEM). The analysis of RNAseq data was detailed in previous sections.

Data from tumor volumes and tumor hypoxia (n≥ 5) were subjected to ANOVA analysis. Results are shown as median ± interquartile range. Regarding tumor metastasis (n≥ 5), metastasis$^+$ mice were assigned a value of 1 while metastasis$^-$ mice were assigned a value of 0. Data was subjected to ANOVA analysis. Data from pericyte coverage did not pass a Kolmogorov-Smirnov normality test, so this data was analyzed through Mann-Whitney two-tailed tests. Results are shown as median ± 90% confidence interval.

Globally, only values of $p < 0.05$ (or FDR < 0.05) were considered as statistically significant. In graphical representations, statistical significance was illustrated as follows:

- *: $p < 0.05$
- **: $p < 0.01$
- ***: $p < 0.001$

RESULTS

RESULTS

Tube formation by melanoma cell lines

Finding appropriate cellular models was necessarily the first step to start our research in melanoma VM.

A number of melanoma cell lines were tested for their ability to develop tube formation on matrigel. A375, C8161 and G361 cell lines were tested as representatives of CM, while the UM cell lines tested were Mum2B and Mum2C (Figure 10). Of all these, only C8161 and Mum2B were capable of tube formation, so they were selected for future experiments.
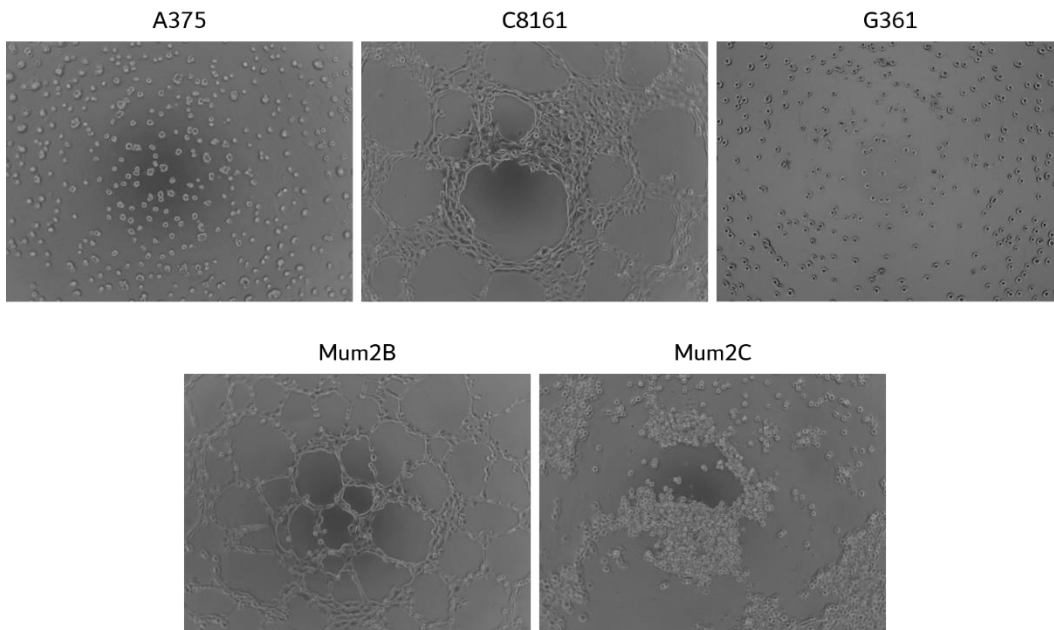
Figure 10. Tube formation on matrigel by different melanoma cell lines. Different CM (top row) and UM (bottom row) melanoma cell lines were cultured on matrigel. Pictures were taken on a light microscope.

C8161 and Mum2B have been previously identified as highly aggressive VM+ cell lines by the group of Mary J. C. Hendrix[300].

A time-course of tube formation was performed. Mature tube formation was achieved after 24h culture on matrigel, so this was the time selected for future experiments.

Expression and phosphorylation of VE-cadherin on VM⁺ melanoma cell lines

VE-cadherin is the main component of endothelial adherens junctions. Moreover, VE-cadherin can be aberrantly expressed by highly aggressive tumor cell lines, where it plays a central role in VM formation[299]. Apart from mere VE-cadherin expression, our research group has recently reported that VE-cadherin phosphorylation on Y658 is vital for VM signaling and tube formation on matrigel[324]. Therefore, we tested our melanoma cell lines for VE-cadherin expression and Y658 phosphorylation.

Indeed, both cell lines displayed VE-cadherin expression, as well as pY658-VE-cadherin (Figure 11). Notably, the expression of VE-cadherin was higher in C8161, as shown by qPCR and western blot, possibly indicating a higher vasculogenic potential of this cell line. As previously reported by our research group, basal pY658 is remarkably high in these VM⁺ cell lines[324]; unlike endothelial cells, C8161 and Mum2B do not need an activating stimulus like VEGF to trigger VE-cadherin phosphorylation.
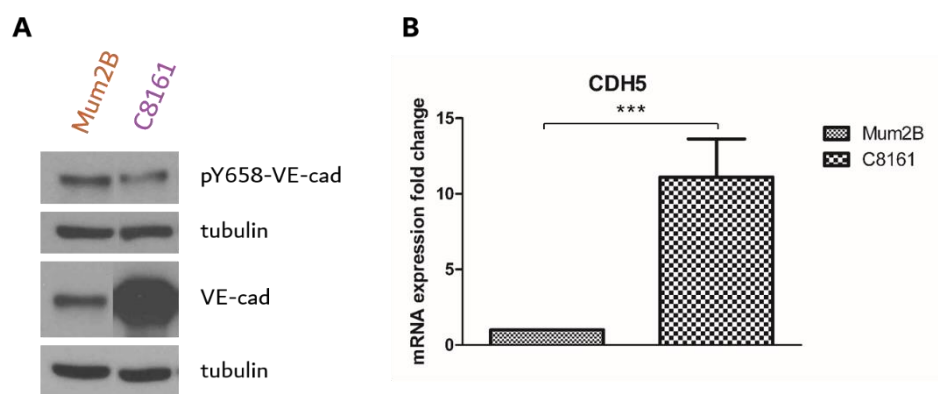
Figure 11. VE-cadherin expression and phosphorylation in VM⁺ melanoma cell lines Mum2B (UM) and C8161 (CM). **A** Western blot showing the constitutive expression of VE-cadherin and its phosphorylation on Y658. **B** qPCR showing the expression of VE-cadherin mRNA. ***: $p < 0.001$ (Student's t-test).

PARP1 and hypoxia affect VM signaling by modulating the phosphorylation of VE-cadherin

The following step was evaluating the influence of PARP inhibition and hypoxia (1% O_2) on VE-cadherin phosphorylation status. Hypoxic conditions and PARP inhibition rendered opposite effects on VE-cadherin (Figure 12).
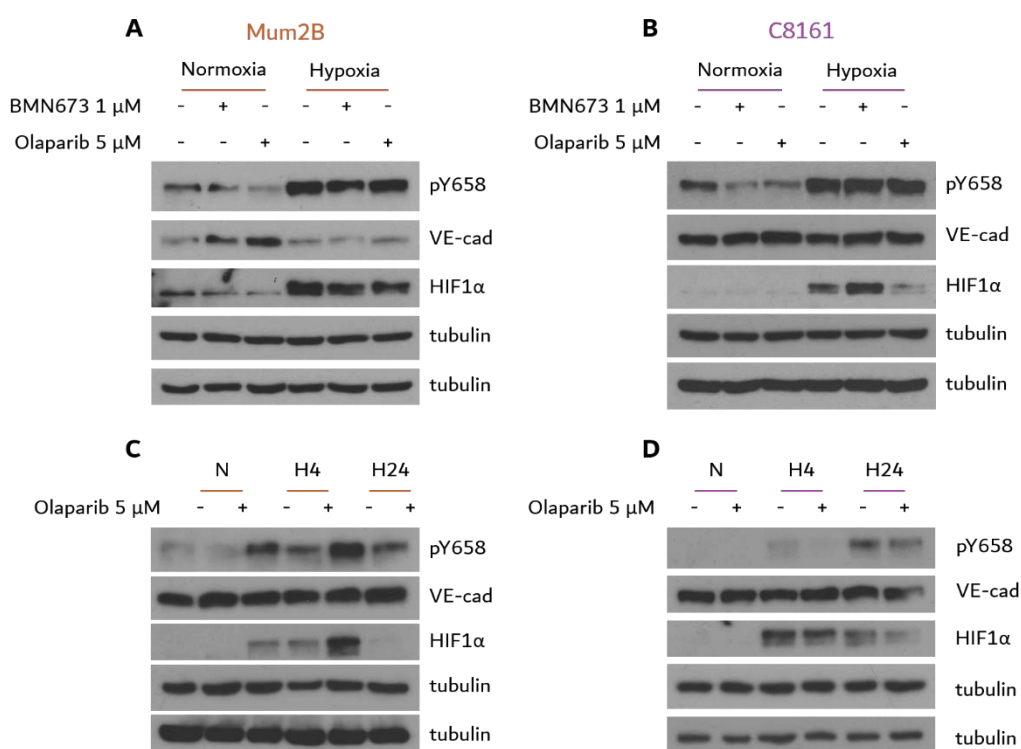
Figure 12. PARPi and hypoxia modulate VE-cadherin phosphorylation on Y658 in VM⁺ melanoma cell lines. **A-B** Mum2B and C8161 were treated with PARP inhibitors BMN673 (1 µM) or olaparib (5 µM), and incubated in normoxia or hypoxia (1% O_2) for 24 hours, or **C-D** 24 hours in normoxia, 20 hours in normoxia plus 4 hours in hypoxia, or 24 hours in hypoxia.

Firstly, hypoxia clearly increased pY658 in both cell lines. This increase occurred in a time-dependent manner (Figure 12C-D), with stronger phosphorylation after longer times of hypoxia (24h compared to 4h of hypoxia). On the other hand, the chemical inhibition of PARP activity with BMN673 (1 µM) or olaparib (5 µM) decreased pY658 (Figure 12A-B),

especially in normoxia but also during short- and long-term hypoxia (Figure 12C-D).

Although most PARPi can inhibit both PARP1 and PARP2, PARP1 specific knockdown with siRNA had a similar effect to BMN673 and olaparib, reducing pY658 in both melanoma cell lines in normoxia and hypoxia (Figure 13). This result highlights the role of PARP1 in the phosphorylation of VE-cadherin. Furthermore, HIF1α knockdown with siRNA decreased pY658 too, suggesting that hypoxia-driven phosphorylation of VE-cadherin depends at least partly on HIF1α (Figure 13).
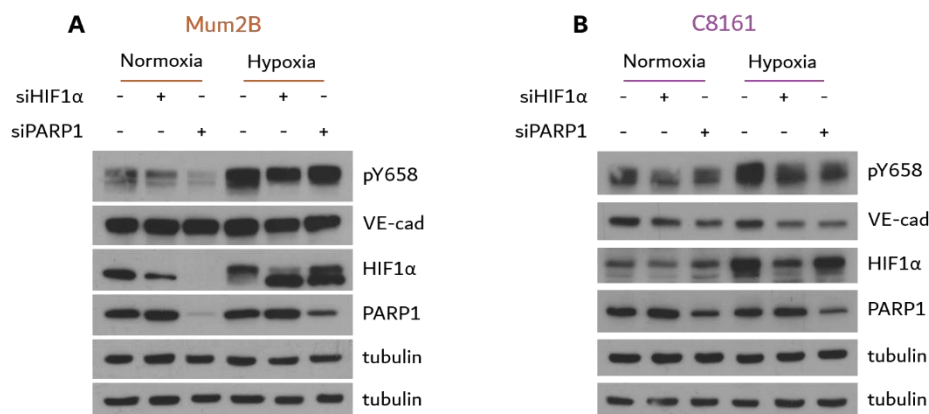
Figure 13. Modulation of pY658 by PARPi and hypoxia is mediated by PARP1 and HIF1α. **A** Mum2B and **B** C8161 were transfected with control siRNA or siRNA against HIF1α or PARP1. After 24 hours, cells were subjected to normoxia or hypoxia for 24 hours.

Hence, PARP1 inhibition might attenuate VM by regulating VE-cadherin signaling, counteracting the effect of HIF1α.

PARP inhibition and hypoxia modulate the expression of VE-cadherin at the transcriptional level

To further investigate the role of PARP1 and hypoxia in VM, we measured the expression of the VE-cadherin gene (CDH5) in response to olaparib and hypoxia in our melanoma cell lines by qPCR (Figure 14). Both cell lines showed a similar trend in CDH5 expression, where hypoxia and

olaparib independently increased CDH5 transcript compared with control, and olaparib treatment during hypoxia rendered the highest CDH5 mRNA levels. In contrast to the effect on VE-cad phosphorylation, these results suggest that PARP1 inhibition and hypoxia have a similar effect promoting VE-cadherin gene expression.
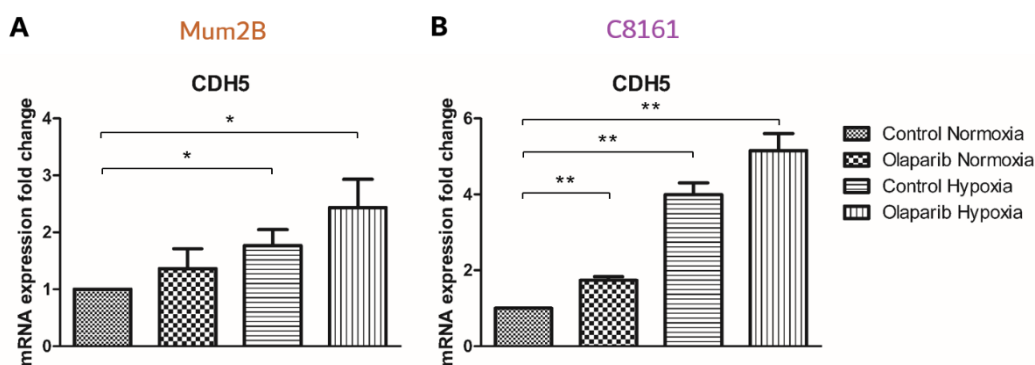
Figure 14. PARP inhibition and hypoxia upregulate the expression of VE-cadherin. **A** Mum2B and **B** C8161 were treated with DMSO or olaparib and incubated in normoxia or hypoxia for 24 hours. Total RNA was extracted for qPCR analysis. *: $p < 0.05$; **: $p < 0.01$ (Student's t-test).

The combination of PARP inhibition and hypoxia enhances the vasculogenic gene expression profile of VM⁺ UM cells during tube formation

Next, we aimed to find out if hypoxia and olaparib modulated the expression of any other genes involved in vascular biology. We performed a whole transcriptome RNAseq using RNA from Mum2B cells grown on matrigel in the absence or presence of hypoxia and olaparib (Figure 15).

Treatment with olaparib significantly changed the expression of 596 genes (Figure 15A), hypoxia significantly modulated 1,897 genes (Figure 15B), while treatment with olaparib plus hypoxia resulted in a significant change in the expression of 4,780 genes (Figure 15C), compared to normoxic controls (FDR< 0.05).

In an attempt to improve our understanding of these results, we examined separately the effect of olaparib and hypoxia by themselves, compared to the combination of both (Figure 16).
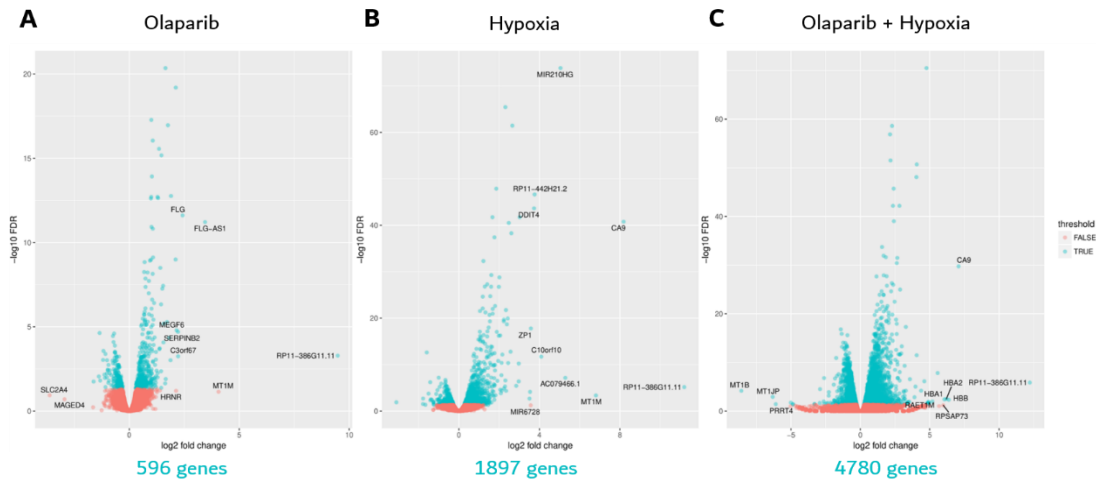
Figure 15. PARP inhibition and hypoxia regulate the expression of hundreds of genes during tube formation. Mum2B were cultured on matrigel, treated with DMSO or olaparib and incubated in normoxia or hypoxia for 24 hours. Cells were detached from matrigel using Corning Cell Recovery Solution™, and total RNA was extracted and subjected to RNAseq. Genes that were modulated by **A** olaparib alone, **B** hypoxia alone, or **C** olaparib treatment during hypoxia, with respect to normoxic controls, were represented in volcano plots. Blue dots symbolize significantly modulated genes (FDR< 0.05), while red dots symbolize non-significantly modulated genes.

Regarding olaparib, we compared the 596 genes that were modulated by olaparib treatment during normoxia in relation to normoxic control (CN/ON), with the 820 genes that were modulated by olaparib treatment during hypoxia in relation to hypoxic control (CH/OH) (Figure 16A). As shown in the Venn diagram, there were 318 genes that were modulated by olaparib in both cases. We could deduce that these genes are fixed targets of PARP, independently of oxygen availability.

As for hypoxia, we compared the 1,897 genes that were modulated by hypoxia alone in relation to normoxic control (CN/CH), with the 2,885 genes that were modulated by hypoxia in the presence of olaparib treatment (ON/OH) (Figure 16B). In this case, there were 1,400 genes that were modulated by hypoxia in both situations, so these are genes that are purely modulated by hypoxia independently of PARP activity.

Finally, we compared the genes that were modulated by olaparib or hypoxia alone, in relation to normoxic control (CN/ON and CN/CH), with

the 4780 genes that were modulated by the combination of olaparib during hypoxia also with reference to normoxic control (CN/OH) (Figure 16C). Firstly, we found that 181 (174+7) genes were independently regulated by both olaparib and hypoxia, therefore being common targets of PARP and hypoxia. There were 319 genes that were always modulated by olaparib but never by hypoxia, and 1,428 genes that were always modulated by hypoxia but never by olaparib. Remarkably, we found 2,859 genes that were significantly modulated only by the combination of olaparib during hypoxia. This suggests that there must be some sort of additive or synergistic interaction between olaparib treatment and hypoxic conditions regarding the regulation of gene expression.
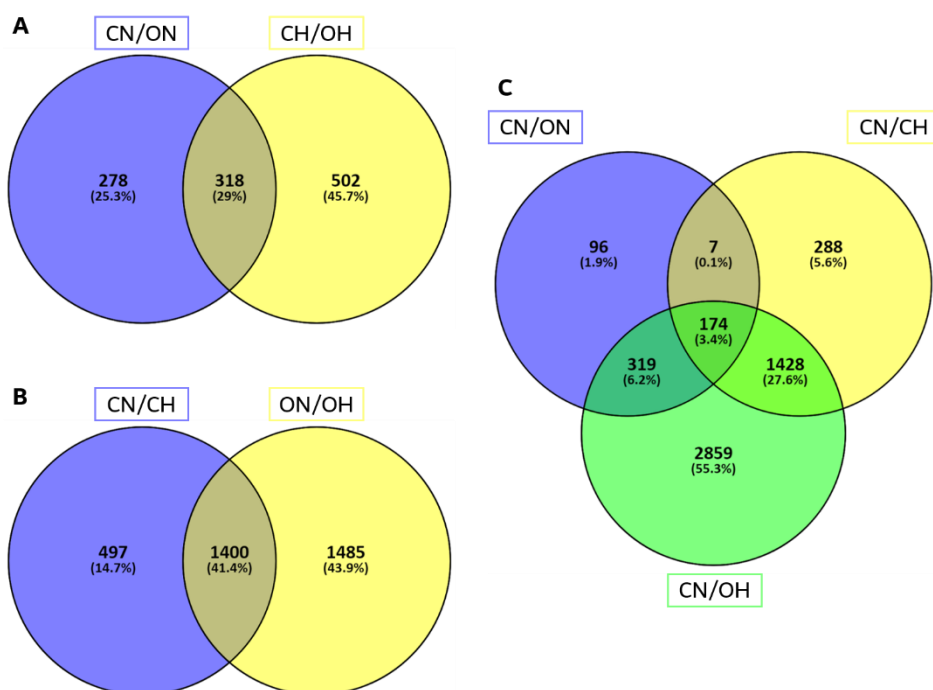
Figure 16. Separate vs combined effect of PARP inhibition and hypoxia on gene expression. RNAseq data for the different conditions was cross-examined to find common and independent targets of PARP and hypoxia, and the results were depicted in Venn diagrams. C: control; O: olaparib treatment; N: normoxia; H: hypoxia.

Gene ontology (GO) did not identify global modulation of any pathways related to vascular function after olaparib treatment or hypoxia alone. However, GO Biological Process (GO-BP) and GSEA showed that several

pathways involved in vessel formation were significantly altered in the olaparib plus hypoxia condition, as compared with normoxic controls (Figure 17). Overall, GO-BP detected 84 genes known to be involved in vascular biology whose expression significantly changed in this condition (Table 7; FDR<0.05). As expected, CDH5 was among these genes, as well as other crucial genes in endothelial cells and vasculature development, such as VEGFA/B/C, PECAM1, CD34, PDGFB, KDR (VEGFR2), NRP1 or Tie1. Moreover, a closer inspection of the RNAseq results revealed significant changes in other genes with important vascular functions that had not been included by GO-BP, such as PTPRB (VE-PTP)[248] or Robo4[227].
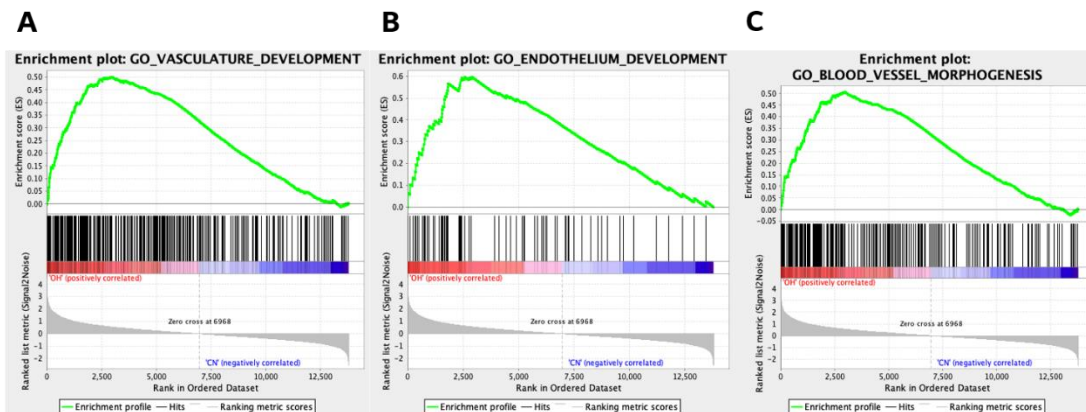
Figure 17. The combination of PARP inhibition and hypoxia globally modulates vascular signaling pathways in VM+ UM cells. RNAseq data comparing gene expression after olaparib plus hypoxia with normoxic controls was subjected to GSEA to generate enrichment plots.

We validated RNAseq results by qPCR for a few of these genes, specifically NRP1, Tie1 and PDGFB, in Mum2B as well as C8161 (Figure 18A-B), in addition to previously analyzed CDH5 (Figure 14). Protein expression of PDGFβ was further validated by ELISA, measuring its concentration in Mum2B-conditioned media (Figure 18C). The expression of PECAM1 and CD34 could not be detected by qPCR.

Altogether, most vasculature-related genes that suffered a significant expression change after olaparib during hypoxia were actually upregulated (Table 7, Figure 18), suggesting the promotion of a vasculogenic gene expression profile in our UM model in this condition.

Upregulated genes			Downregulated genes
PGF	VEGFA	PTGS2	EZR
STC1	PECAM1	IL1B	ATP5B
SH2D2A	CEACAM1	ITGB3	MAPKAPK3
CD34	PROX1	TMEM204	AXL
NCF2	PDGFB	F2RL1	APOLD1
CDH5	ICAM1	CYFIP2	EFNB2
WNT7A	WNT5A	BTG1	SETSIP
VEGFB	NRG1	PTPRS	CCBE1
HEY1	ACVRL1	TNF	
BMPR2	BMP4	VASH1	
MYADM	ITGA5	KDR	
VEGFC	NRP2	ADAMTS12	
TGFB1	SEMA5A	PROX2	
NOTCH4	BCAR1	FOXF1	
HSPB1	SRC	NOTCH1	
MAPK11	MAPK13	CALR	
NRP1	RHOB	KDM6B	
CYBA	SASH1	F11R	
LAMA5	ACVR1	NEDD4	
SEMA3C	ACVR2B	GPX1	
HEG1	PIK3R2	PDPN	
GRB10	ENG	ITGAV	
SRPX2	P2RX4	FYN	
RBPJ	PIK3CA	SHB	
CD40	AMOTL1	MYOF	
LGALS8			

Table 7. Vasculature-related genes regulated by olaparib plus hypoxia in UM. Genetic data was curated from RNAseq results comparing olaparib plus hypoxia with normoxic controls and from the vasculature-related pathways that were highlighted by the GO-BP bioinformatic tool.
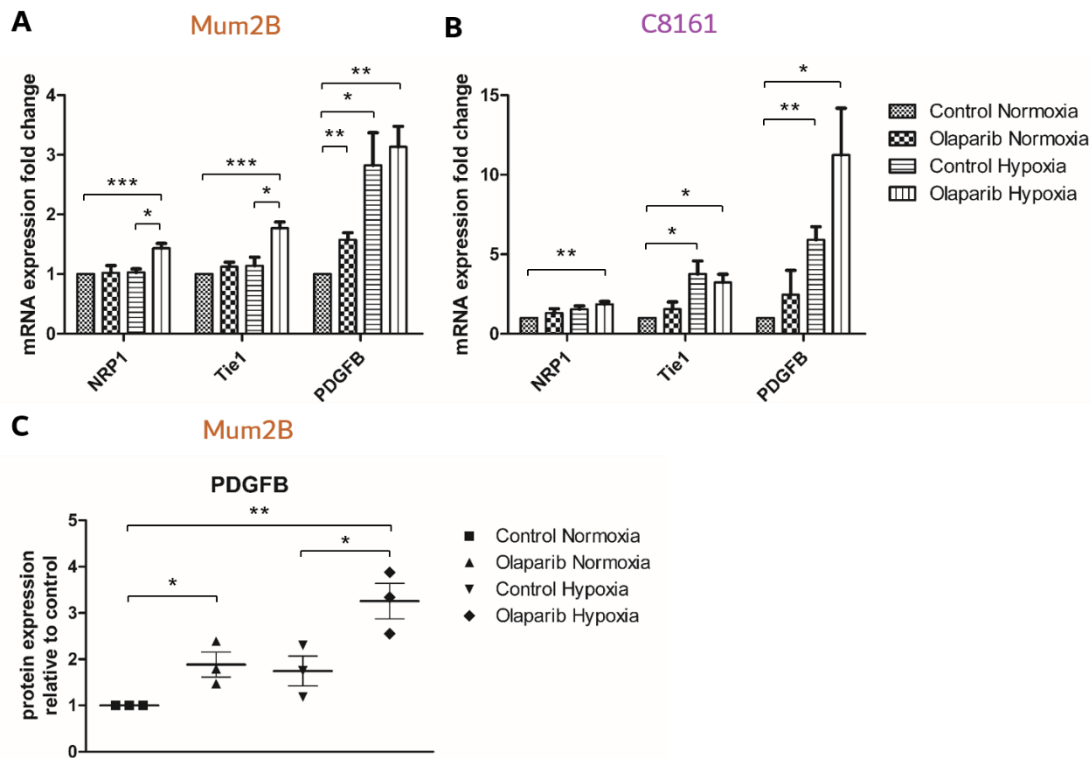
Figure 18. PARP inhibition and hypoxia modulate the expression of vascular genes in UM cells. **A** Mum2B and **B** C8161 were treated with DMSO or olaparib and incubated in normoxia or hypoxia for 24 hours. Total RNA was extracted for qPCR analysis. **C** Mum2B were treated with DMSO or olaparib and incubated in normoxia or hypoxia for 24 hours. Conditioned media were recovered for ELISA against PDGFβ. *: p<0.05; **: p< 0.01; ***: p< 0.001 (Student's t-test).

PARP inhibition modulates lncRNA expression during UM tube formation

In an attempt to understand how PARP inhibition could induce such a shift in gene expression, we focused our attention on the effect of PARP inhibition on the lncRNA landscape, given their prominent role in the regulation of gene expression. For this purpose, we analyzed lncRNA expression changes in response to olaparib in our RNAseq data.

Olaparib increased the expression of 11 lncRNAs and decreased the expression of 9 lncRNAs, making for a total of 20 lncRNAs that were significantly modulated by olaparib (Figure 19, Table 8; FDR< 0.05). FLG-

AS1 was the most upregulated while RP11-706O15.5 was the most downregulated lncRNA.
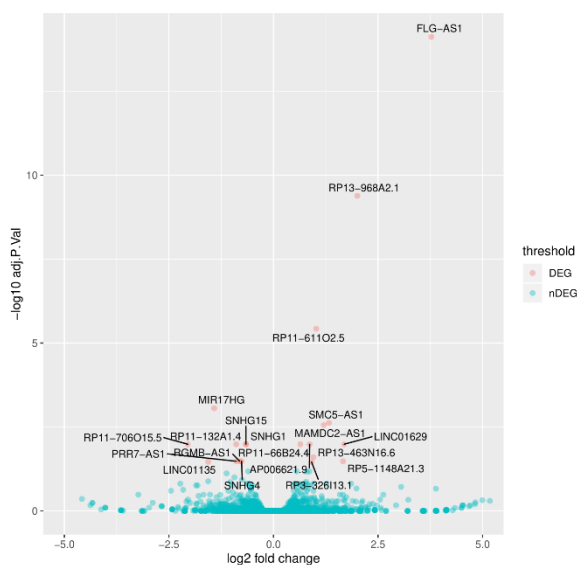
Figure 19. PARP inhibition modulates lncRNA expression during tube formation. The results from figure 15A were curated to focus our attention on lncRNA expression after olaparib treatment. Red dots symbolize significantly modulated lncRNA (FDR< 0.05), while blue dots symbolize non-significantly modulated lncRNA.

Upregulated lncRNA	Downregulated lncRNA
FLG-AS1	SNHG1
RP13-968A2.1	SNHG15
LINC01629	SNHG4
RP5-1148A21.3	RGMB-AS1
SMC5-AS1	PRR7-AS1
MAMDC2-AS1	RP11-132A1.4
RP11-611O2.5	MIR17HG
RP13-463N16.6	LINC01135
RP3-326I13.1	RP11-706O15.5
AP006621.9	
RP11-66B24.4	

Table 8. LncRNA significantly modulated by olaparib in Mum2B during tube formation.

Some lncRNA have been found to modulate gene expression in *cis*, that is, they can enhance or decrease the expression of immediately upstream and/or downstream genes[365]. Thus, we investigated if this regulatory mechanism could apply to any of the lncRNAs modulated by olaparib.

Figure 20. PARP inhibition modulates *cis*-acting lncRNA. Circos plot representation of predicted *cis*-acting lncRNA modulated by olaparib (inner side of the circos) and their target genes (outer side of the circos).

RESULTS

Olaparib-modulated lncRNAs (p-value< 0.05) were coupled with upstream and downstream genes. Next, we checked if *cis*-located genes were modulated by olaparib as well (p-value< 0.05) and we filtered for significant interactions between the gene expression changes in each lncRNA and their respective *cis*-located genes (p-value< 0.05). The results were represented in a circos plot that illustrates gene expression changes mediated by *cis*-acting lncRNA in response to olaparib across the genome (Figure 20). Every olaparib-dependent lncRNA with a predicted *cis*-regulatory action is depicted in the inner side of the circos, while the outer side of the circos shows the respective *cis* target genes associated to each lncRNA.

By means of *cis*-acting lncRNA, PARP inhibition can indirectly affect the expression of numerous genes.

Olaparib-dependent lncRNAs in the context of cancer

Unfortunately, a defined biological role has not been reported yet for most of the lncRNA that were modulated by olaparib. In fact, many of them do not even have definite names, and simply go by the original identifiers that they were given during the course of the Human Genome Project (e.g.: RP11-706O15.5). As a result, estimating the influence that PARP inhibition might exert on UM through lncRNA regulation is not a simple task.

In an attempt to understand the role of olaparib-modulated lncRNA in cancer, we looked them up in the database cBioPortal, which collects extensive genomic data from a great variety of cancer patients and samples. Only the 11 lncRNAs that have been characterized and renamed so far were available for query. Selecting the TCGA PanCancer Atlas cohort, the results showed that in 977 out of 10,967 samples (9%) at least one of the 11 lncRNAs had suffered a genetic alteration (Figure 21). FLG-AS1 was the most frequently altered lncRNA (3% of all samples in the cohort), whereas no LINC01629 alterations were detected in any sample. Most of the reported alterations correspond to genomic amplifications, except in the case of RGMB-AS1, which mostly appeared to undergo genomic deletions.
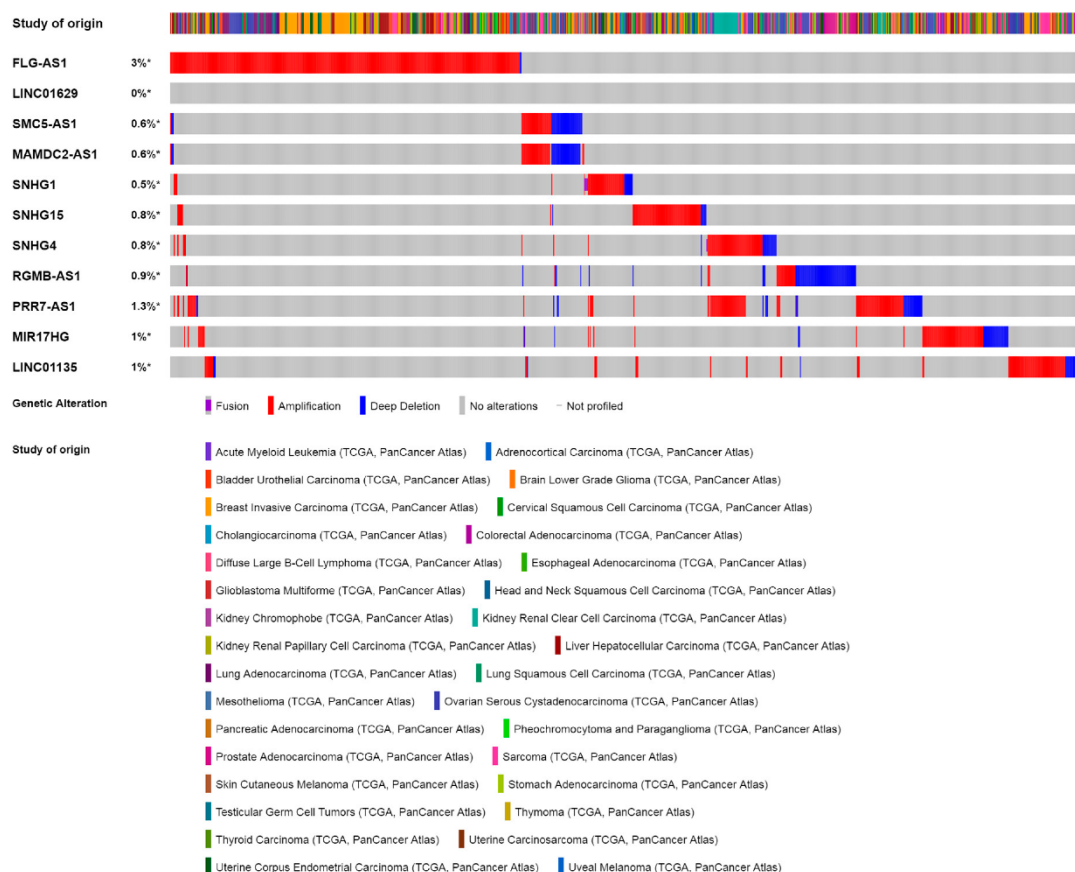
Figure 21. Olaparib-responsive lncRNAs in pan-cancer samples. Oncoprint showing genetic alterations in olaparib-dependent lncRNAs in the PanCancer Atlas cohort, obtained from cBioPortal.

It is important to point out that the TCGA does not usually annotate detailed sequence information from non-coding genes, which is why the mutation data obtained from cBioPortal is restricted to copy number variations (CNV). Furthermore, the great length of lncRNA loci increases their chance of suffering stochastic genetic alterations, especially in the tumor context, characterized by high genomic instability. Thus, it is likely that most of the alterations reported in cBioPortal are simply passenger mutations.

Taking a closer look at lncRNA alteration frequency across the different cancer types (Figure 22), cBioPortal reveals that olaparib-responsive lncRNAs are most frequently altered in sarcoma samples, although only

one sample in the UM cohort harbored alterations in any of these lncRNA. Specifically, one UM sample contained a deletion in SNHG4. However, it is also true that UM is one of the smallest cohorts in the study, with only 80 patients (compared to over 1,000 samples in the non-small cell lung cancer or invasive breast carcinoma cohorts). As for CM, 5% of all samples (24 out of 444) had a genetic alteration in some lncRNA that was modulated by olaparib. Of these, FLG-AS1, PRR7-AS1 and MIR17HG had the highest mutation frequency in CM.
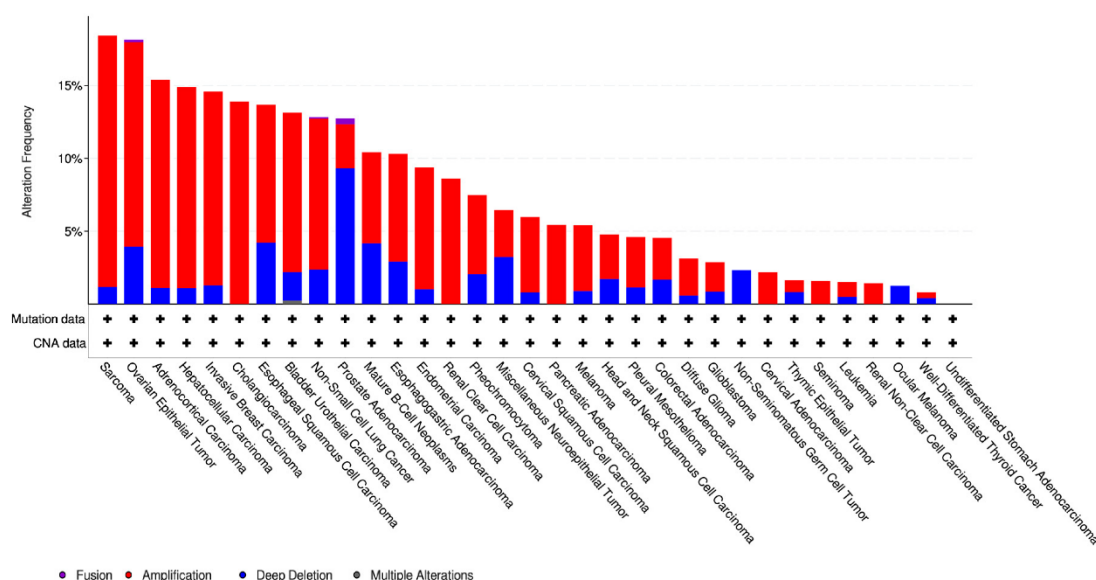
Figure 22. Alteration of olaparib-responsive lncRNAs across different cancer types. Overall alteration frequency of olaparib-modulated lncRNAs in the different cancer types from the PanCancer Atlas cohort, obtained from cBioPortal.

Correlated expression of PARPs and olaparib-dependent lncRNAs in melanoma

Apart from genomic data, cBioPortal collects information regarding gene expression in cancer. We examined the UM and CM cohorts searching for potential correlations between the expression of PARP1 and PARP2 (both direct targets of olaparib) and lncRNAs that were modulated by olaparib treatment in our model. It is important to point out that PARP mRNA expression does not necessarily equate PARP activity, but it can still provide some notion of what the situation might be.

Again, TCGA is mainly focused on protein-coding genes, so information about expression was only available for a few lncRNA: SNHG1, SNHG4, SNHG15 and MIR17HG. All four of these lncRNA were found to be downregulated after olaparib treatment in Mum2B (Table 8). If PARP inhibition results in decreased expression, we might expect some degree of positive correlation between PARP1/2 and these lncRNA, which was true in some cases (Figure 23).
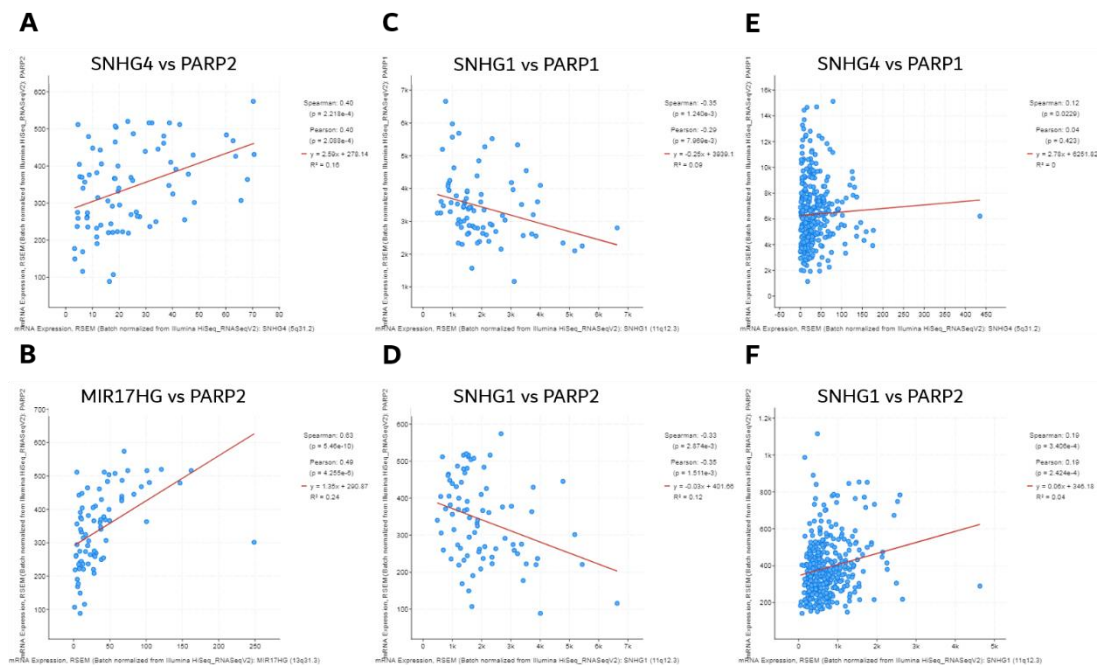
Figure 23. Co-expression of PARP1/2 and lncRNA modulated by olaparib in melanoma. Transcriptional co-expression data for PARP1/2 and olaparib-dependent lncRNAs in the **A-D** UM and **E-F** CM cohorts from TCGA, obtained from cBioPortal. Graphs show significant correlations (q-value< 0.05) between **A** SNHG4 and PARP2, **B** MIR17HG and PARP2, **C** SNHG1 and PARP1, and **D** SNHG1 and PARP2 in UM; and between **E** SNHG4 and PARP1, and **F** SHNG1 and PARP2 in CM.

The expression of SNHG4 and MIR17HG was positively correlated with the expression of PARP2 in UM (Figure 23A-B). In CM, the expression of SNHG4 was positively correlated with PARP1, and SNHG1 with PARP2 (Figure 23E-F). However, the expression of SNHG1 was negatively correlated with PARP1 and with PARP2 in UM (Figure 23C-D). The

expression of SNHG15 was not correlated with any PARP in any melanoma type.

These results suggest a possible association between PARP1/2 and SNHG4 and MIR17HG in melanoma, although the association with SNHG1 is conflicting.

Genomic alterations in olaparib-responsive lncRNAs significantly co-occur with alterations in key tumor suppressor genes

cBioPortal also allows the identification of correlated genomic alterations in different genes. That is, cBioPortal shows if specific alterations in a certain gene significantly co-occur with alterations in other genes within the same tumor samples. Surprisingly, genomic alterations in some of the queried lncRNA had a significant co-occurrence with alterations in well-known tumor suppressors (Figure 24).

Samples containing an amplification in FLG-AS1 were significantly enriched for alterations in the master tumor suppressor TP53 (q-value= 2.761×10^{-3}). On the contrary, amplifications in FLG-AS1 were negatively correlated with genetic alterations in isocitrate dehydrogenase (IDH) 1 (q-value= 0.0204) and PTEN (q-value= 0.0384) (Figure 24A). Alterations in the hypoxia response modulator VHL significantly co-occurred with amplifications in SNHG4 (q-value= 5.98×10^{-9}; Figure 24B) and PRR7-AS1 (q-value= 2.94×10^{-7}; Figure 24D). Finally, samples with a deep deletion of RGMB-AS1 were significantly enriched for alterations in SPOP (q-value< 10^{-10}; Figure 24C).

The fact that amplifications in SNHG4 and PRR7-AS1 co-occur with alterations in the same gene, VHL, is actually not surprising. The loci for these lncRNA are located very close to each other in the long arm of chromosome 5. Therefore, any genomic alterations affecting that region will likely affect both genes, which is why alterations in SNHG4 and PRR7-AS1 have a significant co-occurrence.
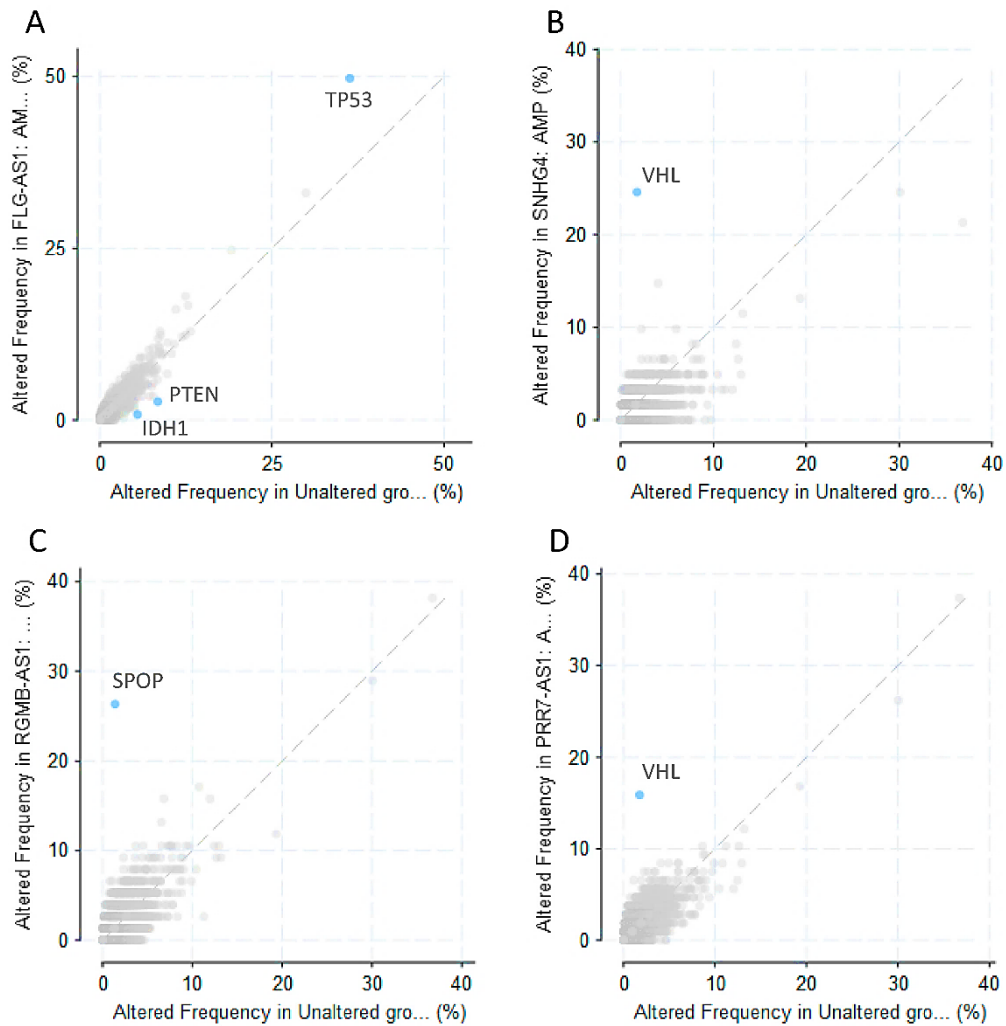
Figure 24. Co-occurrence between alterations in olaparib-responsive lncRNAs and other genes in cancer. **A** Genetic alterations enriched in samples harboring amplifications in FLG-AS1. Amplification of FLG-AS1 is positively correlated with alterations in TP53 and negatively correlated with alterations in IDH1 and in PTEN. **B** Genetic alterations enriched in samples harboring amplifications in SNHG4. Amplification of SNHG4 significantly co-occurs with alterations in VHL. **C** Genetic alterations enriched in samples harboring deep deletions in RGMB-AS1. Deletion of RGMB-AS1 significantly co-occurs with alterations in SPOP. **D** Genetic alterations enriched in samples harboring amplifications in PRR7-AS1. Amplification of PRR7-AS1 significantly co-occurs with alterations in VHL.

RESULTS

Though statistically significant, the biological relevance of all the correlations illustrated in Figure 24 cannot be easily predicted with bioinformatic tools. Further research regarding the potential association between these lncRNA and tumor suppressors is not within the scope of this thesis, but it opens an interesting window to future investigations.

The promoter regions of olaparib-responsive lncRNAs share binding sites for the same transcription factors

Next, we wondered how PARP inhibition could regulate lncRNA expression. As discussed above, PARP1 can influence the activity of sequence-specific transcription factors, so PARP inhibition might affect lncRNA expression by interfering with a hypothetic transcription factor that controls the expression of these lncRNAs.
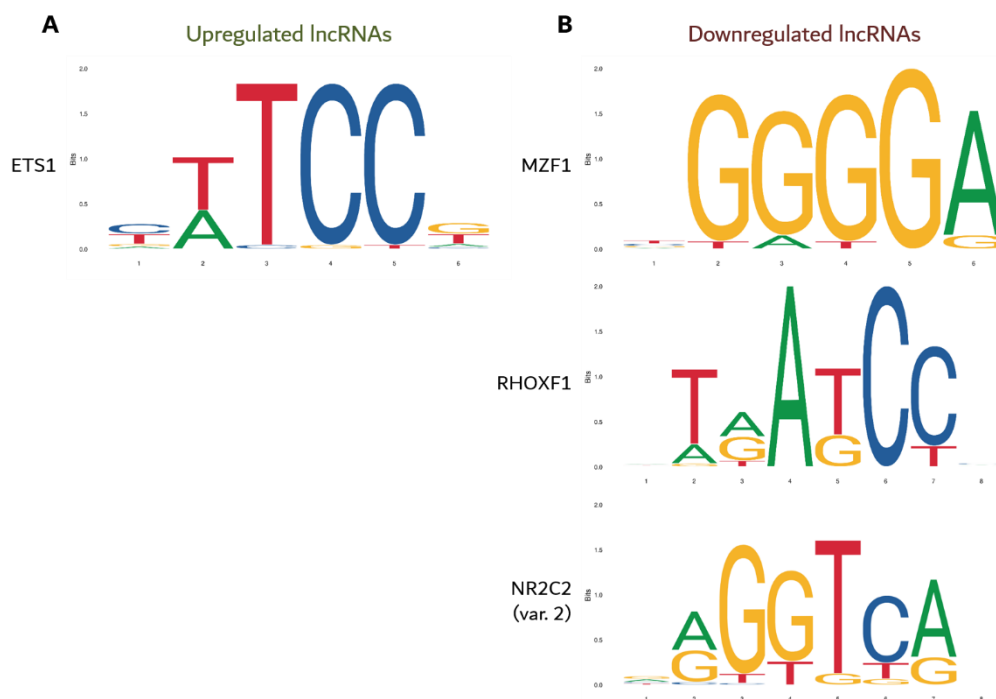
Figure 25. Transcription factors predicted to bind the promoters of olaparib-responsive lncRNAs. Considering a promoter region between −1000 and +100 bp from the transcription start site **A** ETS1 binding sites were present in the promoters of all lncRNAs upregulated by olaparib. **B** MZF1, RHOXF1 and NR2C2 (var. 2) binding sites were present in the promoters of all lncRNAs downregulated by olaparib.

In order to investigate this hypothesis, we located the theoretical promoter region of each of the 20 lncRNAs that were modulated by olaparib. We considered as promoters the genomic region between –1000 and +100 base pairs from each transcription start site. Each of these sequences was introduced in the database JASPAR, which collects data for transcription factor binding sites in the DNA, and examined for all possible transcription factor binding sites with a relative score over 0.95.

Surprisingly, all upregulated and downregulated lncRNA had a few results in common (Figure 25). The transcription factor ETS1 had high-score binding sites in the promoters of all olaparib-upregulated lncRNAs (Figure 25A), while all the promoters of olaparib-downregulated lncRNAs had high-score binding sites for MZF1, RHOXF1 and NR2C2 (Figure 25B).

Olaparib-responsive lncRNAs may participate in complex gene expression networks in melanoma

Due to the relevance of lncRNA in gene expression, we wanted to explore what genes might be affected by lncRNA changes in response to olaparib.

Some reports have shown that lncRNA can modulate the expression of transcription factors and hence alter the expression of all their target genes[362]. The database lncMAP (LncRNA Modulator Atlas in Pan-cancer) uses TCGA data to collect information about lncRNA-mediated transcriptional perturbations in different cancer types. In particular, it lists lncRNA- transcription factor- gene triplets where said lncRNA can modulate the activity of said transcription factor and result in altered expression of said gene. Unfortunately, lncMAP does not contain information regarding UM. Considering that lncRNA-mediated gene expression perturbations are more similar in cancer types of the same origin[362], we selected CM as the most representative cohort for our search.

We searched for all olaparib-responsive lncRNAs, though only 9 of them were annotated in lncMAP. Among these, every lncRNA could modulate the expression of at least two transcription factors, so altogether olaparib-responsive lncRNA may end up affecting a great number of genes (Figure 26). A few of the genes that came up in the search, specifically SCARB1,

CYBRD1, FAM49A, NTN4 and NCKAP5L, were indeed significantly modulated by olaparib in our RNAseq data.
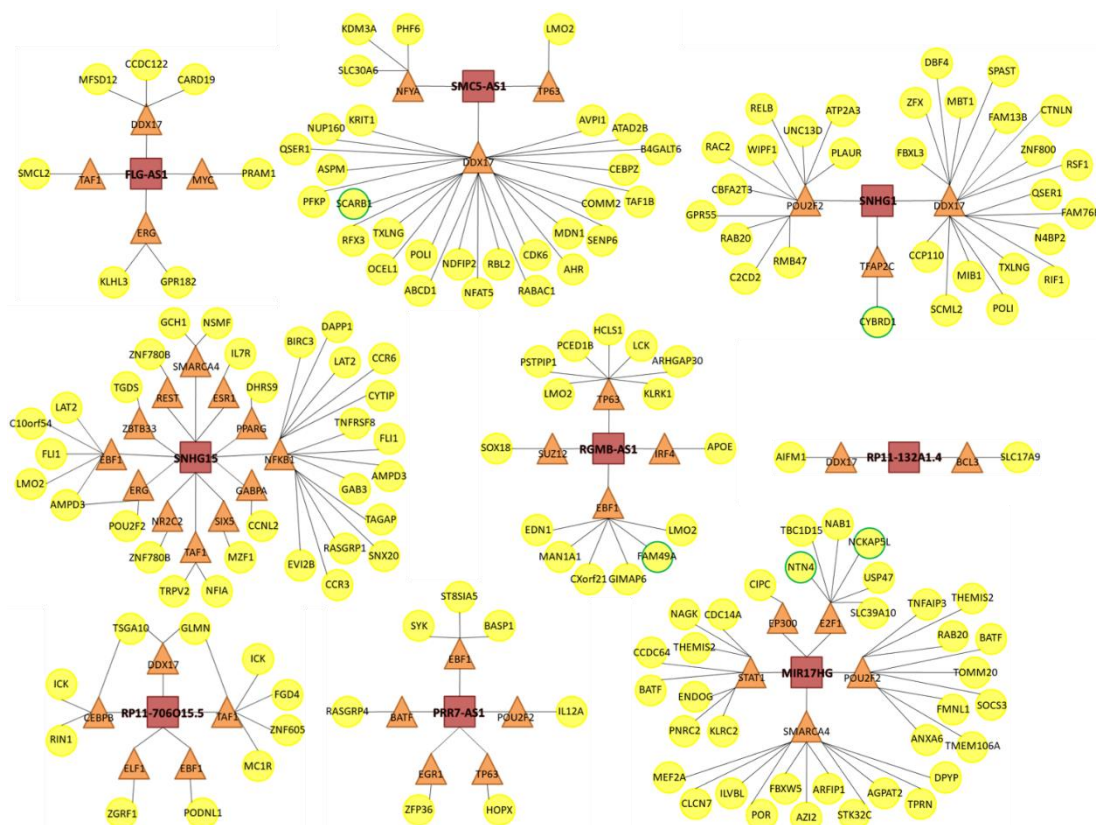
Figure 26. Predicted gene expression perturbations initiated by olaparib-dependent lncRNAs. LncRNAs that were modulated by olaparib were searched in the CM cohort of the database lncMAP. Retrieved data was represented in diagrams where lncRNAs are depicted as red squares, transcription factors are depicted as orange triangles, and target genes are depicted as yellow circles. Genes outlined in green were significantly modulated by olaparib in our UM model.

Therefore, olaparib may affect gene expression networks in melanoma through the modulation of lncRNA expression.

In order to assess whether treatment with PARPi and hypoxia had an effect on the tube formation ability of our VM⁺ melanoma cells, we cultured Mum2B and C8161 on matrigel in the absence or presence of PARPi and hypoxia and analyzed tube formation parameters.
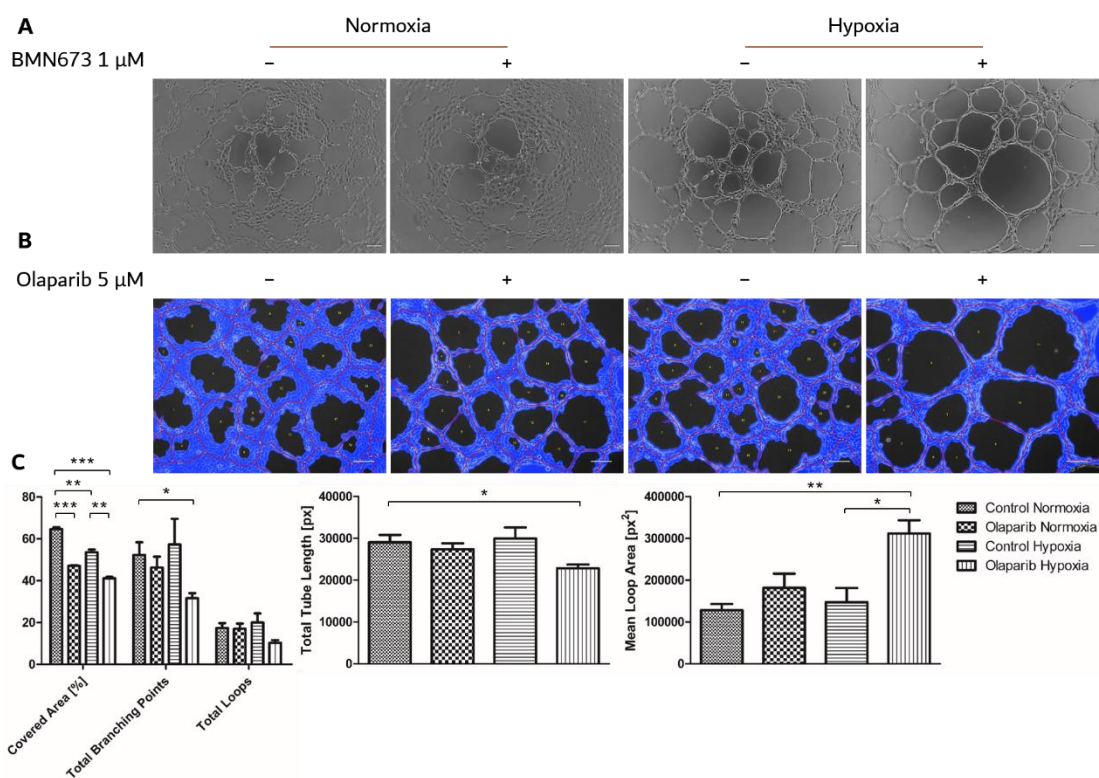
Figure 27. PARPi and hypoxia modulate UM tube formation. Mum2B were cultured on matrigel in the absence or presence of **A** BMN673 or **B** olaparib, and incubated in normoxia or hypoxia for 24 hours. **B-C** Tube formation parameters (covered area, branching points, loops, tube length and loop area) were quantified using the image analysis software WimTube (Wimasis). *: $p<0.05$; **: $p< 0.01$; ***: $p< 0.001$ (Student's t-test). Scale bar: 100 μM.

In Mum2B, PARPi or hypoxia alone did not seem to have any major effect on tube formation (Figure 27A-B). Nevertheless, combined treatment with PARPi during hypoxia seemed to affect the overall morphology of the vasculogenic networks, which now appeared more regular, with better

defined tubes that were more evenly distributed. Quantitatively (Figure 27C), treatment with olaparib during hypoxia significantly reduced covered area, more than olaparib or hypoxia alone. Total branching points and total tube length significantly decreased as well. Finally, there was a significant gain in loop area, since tubes were more spatially dispersed. Strikingly, this network morphology resembles a phenotype of vessel normalization.
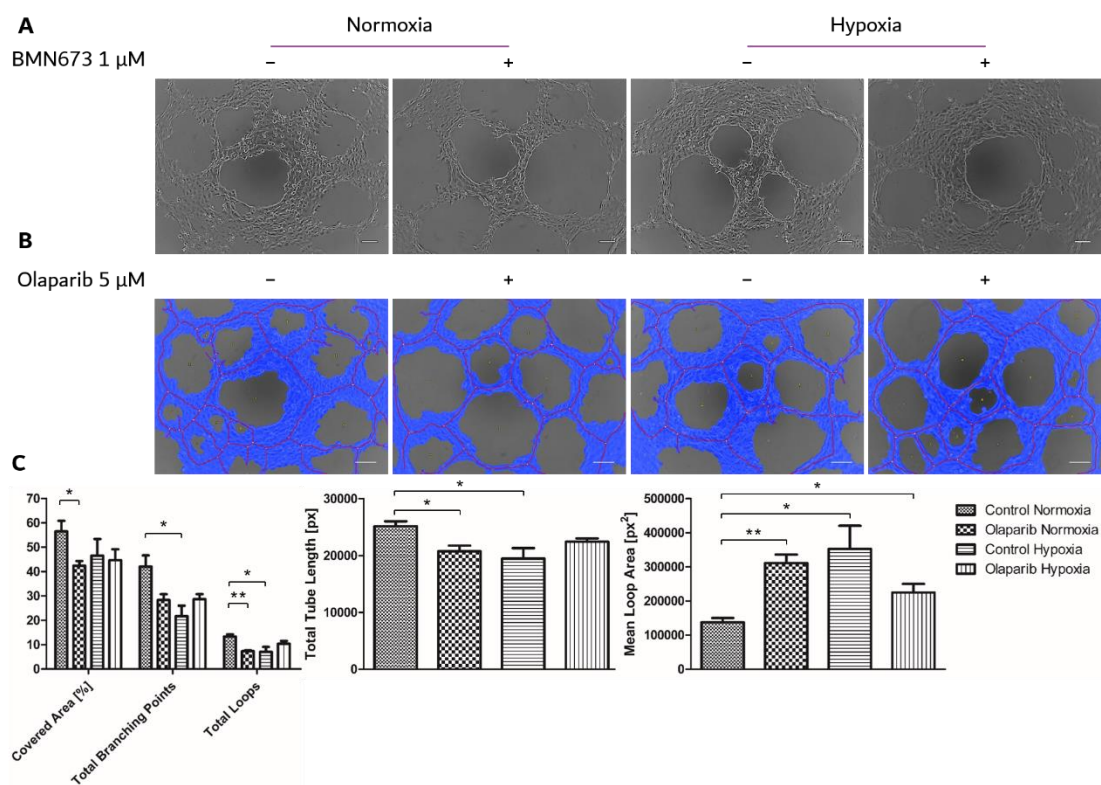
Figure 28. PARPi and hypoxia modulate CM tube formation. C8161 were cultured on matrigel in the absence or presence of **A** BMN673 or **B** olaparib, and incubated in normoxia or hypoxia for 24 hours. **B-C** Tube formation parameters (covered area, branching points, loops, tube length and loop area) were quantified using the image analysis software WimTube (Wimasis). *: p<0.05; **: p< 0.01; ***: p< 0.001 (Student's t-test). Scale bar: 100 µM.

C8161 behaved slightly differently, as basal tube formation in this cell line (Figure 28) was already similar to a "normalized" network. Furthermore, in C8161 PARPi alone were enough to significantly reduce covered area

and total tube length, and to increase mean loop area (Figure 28C). Altogether, it seemed that PARP inhibition alone, without the contribution of hypoxia, could promote the normalized network pattern with narrow, dispersed and evenly distributed tubes in C8161. As previously discussed, VE-cadherin expression in C8161 is much higher than in Mum2B (Figure 11), suggesting a stronger vasculogenic transformation in C8161 that might explain different behavior on matrigel.

In any case, olaparib and hypoxia altered tube formation on matrigel by VM⁺ melanoma cell lines.

PARP inhibition and hypoxia modulate melanoma invasion in matrigel

The network morphology that we observed on matrigel after PARPi treatment and hypoxia prompted the hypothesis that PARP inhibition and hypoxia might somehow interfere with pseudovessel sprouting in our VM⁺ melanoma cell lines.
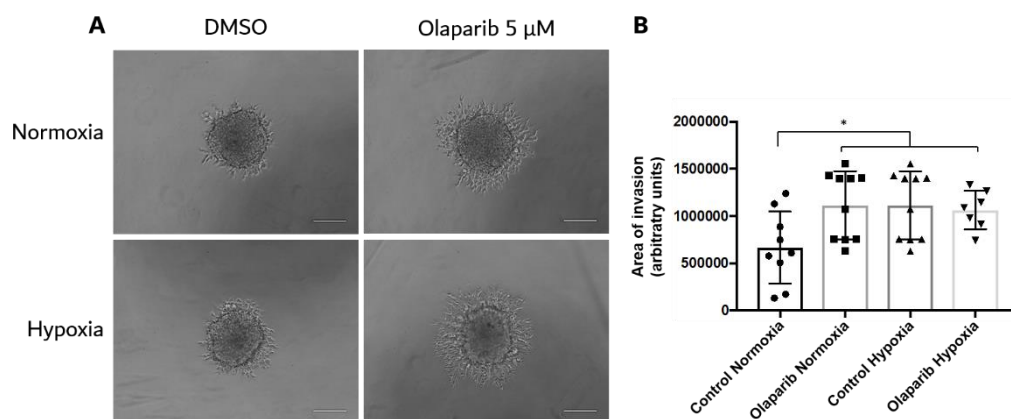
Figure 29. PARPi and hypoxia modulate Mum2B invasion. **A** Mum2B spheroids were generated on agarose and then cultured on matrigel, treated with DMSO or olaparib and incubated in normoxia or hypoxia for 24 hours. **B** The area of invasion was quantified on ImageJ. *: $p < 0.05$. Scale bar: 100 µM.

In the case of actual ECs, sprouting potential can be assessed by culturing endothelial spheroids in some kind of extracellular matrix equivalent, such

as matrigel. This environment triggers endothelial tip cell formation and endothelial sprouting and individual sprouts can be counted and measured as quantitative parameters of sprouting ability. With this purpose, we cultured VM+ melanoma spheroids in matrigel in the absence and presence of olaparib and hypoxia. However, the assay did not go as expected; in spite of the vasculogenic traits of these cell lines, Mum2B and C8161 spheroids did not give rise to discrete sprouts. Instead, they invaded the matrigel, in accordance to their aggressive metastatic origin (Figure 29A). The area of invasion was quantified for Mum2B, and it was increased in every condition with respect to the normoxic control (Figure 29B).

Therefore, olaparib and hypoxia may modulate melanoma cell invasive ability. On the other hand, analyzing tip cell sprouting in VM+ cell lines requires a different approach.

Involvement of pericytes in tube formation by VM+ melanoma cells

The RNAseq revealed a number of vascular genes that were upregulated by olaparib and hypoxia. One of them was particularly noteworthy: PDGFB, which is crucial in pericyte recruitment and hence in blood vessel maturation[240]. In tumor vasculature, pericyte coverage is generally regarded as a sign of vascular normalization[238].

As shown above, we confirmed by qPCR that PDGFB expression is upregulated by olaparib and hypoxia alone but especially in combination (Figure 18A-B). Furthermore, PDGFβ secretion measured by ELISA was significantly increased by olaparib too, especially during hypoxia (Figure 18C). Therefore, we hypothesized that PARP inhibition might play a role in the recruitment of pericytes to VM pseudovessels.

In an attempt to evaluate if pericytes interacted with VM networks on matrigel, and whether this interaction was modulated by PARP inhibition and hypoxia, we decided to co-culture Mum2B with human brain vascular pericytes. Prior to that, we needed a way to distinguish one cell type from the other in the co-culture. Therefore, we used lentiviral vectors to transduce RFP to Mum2B and GFP to pericytes, generating stably fluorescent cell lines.

We then co-cultured RFP-Mum2B with GFP-pericytes on matrigel in the absence or presence of olaparib and hypoxia, and took images of the resulting tube formation on a fluorescent microscope (Figure 30). As reported by other authors[342], pericytes successfully integrated in the VM networks.
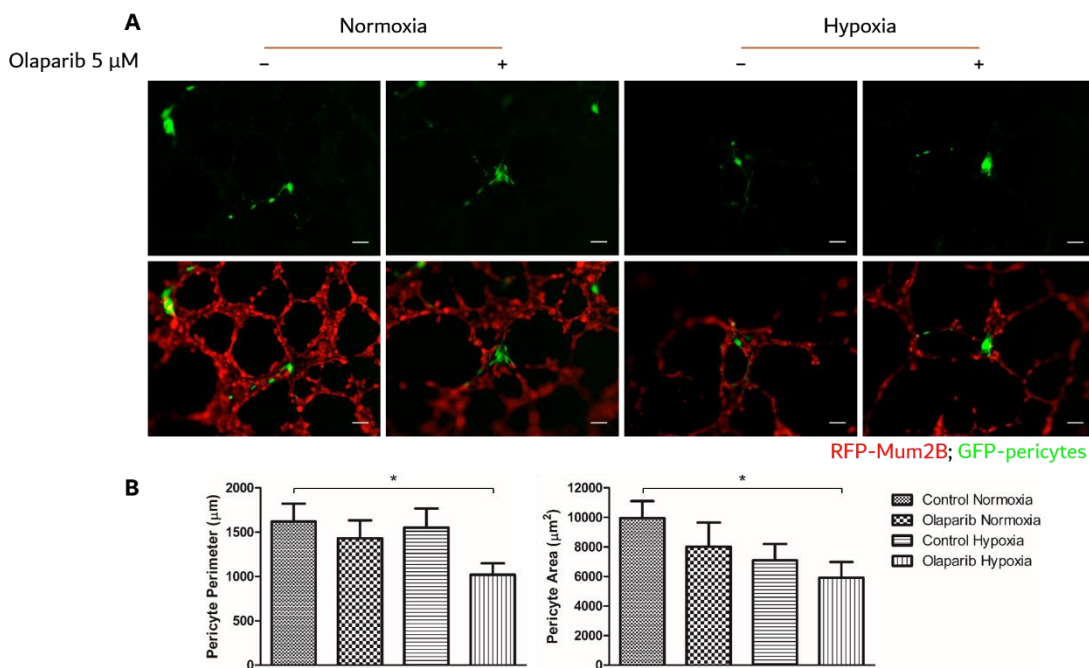
Figure 30. Pericytes take part in UM VM networks on matrigel. **A** Mum2B and pericytes were stably transduced with lentiviral vectors coding for RFP or GFP, respectively. Fluorescent cell lines were co-cultured on matrigel at a proportion of 20:1, treated with DMSO or olaparib and incubated in normoxia or hypoxia for 24 hours. **B** Pericyte parameter and area were quantified on ImageJ. *: $p < 0.05$ (Student's t-test). Scale bar: 100 μM.

However, this method does not allow a proper measurement of pericyte recruitment, since the amount of pericytes added to the co-culture is fixed. Alternatively, we could assess Mum2B-pericyte association, quantifying the perimeter and the area of pericytes as a measure of the surface of interaction and their extension over the tubes (Figure 30B). Contrary to our expectations, both the perimeter and the area of pericytes gradually decreased with olaparib and hypoxia, reaching a statistically significant reduction in the combination treatment. However, observation under the microscope indicated that the treatment with olaparib during hypoxia

might affect the viability of the pericytes, which often had a completely spherical shape, sometimes located within VM loops without interacting with any other cells. Therefore, the decreased interaction might not be due to decreased pericyte recruitment signals from Mum2B, but to a poor adaptation of pericytes to the experimental conditions.

Generation of human UM xenografts in mice

All the limitations that we found working *in vitro* encouraged us to try an *in vivo* approach.

We generated human UM xenografts using the cell lines Mum2B and Mum2C as a model of VM$^+$ and VM$^-$ UM, respectively. UM cells were injected subcutaneously into immunocompromised mice. Tumor volumes were measured regularly in the next few days. When they reached a size of approximately 100 mm^3, tumor-bearing mice were randomized for further treatment with vehicle or olaparib (50 mg/kg) for each cell line. Mice were treated three times a week for three weeks' time.

PARP inhibition does not affect tumor growth *in vivo* but it affects the incidence of metastasis in a VM context

Upon sacrifice, tumors were measured, harvested and fixed for further investigations, and mice were explored for the presence of metastasis.

Tumor size was similar in all the experimental groups, with no significant effect that could be attributed to treatment or to the different cell lines (Figure 31A). Nevertheless, there were some important qualitative differences between Mum2B- and Mum2C-derived tumors. Mum2C local tumors appeared to be tightly encapsulated and clearly delimited from surrounding tissues, whereas Mum2B tumors looked more invasive, sometimes with no clear boundaries between tumor and healthy tissue. Secondly, Mum2C tumors looked unusually bloody, which could indicate vascularization issues.

On the other hand, careful examination of internal organs revealed a variation in the incidence of metastasis in the different experimental groups (Figure 31B). Firstly, in the vehicle groups, fewer Mum2C-bearing

mice presented metastasis than Mum2B-bearing mice, which is consistent with the different invasive appearances. However, this difference was not statistically significant. Secondly, treatment with olaparib reduced the incidence of metastasis in both cell lines to the same baseline of only 1 mouse with metastasis. This reduction was statistically significant in Mum2B mice. Furthermore, treatment with olaparib seemed to affect not only the presence of metastasis but also the size of metastatic tumors: as shown in Figure 31C, the only metastasis found in Mum2B-bearing mice treated with olaparib was considerably smaller than metastases found in mice treated with vehicle. All metastases in the different groups were found in the peritoneal cavity.
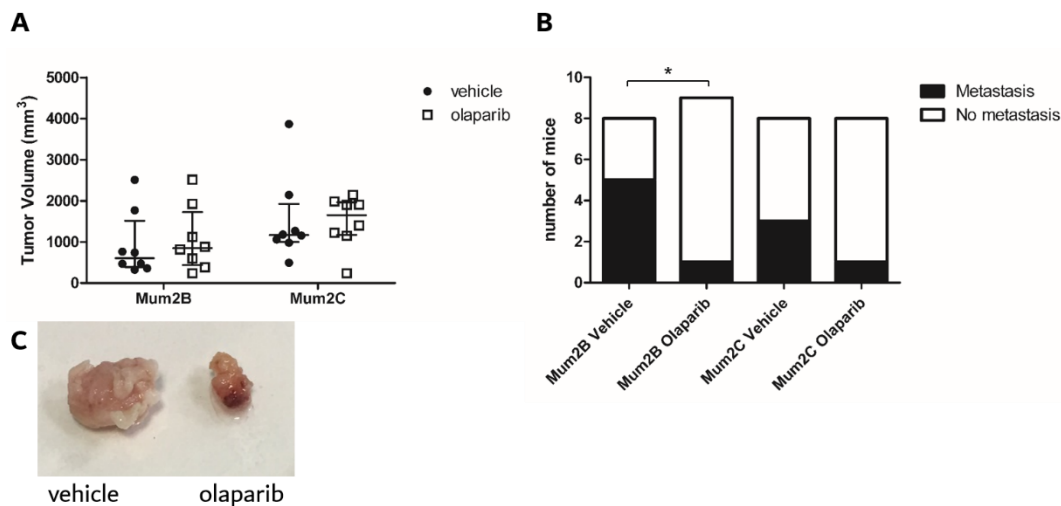
Figure 31. PARP inhibition affects the incidence and size of UM metastasis *in vivo*. Human subcutaneous UM xenografts were generated in immunocompromised mice, which were then treated with vehicle or olaparib (50 mg/kg) for three weeks. **A** Final tumor volume was measured with a caliper in all mice before sacrifice. There were no significant differences among the different experimental groups. **B** Upon sacrifice, mice were dissected and explored for the presence of metastasis. **C** Mum2B metastases harvested from vehicle- and olaparib-treated mice.

Thus, PARP inhibition had a role in controlling the metastatic spread of VM+ UM tumors.

Mum2B- but not Mum2C-derived tumors present VM pseudovessels *in vivo*
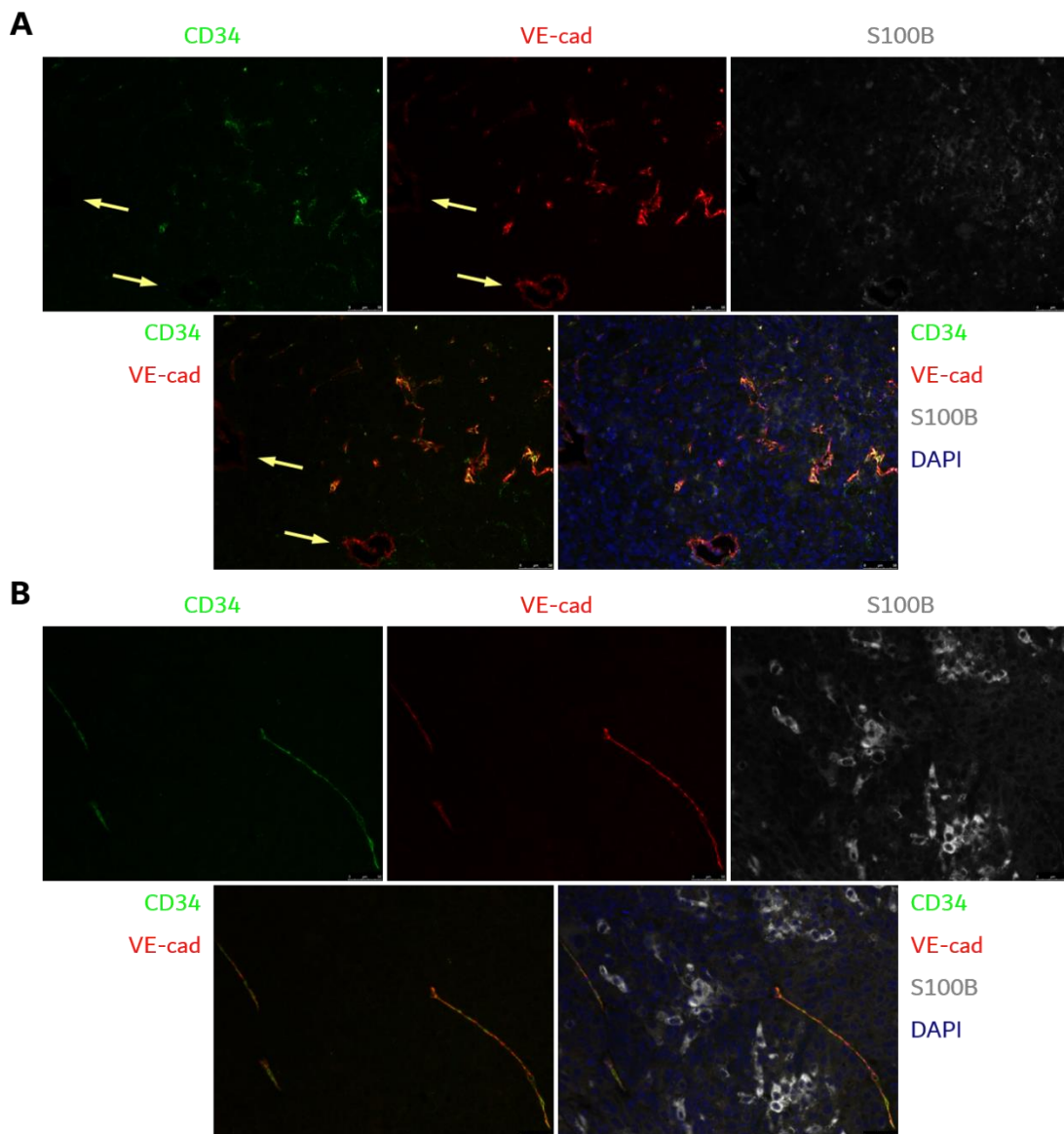
Figure 32. Tumor vasculature in human UM xenografts. **A** Mum2B and **B** Mum2C tumor sections were co-immunostained for CD34, VE-cadherin and S100B. Arrows show CD34⁻/VE-cadherin⁺ VM pseudovessels.

Harvested tumors were immediately fixed in formalin and subsequently embedded in paraffin at the Anatomical Pathology Department of the

University of Granada, by the team of Dr Francisco O'Valle. Tumor samples were then sectioned and stained at the Histology Unit of Dr Peter Carmeliet research group, and images were acquired at their facilities.

In order to identify VM pseudovessels among the tumor vasculature, co-immunofluorescent stainings for CD34, VE-cadherin and S100B were performed (Figure 32). CD34 was considered an EC specific marker, while S100B was used as a melanoma cell marker. VE-cadherin is expressed in both ECs and VM$^+$ melanoma cells, so its co-localization with either CD34 or S100B should serve as a discerning feature between true endothelial vessels and VM pseudovessels.

Microscopic imaging revealed remarkable differences in tumor vasculature from Mum2B compared to Mum2C tumors. To begin with, CD34$^-$/VE-cadherin$^+$ VM pseudovessels were found in all of Mum2B tumors (Figure 32A, arrows), but not in Mum2C tumors (Figure 32B). As previously reported[300], VM formation seemed to be specially abundant in the peripheral region of the tumors. Moreover, the overall morphology of blood vessels was notably different; while the vessels in Mum2B tumors were highly sinuous and irregular, Mum2C tumors were dominated by straight blood vessels. However, Mum2C tumors had a very high infiltration of erythrocytes, with many regions of what we identified as blood lakes. This is consistent with the bloody appearance that Mum2C tumors had when first harvested, and it suggests that their apparently improved blood vessel morphology does not suffice to maintain a normal irrigation and blood flow.

Tumor hypoxia is not affected by VM or PARP inhibition *in vivo*

Tumor hypoxia is a very important sign of tumor prognosis, as well as of tumor vessel functionality, so we were very interested in evaluating this parameter in our UM xenografts.

For this purpose, pimonidazole hydrochloride (60 mg/kg) was injected in tumor-bearing mice 60 min prior to sacrifice. Pimonidazole forms covalent adducts with thiol groups in hypoxic conditions, so the presence of these

adducts can serve as a marker of hypoxic regions. Pimonidazole adducts were detected in tumor samples using hypoxyprobe (Figure 33A-D).
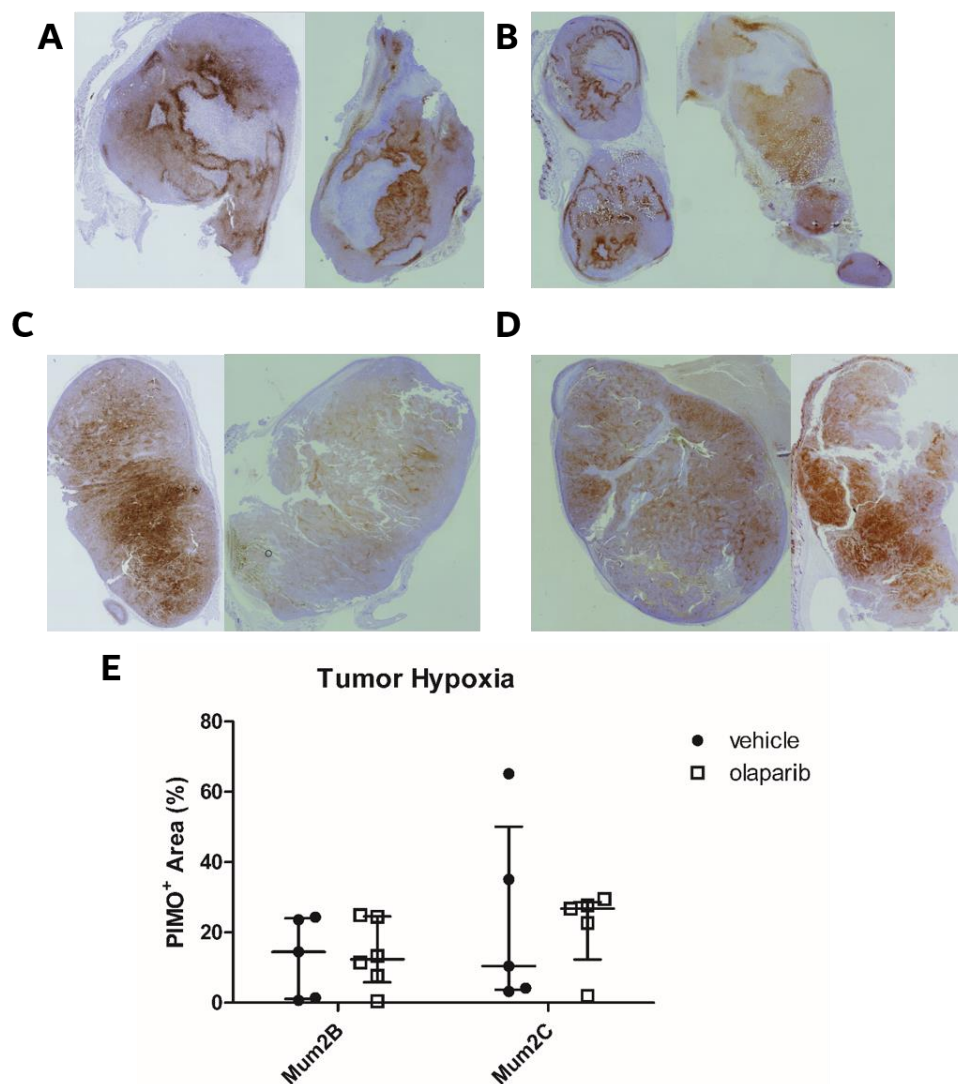
Figure 33. Tumor hypoxia is not affected by VM or olaparib in human UM xenografts. Tumor-bearing mice received an intraperitoneal injection of pimonidazole hydrochloride (60 mg/kg) 60 min before sacrifice. **A-B** Mum2B and **C-D** Mum2C tumor sections were stained with hypoxyprobe for the detection of pimonidazole adducts (brown). **A** and **C** were treated with vehicle. **B** and **D** were treated with olaparib. **E** No significant differences in tumor hypoxia were detected among the different experimental groups.

Neither the presence of VM nor olaparib treatment seemed to affect overall tumor hypoxia in our human UM xenografts (Figure 33E).

Pericyte association to VM pseudovessels *in vivo*

Another vascular parameter that we were interested in was pericyte recruitment. As discussed above, PARP inhibition promoted the expression and secretion of PDGFβ in VM⁺ melanoma cells (Figure 18), which might be related to pericyte recruitment. We showed that pericytes interacted with VM networks *in vitro* (Figure 30), but we needed to confirm whether this association took place in an *in vivo* environment as well.
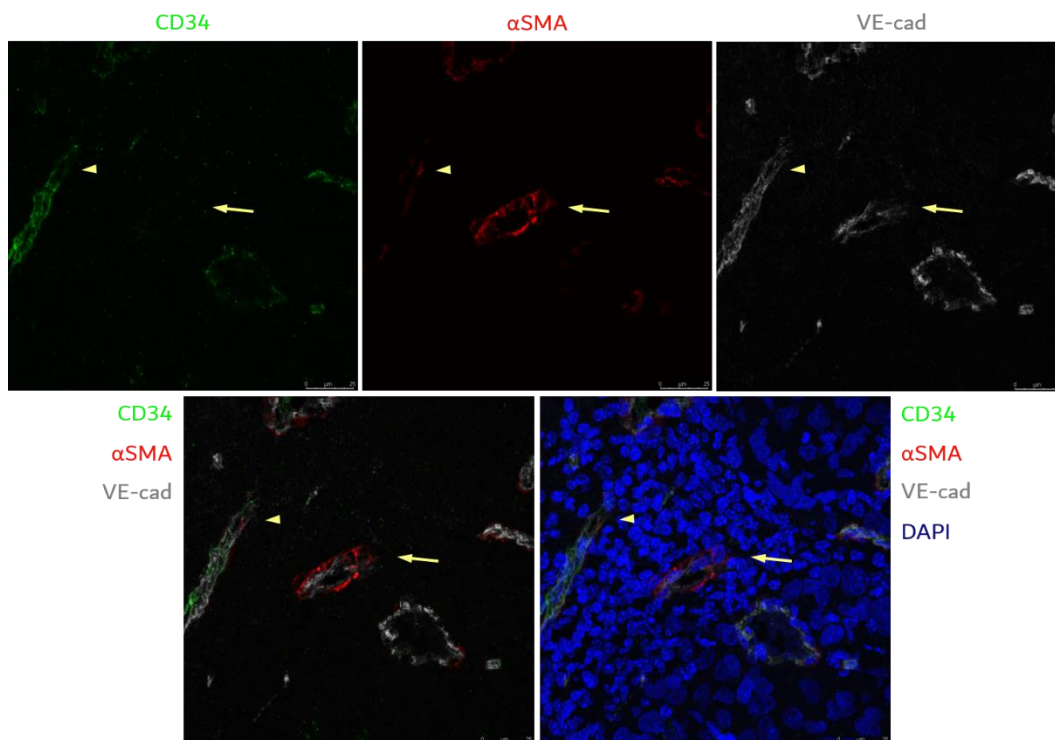
Figure 34. Pericyte association to EC and VM pseudovessels *in vivo*. Mum2B tumor sections were co-immunostained for CD34, αSMA and VE-cadherin. Arrowheads show a CD34⁺/VE-cadherin⁺ endothelial vessel covered by pericytes (αSMA⁺). Arrows show a CD34⁻/VE-cadherin⁺ VM pseudovessel that is covered by pericytes (αSMA⁺).

Tumor samples were subjected to co-immunofluorescent stainings for CD34, VE-cadherin and the mural cell marker αSMA (Figure 34). In this model, CD34/VE-cadherin/αSMA co-localization can be considered as pericyte coverage in endothelial vessels, while CD34$^-$/VE-cadherin$^+$/αSMA$^+$ staining indicates pericyte coverage in VM pseudovessels.

Indeed, examination of Mum2B tumor sections under a fluorescent microscope revealed the association of pericytes to VM pseudovessels *in vivo* (Figure 34, arrow), supporting the observations of Thijssen et al[342].

PARP inhibition has opposing effects on pericyte recruitment to EC vs VM vessels *in vivo*

In order to assess a possible influence of olaparib on pericyte recruitment, pericyte coverage in Mum2B tumor vessels was quantified on ImageJ (Figure 35).

Taking all vessels together, global pericyte coverage did not seem to vary between olaparib- and vehicle-treated mice (Figure 35A). However, significant differences could be detected if we analyzed endothelial and VM vessels separately. In the case of CD34$^+$/VE-cadherin$^+$ vessels, that is, genuine endothelial vessels, the results showed that median pericyte recruitment was reduced after olaparib treatment (Figure 35B). Surprisingly, when we focused our attention on VM CD34$^-$/VE-cadherin$^+$ pseudovessels we observed a different outcome: olaparib significantly increased median pericyte coverage of VM pseudovessels (Figure 35C). The results concerning VM are consistent with our *in vitro* results about PDGFβ expression and secretion, but the involvement of pericytes in endothelial vessels in response to olaparib requires further research.

Thus, PARP inhibition increased pericyte recruitment specifically to VM pseudovessels, but it had the opposite effect on pericyte recruitment to endothelial vessels.
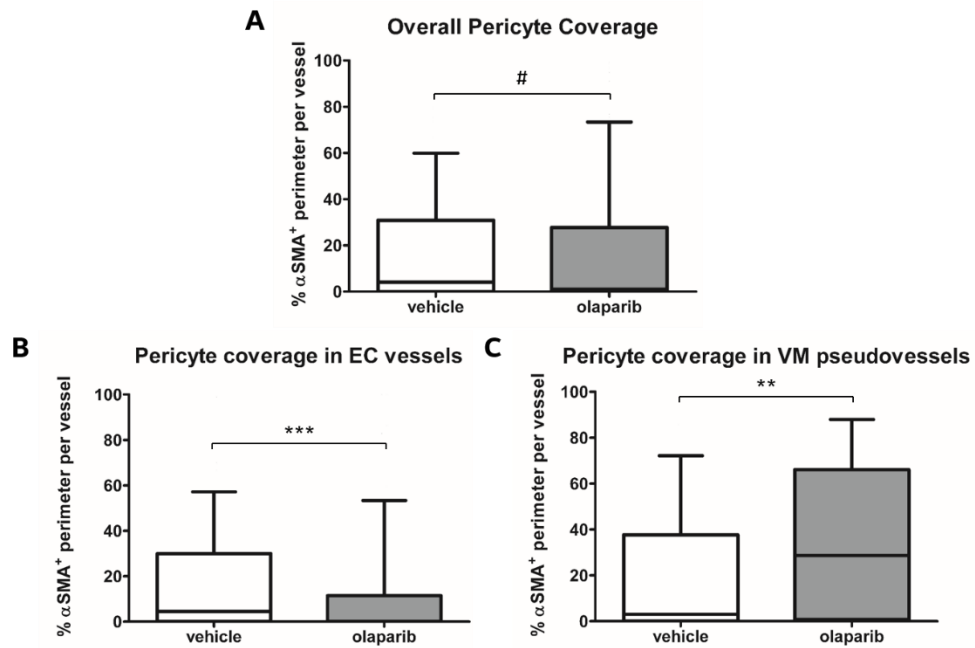
Figure 35. PARP inhibition has opposing effects on pericyte recruitment to EC vs VM vessels *in vivo*. Pericyte coverage in Mum2B tumor vasculature was measured on ImageJ as the percentage of **A** VE-cad$^+$, **B** CD34$^+$/VE-cadherin$^+$ or **C** CD34$^-$/VE-cadherin$^+$ vessel perimeter that co-localized with αSMA. #: non-significant; **: p<0.01; ***: p<0.001 (two-tailed Mann Whitney test).

DISCUSSION

DISCUSSION

Cancer affects millions of people around the world. Decades of research have uncovered a great amount of knowledge concerning cancer biology, but cancer is still the second leading cause of death worldwide, and the predicted trend for future years is anything but hopeful. Melanoma comprises a number of malignancies all derived from melanocytes. CM is the most prevalent type of melanoma, and it is the cancer type whose incidence has grown the most in recent decades. UM is not as prevalent but it is the most frequent eye cancer in adults, and its high metastatic risk makes it a very aggressive cancer type[7]. Current therapies have proved insufficient in the management of both CM and UM, meaning that more research is required in order to discover new therapeutic opportunities.

Though cancer research focused all the attention on tumor cells for a long time, the notion that tumors are simply a mass of cancer cells is currently outdated[3]. The last few decades have seen a growing interest in the study of other cell types present within tumor tissues. Among these, ECs that take part in tumor vasculature have been one of the main pillars of recent cancer investigations.

The purpose of this thesis was centered on studying tumor vascularization as carried out by tumor cells themselves. This is possible due to the ability of highly aggressive tumor cells to acquire a plastic phenotype, expressing cell markers and mirroring behaviors typical of other cell types, namely of ECs[366]. This is the core of the VM process, where cancer cells acquire endothelial traits and develop vessel-like structures capable of carrying blood without the participation of ECs[300]. This pseudovessel architecture favors the escape of tumor cells into the bloodstream, which is a preliminary step of metastatic spread. For all these reasons, VM is associated with metastasis, resistance to antiangiogenic therapies and poor prognosis in cancer patients[299]. However, the molecular mechanisms that support VM development remain poorly understood.

A critical initiator of VM, angiogenesis and many other malignant processes is tumor hypoxia[185,299]. As a result, tumor hypoxia is a prominent marker of poor prognosis. The hypoxia response is mediated by HIF, whose

stability and function have been shown to be influenced by PARP1 and parylation[129–132]. PARP1 is best-known for its role in DNA repair, although PARP1 has been implicated in many other cellular processes, including the regulation of gene expression[80]. Moreover, our group showed that PARP inhibition could modulate tube formation *in vitro* and decrease the phosphorylation of non-vascular VE-cadherin on Y658[327]. VE-cadherin plays a pivotal role in VM development[299], and we have recently reported that its phosphorylation on Y658 is crucial in VM formation[324], which raises PARP inhibition as an attractive opportunity for the targeting of VM. Various PARPi, among them olaparib, are already approved for the treatment of several cancer types in certain patients, highlighting their clinical relevance and safety[104].

This thesis aims to explore the consequences of PARP inhibition in the context of melanoma VM, which could expand the therapeutic benefit of PARPi in cancer treatment while potentially targeting a malignant trait which so far remains untreatable. Our study resolves that PARP inhibition has a wide effect on VM+ tumor cells especially under hypoxic conditions, favoring a phenotype that allows tumor cells to not just mimic vessel formation but also to emulate blood vessel maturation, namely by promoting pericyte recruitment.

Modulation of VM signaling by PARP1 and hypoxia

We have previously reported that VE-cadherin is constitutively expressed and phosphorylated on Y658 in VM+ UM and CM cells[324]. This is abnormal for two reasons: (1) VE-cadherin expression is supposed to be specific of ECs; and (2), in an EC context, VE-cadherin is only phosphorylated upon specific stimuli, like histamine or VEGF[321,326]. During VM, VE-cadherin is phosphorylated on Y658 by FAK[324], so the reason for this constitutive phosphorylation could be the hyperactivation of FAK in response to constitutive GNAQ/11 signaling in melanoma[74]. In ECs, the phosphorylation status of VE-cadherin is a central regulator of vessel permeability[321], and in tumors it is associated with increased tumor cell transmigration across the endothelial barrier and so with metastasis[326]. In tumor cells, we reported that pY658-VE-cadherin promoted the VM malignant phenotype[324].

DISCUSSION

In this study, we have shown that the phosphorylation of VE-cadherin on Y658 was greatly enhanced in hypoxic conditions. This effect seemed to be mediated by HIF1α, since HIF1α knockdown reduced pY658-VE-cadherin. Interestingly, hypoxia has been shown to decrease pY658-VE-cadherin in ECs via the HIF2α-mediated upregulation of the endothelial-specific phosphatase VE-PTP, revealing another way in which VE-cadherin regulation differs in ECs compared to a VM context.

Consistent with previous results[327], PARP inhibition as well as PARP1 knockdown reduced pY658-VE-cadherin, and we found that this can happen not only normoxia but also in hypoxia. The molecular mechanism that may lead to decreased phosphorylation of a plasma membrane protein after the inhibition of nuclear PARP remains unexplored. The direct phosphorylation of VE-cadherin is attributed to a number of kinases, such as FAK, Pyk2 or Src[321,322,324,326]. Since PARP1 can be implicated in the modulation of gene expression at multiple levels, we could assume that PARPi-mediated changes in gene expression may interfere with the expression or activation of these kinases. However, RNAseq results did not show a direct downregulation of any of these kinases after olaparib treatment, so PARPi must alter the expression of some other protein upstream of the mentioned kinases.

Integrins are prominent activators of FAK[367]. A few of them (ITGA2, ITGB3 and ITGB2) were found to be modulated by olaparib in our RNAseq, though in all cases they suffered an upregulation, which should lead to increased FAK activity and hence pY658-VE-cadherin. During hypoxia, olaparib downregulated ezrin, which is another activator of FAK[368]. Nevertheless, olaparib did not affect the expression of ezrin in normoxia, so the reduction of pY658-VE-cadherin by PARPi during normoxia remains unexplained. Similarly, VE-PTP, which directly dephosphorylates VE-cadherin in ECs[369], was found to be upregulated by olaparib plus hypoxia, providing another possible explanation for the olaparib-mediated decrease of pY658-VE-cadherin in hypoxia but not in normoxia. Zlot et al reported that stanniocalcin 1 (STC1) could inhibit hepatocyte growth factor (HGF)- but not VEGF-induced activation of FAK[370]. Data from our RNAseq show that STC1 is upregulated by olaparib

in normoxia and hypoxia, but whether STC1 plays a role in regulating FAK during VM remains unknown.

In any case, hypoxia is posed as a promoter of VM-related melanoma malignancy through the increase of pY658-VE-cadherin, while PARPi can restrain this phosphorylation and the pro-malignant VM signaling that it initiates. Moreover, based on the observations of endothelial vasculature, decreased VE-cadherin phosphorylation might lead to decreased pseudovessel permeability, therefore reducing the high metastatic potential provided by VM pseudovessels.

Transcriptional modulation of UM gene expression by olaparib and hypoxia and role of lncRNA

Our –omics approach to understand the role of PARPi and hypoxia in the modulation of VM led to the identification of thousands of genes that were regulated by these factors during tube formation *in vitro*. Interestingly, the combination of olaparib plus hypoxia resulted in the significant modulation of over 2,000 genes that were not modulated by olaparib or hypoxia alone. This suggests that there may be some kind of additive or synergistic interaction between PARPi and hypoxia. Remarkably, olaparib treatment during hypoxia resulted in the modulation of at least 84 genes related to the vascular function, so much so that GSEA highlighted a number of vasculature-related pathways that were significantly modulated in this condition compared to normoxic controls: vasculature development, endothelium development, blood vessel morphogenesis and endothelial cell differentiation, among others. A closer inspection of the RNAseq data as well as the validation carried out for some of the pertinent genes revealed that PARP inhibition during hypoxia mostly promoted an upregulation of vasculature-related genes, suggesting that the combination of PARPi and hypoxia can enhance the endothelial-like phenotype of VM$^+$ tumor cells.

As to the question of how PARP inhibition can have such a widespread effect on gene expression, there can be multiple reasons. Firstly, PARP1 has been implicated in the regulation of chromatin structure by histone modifications and chromatin insulators[115–118], among others. Furthermore,

DISCUSSION

PARP1 can alter the transcriptional activity of sequence-specific transcription factors, including HIFs[129–132]. Here, we propose that PARP inhibition affects the transcriptional activity of ETS1 and MZF1, RHOXF1 and/or NR2C2, resulting in the differential expression of a number of lncRNA, which in turn might regulate gene expression themselves.

Indeed, several reports have correlated PARP1 with some of these transcription factors, specifically ETS1[371,372] and myeloid zinc finger 1 (MZF1)[373]. ETS1 was the founding member of the ETS domain family of transcription factors. It has been repeatedly implicated in cancer progression, since it promotes a number of malignant traits such as invasion and EMT. More importantly for the purpose of this thesis, ETS1 can play an important role in angiogenesis, contributing to EC survival and enhancing VEGF dependent transcription[374–376]. Reportedly, ETS1 interacts with and is parylated by PARP1. PARP inhibition was shown to promote ETS1 nuclear translocation and transcriptional activity[371]. This is consistent with our results in VM+ tumor cells, where all lncRNAs that were upregulated by olaparib contained binding sites for ETS1 in their promoters. On the other hand, MZF1 belongs to the SCAN-zinc finger family of transcription factors and it has also been associated with many cancer types. Reportedly, MZF1 expression can be upregulated by PARP1-mediated activation of the transcription factor E2F1, though the requirement of PARP1 activity for E2F1 activation is controversial[373,377]. In our model, PARP inhibition with olaparib downregulated the expression of lncRNAs whose promoters contained MZF1 binding sites, supporting a role for the parylation-dependent regulation of MZF1. In particular, PARP inhibition could presumably reduce the expression of MZF1 and hence of predicted MZF1 target lncRNAs. In principle, the modulation of just these two transcription factors could suffice to explain the effect of PARP inhibition on lncRNA expression, as ETS1 could be responsible for all the upregulated lncRNAs, while MZF1 could mediate the expression change in all the downregulated lncRNAs.

In total, PARP inhibition altered the expression of 20 lncRNAs, listed in Table 8. The expression of FLG-AS1, the most upregulated lncRNA in the list, has been associated to healthy oral mucosa compared to oral squamous cell carcinoma[378]. RP3-326I13.1 can be upregulated by DNA damage,

which is likely to happen after PARP inhibition in tumor cells, therefore explaining the upregulation of this lncRNA by olaparib treatment[379]. Three of the downregulated lncRNA are classed as small nucleolar RNA host genes (SNHG): SNHG1, SNHG15 and SNHG4. SNHG in general and these three in particular have been associated to cancer progression, malignancy and poor prognosis in a wide variety of cancer types[380–385], meaning that their olaparib-dependent decrease might reduce all these negative effects. RGMB-AS1 and MIR17HG, both downregulated by olaparib as well, have been implicated in plenty of cancer types too[386–388]. Altogether, it seems that olaparib treatment promotes a favorable lncRNA landscape, promoting the expression of lncRNAs correlated with healthy tissues, such as FLG-AS1, while decreasing the expression of a number of pro-malignant lncRNAs.

Surprisingly, we found that CNV alterations involving a few olaparib-responsive lncRNAs had a statistically significant correlation with alterations in very relevant tumor suppressors in samples from cancer patients. TP53, which codes for the renowned tumor suppressor p53, was altered in over half of the samples harboring FLG-AS1 amplification (192 out of 376 samples), though the biological significance of this correlation remains unknown. On the contrary, FLG-AS1 amplification seemed to be mutually exclusive with alterations in PTEN and IDH1. A more detailed inspection of cBioPortal pointed towards the differential incidence of all these alterations in distinct cancer types as the reason for the negative correlation; while PTEN and IDH1 alterations are especially frequent in endometrial carcinoma and glioma, respectively, FLG-AS1 amplifications occurred mostly in hepatocellular, breast and lung adenocarcinomas. VHL alterations were enriched in samples containing SNHG4 and/or PRR7-AS1 amplification. The loci for SNHG4 and PRR7-AS1 are located very close to each other in the long arm of chromosome 5. In consequence, any genomic alterations involving that region will probably affect both genes, which means that alterations in SNHG4 and PRR7-AS1 significantly co-occur and that is why they are both correlated with alterations in the same gene. Alterations in VHL, SNHG4 and PRR7-AS1 are most frequent in clear cell renal cell carcinoma, which might explain their correlation. VHL mutations are a well-known driver of renal cell carcinoma[389]. Interestingly, one report showed that SNHG4 can promote the progression

of this cancer type[390], though the correlation with VHL has not been investigated. To our knowledge, no reports have ever been published about PRR7-AS1. Lastly, samples with a deep deletion of RGMB-AS1 were significantly enriched for alterations in SPOP. Co-alteration of RGMB-AS1 and SPOP was restricted to prostate adenocarcinoma. SPOP mutations are classed as drivers of prostate adenocarcinoma, and they are correlated with deletions in chromodomain helicase DNA binding protein 1 (CHD1)[391]. Surprisingly, the loci for CHD1 and RGMB-AS1 are located in the same cytogenetic band of chromosome 5, so a deletion of that region always involves the loss of both genes. While the role of CHD1 deletion in prostate cancer has been investigated, no information has been published regarding the loss of RGMB-AS1 in this cancer type.

Although we cannot provide any firm biological argument for these correlations or easily guess the implication of PARP inhibition with them, the unquestionable importance of all these tumor suppressor genes encourages further research into this topic. Moreover, it is noteworthy that many of the mutations listed above, such as PTEN, IDH1 or SPOP mutations have been reported to sensitize tumor cells to treatment with PARPi[392–396].

On a final note, as far as lncRNA are concerned, we tried to investigate the overall effect that the change in lncRNA landscape triggered by olaparib could have on gene expression. We used the database lncMAP to predict what and how many transcription factors and subsequent target genes might be influenced by changes in the expression of olaparib-responsive lncRNA. Although lncRNA are known for their high cell type specificity, it was reported that a subset of lncRNA-dependent perturbations in gene expression are conserved across many cancer types. Moreover, cancer types of a similar tissue origin shared more lncRNA-mediated transcriptional perturbations[362]. Based on this, and in the absence of a UM cohort, we chose the CM cohort to estimate the transcriptional significance of olaparib-responsive lncRNAs. Although the search only showed five genes whose expression was actually modulated by olaparib in our UM model, it could give us a general idea of how much the gene expression profile can be affected by the modulation of lncRNA expression in response to olaparib in a given cancer type.

Focusing on tumor vasculature again, we found a few genes with a great relevance in vascular biology that were upregulated by olaparib plus hypoxia in both of our VM+ melanoma cell lines, namely NRP1, Tie1 and PDGFB.

NRP1 is a transmembrane receptor than can bind multiple ligands. Importantly, NRP1 can act as a co-receptor of VEGFR2 for the binding of VEGF, increasing VEGF/VEGFR2-mediated signaling[397]. As a result, NRP1 has a key importance in vasculogenesis and angiogenesis[398–400]. In particular, it has been repeatedly associated with the promotion of endothelial tip cell formation and migration, having a crucial role in the formation of filopodia and also guiding directional migration of endothelial sprouts.[214,215,220,401,402]. In fact, overexpression of NRP1 in mice was shown to induce excessive capillary and blood vessel formation[403]. However, increased expression of NRP1 in our VM models after olaparib plus hypoxia was accompanied by a reduction in the number of branching points during tube formation on matrigel, resulting in sparser tubular networks. Unfortunately, our attempt to have a better understanding of tip cell formation and sprouting in VM cells did not work as expected; our sprouting assay ended up being an invasion assay, so we could not evaluate the impact of olaparib and hypoxia on tip cell formation. On the other hand, if we adhere to the evidence that NRP1 promotes tip cell formation, there must be a mechanism over-compensating for NRP1 in our VM models so that the overall result is a decrease in tube branching. In other words, if a decrease in branching is not caused by reduced tip cell formation, we should consider the possibility that it may be caused by increased vessel regression. This hypothesis is proposed for future studies.

Tie1 is an endothelial receptor analogous to Tie2. Their intracellular domains share over 75% similarity, but their extracellular domains are only 30% similar. As a result, Tie2 is a well-characterized receptor for ANGPTs, but not Tie1[290]. In fact, Tie1 was classed as an orphan receptor for decades, until a recent publication described the ability of leukocyte cell-derived chemotaxin 2 (LECT2) to bind Tie1[404]. Despite its inability to anchor ANGPTs, Tie1 has proved very important in vascular biology. The

function of Tie1 depends on its ability to dimerize with Tie2, although whether this dimerization activates or attenuates ANGPT/Tie2-dependent signaling is not clear, and it could be context-dependent[405–408]. In tumor vasculature, Tie1 has been mostly associated to tumor progression and metastasis through the inhibition of Tie2-mediated vascular stabilization and normalization, while Tie1 deletion or blockage have been shown to reduce tumor growth and metastasis[291,409,410]. In fact, the abnormal expression of Tie1 in VM[+] UM was described in Maniotis's initial report about VM[300]. This contrasts with early studies that highlighted a vital role of Tie1 in promoting the structural integrity of embryonic blood vessels[411]. Moreover, Garcia et al showed that Tie1 deficiency triggered endothelial–mesenchymal transition (EndoMT)[412], a process where ECs undergo a partial loss of EC markers and to acquire mesenchymal-like characteristics. EndoMT can promote tumor malignancy through the generation of cancer-associated fibroblasts and also by favoring tumor cell transendothelial migration, a pre-requisite for metastasis[413]. Therefore, the deficiency of Tie1 may have detrimental consequences in cancer. Notably, our research group reported that PARP inhibition could inhibit EndoMT[327], which is consistent with an upregulation of Tie1 by PARPi, as reported here. With all this information, the effect that olaparib-induced Tie1 could have on VM is unclear. On the one hand, Tie1 reportedly inhibits Tie2-dependent vessel normalization, but on the other hand the tubular networks that we observed after PARPi and hypoxia resembled a normalized vessel architecture. Most importantly, PARP inhibition reduced metastasis in our *in vivo* models. As in the case of NRP1, further research is required to elucidate the exact role of Tie1 in VM and to find out whether other molecular mechanisms may compensate for increased Tie1 expression after olaparib treatment.

In the case of PDGFB, our results are more consistent with the available literature. PDGFβ, whose expression and secretion were upregulated by olaparib, is well-known for its crucial role in pericyte recruitment[240]. Although *in vitro* experiments suggested a decreased interaction between Mum2B and pericytes in the olaparib plus hypoxia condition, this seemed to be the result of reduced pericyte viability, which could be due to the general maladaptation of pericytes to *in vitro* culture. Indeed, *in vivo* experiments demonstrated significantly increased pericyte recruitment to

VM pseudovessels in olaparib-treated mice, consistent with a higher expression and secretion of PDGFβ by VM$^+$ UM cells induced by olaparib treatment.

Human UM xenografts in mice could offer essential information regarding the potential of olaparib as an antitumor agent in VM$^+$ tumors. We observed that neither PARP inhibition nor the presence of VM had any impact on the local growth of subcutaneous tumors. Bearing in mind that neither of the cell lines that we used shows signs of BRCAness, it is not surprising that PARP inhibition did not affect tumor growth.

However, we could see important differences in the incidence of metastasis. In vehicle-treated mice, Mum2B-bearing mice (VM$^+$) had a slightly higher incidence of metastasis than Mum2C-bearing mice (VM$^-$), implying a pro-metastatic potential of VM, although this difference was not statistically significant. In Mum2C-bearing mice, treatment with olaparib caused a slight, non-significant reduction of metastasis. A trend towards reduced metastasis in response to PARP inhibition in a non-BRCAness and non-VM context could be attributed to other effects of PARP inhibition, such as decreased inflammation, decreased EndoMT or decreased stemness[122,327,414]. Interestingly, treatment with olaparib triggered a significant reduction of metastasis in Mum2B-bearing mice. Since this significant reduction did not happen in VM$^-$ Mum2C-derived tumors, we propose that the ability of PARPi to reduce metastasis may rely more specifically on the presence of VM.

The staining of tumor sections with endothelial marker CD34, dual EC/VM marker VE-cadherin and mural cell marker αSMA revealed the presence of pericytes in VM pseudovessels, as already reported by Thijssen et al[342]. Surprisingly, olaparib treatment had opposing effects on pericyte recruitment: pericyte coverage was reduced in endothelial vessels, whereas it was increased in VM pseudovessels. Improved pericyte recruitment to VM pseudovessels is consistent with our results concerning PDGFB. As for endothelial vessels, we are still investigating whether PARP inhibition modulates PDGFB and pericyte recruitment in ECs in a non-VM context. In the meantime, the reason for the opposite outcomes in EC- and tumor cell-derived vessels found within Mum2B tumors can

DISCUSSION

only be hypothesized. Presumably, PARP inhibition will predominantly affect tumor cells rather than other cells, since the genomic instability inherent to cancer cells triggers DNA damage-mediated PARP activation. Therefore, PARP inhibition would enact the molecular mechanisms leading to PDGFB upregulation in VM tumor cells but not in ECs, leading to a promotion of pericyte recruitment specifically towards VM pseudovessels. However, overall pericyte coverage was not affected by olaparib treatment, meaning that no new pericytes joined the tumor vasculature in response to olaparib. Instead, we found a decrease in the pericyte coverage of endothelial vessels. Altogether, these findings suggest that there might be a competition between endothelial and VM vessels for the recruitment of the pericytes available within a certain tumor. In this situation, the presence of olaparib, by promoting PDGFβ signals specifically in VM cells, would favor pericyte coverage in VM, hence shifting the tumor pericyte population towards VM pseudovessels and away from endothelial vessels. This could also explain why tumor hypoxia did not change in response to olaparib: the positive effect derived from improved VM pseudovessels would be counteracted by the negative effect caused by endothelial vessel abnormalization.

In any case, improved pericyte coverage of VM pseudovessels accompanied by reduced pY658-VE-cadherin after PARP inhibition might induce some degree of pseudovessel normalization that may well be the reason for reduced metastasis after olaparib treatment. This highlights the importance of VM in metastatic spread: even though pericyte coverage of endothelial vessels was reduced and tumor hypoxia did not change, apparent normalization of VM vessels still diminished the incidence of metastasis. A more certain way to confirm that differential pericyte coverage is responsible for the reduced metastatic incidence after olaparib would be the generation of PDGFB-KO VM[+] cell lines. In this way, we could develop PDGFB-wildtype and PDGFB-KO VM[+] tumor xenografts, and evaluate the effect of olaparib on metastatic spread in both groups; if olaparib could decrease the metastasis of PDGFB-wildtype but not PDGFB-KO tumors, we could assume that the impact of olaparib on the metastasis of VM[+] tumors depends on pericyte coverage.

The combination of PARPi as VM normalizing agents with EC vessel normalizing drugs would be of great interest for future research as well. Hopefully, the combined treatment might induce pericyte recruitment and vessel normalization in both types of vasculature, and lead to a more effective reduction of metastasis. On the contrary, the combination of normalizing agents might balance the competition for pericytes, decreasing the proportion of pericyte-covered VM pseudovessels compared to single treatment with olaparib. Still, it is a possibility very much worth exploring.

	↑ Vasculogenic gene expression ↑↑	
↑	Melanoma tube branching	↓
↑	Melanoma tube density	↓
↑	pY658-VE-cadherin	↓
↓	Melanoma PDGFβ	↑
?	EC PDGFβ	?
↓	VM pericyte coverage	↑
↓	EC pericyte coverage	↓↓
↑	Tumor hypoxia	↑
↑	Tumor growth	↑
↑	Metastatic spread	↓
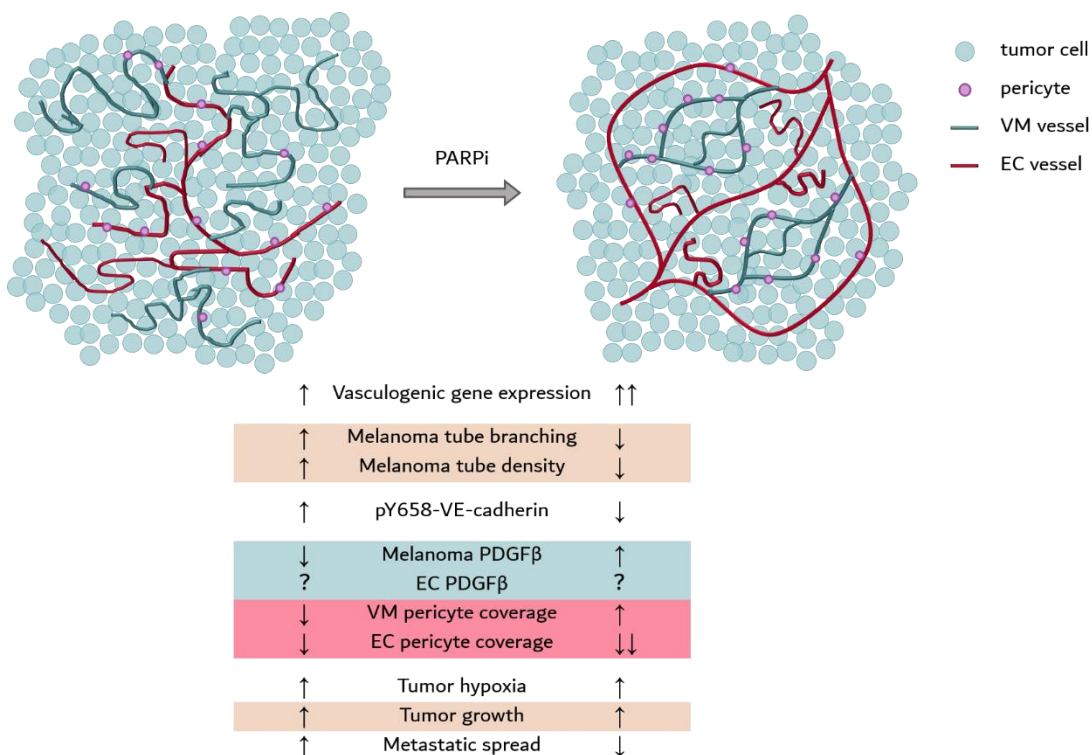
Figure 36. PARP inhibition modulates VM in melanoma. PARP inhibition in VM⁺ melanoma cells induces a number of changes (pro-vasculogenic gene expression, reduced pY658-VE-cadherin, increased PDGFβ) that may favor a partial normalization of VM pseudovessels, as illustrated by increased pericyte recruitment *in vivo*. Altogether, these changes lead to reduced metastasis in VM⁺ tumors.

In summary, our study reveals a role for PARP1 in the regulation of melanoma VM, especially during hypoxia, whether artificial *in vitro* hypoxia or *in vivo* tumor hypoxia. *In vitro*, PARP inhibitor olaparib

significantly modulated the expression of hundreds of genes during tube formation on matrigel, partly through the modulation of the lncRNA expression landscape. PARP inhibition during hypoxia significantly modulated the expression of over 80 genes implicated in vascular biology, resulting in the global modulation of a number of vasculature-related signaling pathways and seemingly enhancing the endothelial-like characteristics of VM⁺ melanoma cells. Moreover, PARP1 chemical inhibition or genetic knockdown reduced the phosphorylation of VE-cadherin on Y658. This reduction may hinder pro-malignant VM signaling and potentially decrease pseudovessel permeability by improving VE-cadherin adhesions. Adding in an upregulation of PDGFβ expression and secretion by olaparib, it would seem that treatment with PARPi favors a mature endothelial-like phenotype. Indeed, melanoma tubular networks on matrigel seemed to undergo a certain degree of structural normalization after PARP inhibition. Finally, olaparib treatment resulted in improved pericyte coverage of VM pseudovessels *in vivo*, concomitant with a decrease in the incidence and size of metastatic VM⁺ tumors. In conclusion, PARP inhibition may reduce metastatic spread in the context of VM by inducing VM pseudovessel normalization.

CONCLUSIONS

CONCLUSIONS

1. PARP inhibition and hypoxia modulate the expression of thousands of genes during melanoma tube formation on matrigel.

2. The combination of hypoxia plus PARP inhibition during tube formation results in the global transcriptional modulation of signaling pathways implicated in vascular biology, seemingly enhancing the endothelial-like characteristics of VM+ melanoma cells.

3. PARP inhibition modulates the lncRNA expression landscape during melanoma tube formation, possibly by regulating transcription factors ETS1 and MZF1.

4. The modulation of the lncRNA expression landscape can predictedly affect the expression of many other genes in melanoma, amplifying the effect of PARP inhibition on gene expression.

5. Hypoxia increases the phosphorylation of VE-cadherin on Y658, whereas PARP inhibitors and PARP1 knockdown decrease this phosphorylation.

6. PARP inhibition increases the expression and secretion of PDGFβ, especially during hypoxia.

7. PARP inhibition during hypoxia modulates melanoma tube formation on matrigel, inducing a network architecture that resembles vessel normalization.

8. PARP inhibition *in vivo* improved the pericyte coverage of VM pseudovessels specifically, while reducing the pericyte coverage of endothelial vessels in VM+ tumors.

9. PARP inhibition reduced the incidence and size of metastasis specifically in VM+ tumor xenografts.

REFERENCES

REFERENCES

1. Vogelstein, B. & Kinzler, K. W. Cancer genes and the pathways they control. *Nature Medicine* vol. 10 789–799 (2004).

2. Hanahan, D. & Weinberg, R. A. The Hallmarks of Cancer. *Cell* vol. 100 57–70 (2000).

3. Hanahan, D. & Weinberg, R. A. Hallmarks of Cancer: The Next Generation. *Cell* vol. 144 646–674 (2011).

4. Washington, C. M. & Leaver, D. *Principles and Practice of Radiation Therapy.* (2015).

5. Skeel, R. T. & Khleif, S. N. *Handbook of Cancer Chemotherapy.* (Lippincott Williams & Wilkins, 2011).

6. Shain, A. H. & Bastian, B. C. From melanocytes to melanomas. *Nature Reviews Cancer* vol. 16 345–358 (2016).

7. Pandiani, C., Béranger, G. E., Leclerc, J., Ballotti, R. & Bertolotto, C. Focus on cutaneous and uveal melanoma specificities. *Genes and Development* vol. 31 724–743 (2017).

8. Pingault, V. *et al.* Review and update of mutations causing Waardenburg syndrome. *Human Mutation* vol. 31 391–406 (2010).

9. Lavezzo, M. M. *et al.* Vogt-Koyanagi-Harada disease: Review of a rare autoimmune disease targeting antigens of melanocytes. *Orphanet Journal of Rare Diseases* vol. 11 1–21 (2016).

10. Yamaguchi, Y. & Hearing, V. J. Melanocytes and their diseases. *Cold Spring Harb. Perspect. Med.* **4**, a017046 (2014).

11. Albano, L. *et al.* Primary sellar melanocytoma: pathological, clinical and treatment review. *Journal of Endocrinological Investigation* vol. 43 575–585 (2020).

12. Hu, D. N., Yu, G., McCormick, S. A. & Finger, P. T. Population-Based Incidence of Conjunctival Melanoma in Various Races and Ethnic Groups and Comparison With Other Melanomas. *Am. J. Ophthalmol.* **145**, 418-423.e1 (2008).

13. Triay, E., Bergman, L., Nilsson, B., All-Ericsson, C. & Seregard, S. Time trends in the incidence of conjunctival melanoma in Sweden. *Br. J. Ophthalmol.* **93**, 1524–1528 (2009).

14. Yu, G. P., Hu, D. N., McCormick, S. & Finger, P. T. Conjunctival melanoma: Is it increasing in the United States? *Am. J. Ophthalmol.* **135**, 800–806 (2003).

15.   Postow, M. A., Hamid, O. & Carvajal, R. D. Mucosal melanoma: Pathogenesis, clinical behavior, and management. *Curr. Oncol. Rep.* **14**, 441–448 (2012).

16.   McLaughlin, C. C. *et al.* Incidence of noncutaneous melanomas in the U.S. *Cancer* **103**, 1000–1007 (2005).

17.   Bai, X. *et al.* MAPK pathway and TERT promoter gene mutation pattern and its prognostic value in melanoma patients: A retrospective study of 2,793 cases. *Clin. Cancer Res.* **23**, 6120–6128 (2017).

18.   Chi, Z. *et al.* Clinical presentation, histology, and prognoses of malignant melanoma in ethnic Chinese: A study of 522 consecutive cases. *BMC Cancer* **11**, 1–10 (2011).

19.   Schadendorf, D. *et al.* Melanoma. *Nat. Rev. Dis. Prim.* **1**, 1–20 (2015).

20.   Ossio, R., Roldán-Marín, R., Martínez-Said, H., Adams, D. J. & Robles-Espinoza, C. D. Melanoma: A global perspective. *Nature Reviews Cancer* vol. 17 393–394 (2017).

21.   Bevona, C. *et al.* Cutaneous Melanomas Associated with Nevi. *Archives of Dermatology* vol. 139 1620–1624 (2003).

22.   Gandini, S. *et al.* Meta-analysis of risk factors for cutaneous melanoma: I. Common and atypical naevi. *Eur. J. Cancer* **41**, 28–44 (2005).

23.   Abbasi, N. R. *et al.* Early diagnosis of cutaneous melanoma: Revisiting the ABCD criteria. *Journal of the American Medical Association* vol. 292 2771–2776 (2004).

24.   Grob, J. J. & Bonerandi, J. J. The 'Ugly Duckling' Sign: Identification of the Common Characteristics of Nevi in an Individual as a Basis for Melanoma Screening. *Arch. Dermatol.* **134**, 103-a-104 (1998).

25.   Shaikh, W. R., Xiong, M. & Weinstock, M. A. The contribution of nodular subtype to melanoma mortality in the United States, 1978 to 2007. *Arch. Dermatol.* **148**, 30–36 (2012).

26.   Scolyer, R. A., Long, G. V. & Thompson, J. F. Evolving concepts in melanoma classification and their relevance to multidisciplinary melanoma patient care. *Mol. Oncol.* **5**, 124–136 (2011).

27.   Demierre, M. F., Chung, C., Miller, D. R. & Geller, A. C. Early detection of thick melanomas in the United States: Beware of the nodular subtype. *Arch. Dermatol.* **141**, 745–750 (2005).

28.   Kalkhoran, S. *et al.* Historical, clinical, and dermoscopic characteristics of thin nodular melanoma. *Arch. Dermatol.* **146**, 311–318 (2010).

29.   Liu, W. *et al.* Rate of growth in melanomas: Characteristics and associations of rapidly growing melanomas. *Archives of Dermatology* vol. 142 1551–1558 (2006).

REFERENCES

30.   Lattanzi, M. *et al.* Primary Melanoma Histologic Subtype: Impact on Survival and Response to Therapy. *JNCI J. Natl. Cancer Inst.* **111**, 180–188 (2019).

31.   Allais, B. S. *et al.* Five-Year Survival in Patients with Nodular and Superficial Spreading Melanomas in the US Population. *J. Am. Acad. Dermatol.* **0**, (2020).

32.   DeWane, M. E., Kelsey, A., Oliviero, M., Rabinovitz, H. & Grant-Kels, J. M. Melanoma on chronically sun-damaged skin: Lentigo maligna and desmoplastic melanoma. *Journal of the American Academy of Dermatology* vol. 81 823–833 (2019).

33.   Chen, Y. A. *et al.* Translational pathology, genomics and the development of systemic therapies for acral melanoma. *Seminars in Cancer Biology* vol. 61 149–157 (2020).

34.   Bradford, P. T., Goldstein, A. M., McMaster, M. L. & Tucker, M. A. Acral lentiginous melanoma: Incidence and survival patterns in the United States, 1986-2005. *Arch. Dermatol.* **145**, 427–434 (2009).

35.   Phan, A. *et al.* Acral lentiginous melanoma: a clinicoprognostic study of 126 cases. *Br. J. Dermatol.* **155**, 561–569 (2006).

36.   Minagawa, A., Omodaka, T. & Okuyama, R. Melanomas and Mechanical Stress Points on the Plantar Surface of the Foot. *N. Engl. J. Med.* **374**, 2404–2406 (2016).

37.   Bastian, B. C. The molecular pathology of melanoma: An integrated taxonomy of melanocytic neoplasia. *Annu. Rev. Pathol. Mech. Dis.* **9**, 239–271 (2014).

38.   Holderfield, M., Deuker, M. M., McCormick, F. & McMahon, M. Targeting RAF kinases for cancer therapy: BRAF-mutated melanoma and beyond. *Nature Reviews Cancer* vol. 14 455–467 (2014).

39.   Davies, H. *et al.* Mutations of the BRAF gene in human cancer. *Nature* **417**, 949–954 (2002).

40.   The Genome Cancer Atlas Network. Genomic Classification of Cutaneous Melanoma. *Cell* **161**, 1681–1696 (2015).

41.   Subbiah, V., Baik, C. & Kirkwood, J. M. Clinical Development of BRAF plus MEK Inhibitor Combinations. *Trends in Cancer* vol. 6 797–810 (2020).

42.   Li, S., Balmain, A. & Counter, C. M. A model for RAS mutation patterns in cancers: finding the sweet spot. *Nature Reviews Cancer* vol. 18 767–777 (2018).

43.   Moore, A. R., Rosenberg, S. C., McCormick, F. & Malek, S. RAS-targeted therapies: is the undruggable drugged? *Nature Reviews Drug Discovery* vol. 19 533–552 (2020).

44.   Vigil, D., Cherfils, J., Rossman, K. L. & Der, C. J. Ras superfamily GEFs and GAPs: Validated and tractable targets for cancer therapy? *Nature Reviews*

Cancer vol. 10 842–857 (2010).

45. Singh, A. D., Turell, M. E. & Topham, A. K. Uveal melanoma: Trends in incidence, treatment, and survival. *Ophthalmology* **118**, 1881–1885 (2011).

46. Weis, E., Shah, C. P., Lajous, M., Shields, J. A. & Shields, C. L. The association between host susceptibility factors and uveal melanoma: A meta-analysis. *Arch. Ophthalmol.* **124**, 54–60 (2006).

47. Virgili, G. *et al.* Incidence of Uveal Melanoma in Europe. *Ophthalmology* **114**, 2309-2315.e2 (2007).

48. Singh, A. D. & Topham, A. Survival rates with uveal melanoma in the United States: 1973-1997. *Ophthalmology* **110**, 962–965 (2003).

49. Kujala, E., Mäkitie, T. & Kivelä, T. Very Long-Term Prognosis of Patients with Malignant Uveal Melanoma. *Investig. Ophthalmol. Vis. Sci.* **44**, 4651–4659 (2003).

50. Shields, C. L. *et al.* Metastasis of uveal melanoma millimeter-by-millimeter in 8033 consecutive eyes. *Arch. Ophthalmol.* **127**, 989–998 (2009).

51. Diener-West, M. *et al.* Development of metastatic disease after enrollment in the COMS trials for treatment of choroidal melanoma: Collaborative Ocular Melanoma Study Group Report No. 26. *Arch. Ophthalmol.* **123**, 1639–1643 (2005).

52. Midena, E., De Belvis, V., Dei Tos, A. P. & Antonini, C. Isolated brain metastasis of malignant choroidal melanoma 27 years after enucleation. *Arch. Ophthalmol.* **117**, 1553–1556 (1999).

53. Gragoudas, E. S. *et al.* Survival of Patents with Metastases from Uveal Melanoma. *Ophthalmology* **98**, 383–390 (1991).

54. Chattopadhyay, C. *et al.* Uveal melanoma: From diagnosis to treatment and the science in between. *Cancer* **122**, 2299–2312 (2016).

55. Van Raamsdonk, C. D. *et al.* Mutations in GNA11 in Uveal Melanoma. *N. Engl. J. Med.* **363**, 2191–2199 (2010).

56. Campbell, A. P. & Smrcka, A. V. Targeting G protein-coupled receptor signalling by blocking G proteins. *Nature Reviews Drug Discovery* vol. 17 789–803 (2018).

57. Takasaki, J. *et al.* A novel Gαq/11-selective inhibitor. *J. Biol. Chem.* **279**, 47438–47445 (2004).

58. Schrage, R. *et al.* The experimental power of FR900359 to study Gq-regulated biological processes. *Nat. Commun.* **6**, 1–17 (2015).

59. Robertson, A. G. *et al.* Integrative Analysis Identifies Four Molecular and Clinical Subsets in Uveal Melanoma. *Cancer Cell* **32**, 204-220.e15 (2017).

REFERENCES

60. Moore, A. R. *et al.* Recurrent activating mutations of G-protein-coupled receptor CYSLTR2 in uveal melanoma. *Nat. Genet.* **48**, 675–680 (2016).

61. Goldsmith, Z. G. & Dhanasekaran, D. N. G Protein regulation of MAPK networks. *Oncogene* vol. 26 3122–3142 (2007).

62. Van Raamsdonk, C. D. *et al.* Frequent somatic mutations of GNAQ in uveal melanoma and blue naevi. *Nature* **457**, 599–602 (2009).

63. Yu, F. X. *et al.* Regulation of the Hippo-YAP pathway by G-protein-coupled receptor signaling. *Cell* **150**, 780–791 (2012).

64. Zhao, B., Li, L., Lei, Q. & Guan, K. L. The Hippo-YAP pathway in organ size control and tumorigenesis: An updated version. *Genes and Development* vol. 24 862–874 (2010).

65. Yu, F. X. *et al.* Mutant Gq/11 promote uveal melanoma tumorigenesis by activating YAP. *Cancer Cell* **25**, 822–830 (2014).

66. Li, H. *et al.* YAP/TAZ Activation Drives Uveal Melanoma Initiation and Progression. *Cell Rep.* **29**, 3200-3211.e4 (2019).

67. Prescher, G. *et al.* Prognostic implications of monosomy 3 in uveal melanoma. *Lancet* **347**, 1222–1225 (1996).

68. Harbour, J. W. *et al.* Frequent mutation of BAP1 in metastasizing uveal melanomas. *Science (80-.).* **330**, 1410–1413 (2010).

69. Gupta, M. P. *et al.* Clinical characteristics of uveal melanoma in patients with germline BAP1 mutations. *JAMA Ophthalmol.* **133**, 881–887 (2015).

70. Carbone, M. *et al.* Biological Mechanisms and Clinical Significance of BAP1 Mutations in Human Cancer. *Cancer discovery* vol. 10 1103–1120 (2020).

71. Martin, M. *et al.* Exome sequencing identifies recurrent somatic mutations in EIF1AX and SF3B1 in uveal melanoma with disomy 3. *Nat. Genet.* **45**, 933–936 (2013).

72. Harbour, J. W. *et al.* Recurrent mutations at codon 625 of the splicing factor SF3B1 in uveal melanoma. *Nat. Genet.* **45**, 133–135 (2013).

73. Chen, X. *et al.* Combined PKC and MEK inhibition in uveal melanoma with GNAQ and GNA11 mutations. *Oncogene* **33**, 4724–4734 (2014).

74. Feng, X. *et al.* A Platform of Synthetic Lethal Gene Interaction Networks Reveals that the GNAQ Uveal Melanoma Oncogene Controls the Hippo Pathway through FAK. *Cancer Cell* **35**, 457-472.e5 (2019).

75. Paradis, J. S. *et al.* Synthetic Lethal Screens Reveal Co-Targeting FAK and MEK as a Multimodal Precision Therapy for GNAQ-Driven Uveal Melanoma. *Clin. Cancer Res.* clincanres.3363.2020 (2021) doi:10.1158/1078-0432.ccr-20-3363.

76. Brown, N. F. *et al.* A study of the focal adhesion kinase inhibitor GSK2256098 in patients with recurrent glioblastoma with evaluation of tumor penetration of [11 C]GSK2256098. *Neuro. Oncol.* **20**, 1634–1642 (2018).

77. Onken, M. D. *et al.* Targeting nucleotide exchange to inhibit constitutively active G protein a subunits in cancer cells. *Sci. Signal.* **11**, (2018).

78. Lapadula, D. *et al.* Effects of oncogenic Gαq and Gα11 inhibition by FR900359 in uveal melanoma. *Mol. Cancer Res.* **17**, 963–973 (2019).

79. Annala, S. *et al.* Direct targeting of Gαq and Gα11 oncoproteins in cancer cells. *Sci. Signal.* **12**, 5948 (2019).

80. Gupte, R., Liu, Z. & Kraus, W. L. PARPs and ADP-ribosylation: Recent advances linking molecular functions to biological outcomes. *Genes Dev.* **31**, 101–126 (2017).

81. Chambon, P., Weill, J. D. & Mandel, P. Nicotinamide mononucleotide activation of a new DNA-dependent polyadenylic acid synthesizing nuclear enzyme. *Biochem. Biophys. Res. Commun.* **11**, 39–43 (1963).

82. Chambon, P., Weill, J. D., Doly, J., Strosser, M. T. & Mandel, P. On the formation of a novel adenylic compound by enzymatic extracts of liver nuclei. *Biochem. Biophys. Res. Commun.* **25**, 638–643 (1966).

83. Nishizuka, Y., Ueda, K., Nakazawa, K. & Hayaishi, O. Studies on the polymer of adenosine diphosphate ribose: I. Enzymic formation from nicotinamide adenine dinuclotide in mammalian nuclei. *J. Biol. Chem.* **242**, 3164–3171 (1967).

84. Stone, P. R. & Shall, S. Poly(Adenosine Diphosphoribose) Polymerase in Mammalian Nuclei. Characterization of the Activity in Mouse Fibroblasts (LS Cells). *Eur. J. Biochem.* **38**, 146–152 (1973).

85. Dungan, S. M., Berger, B., Zervoudakis, R. J. & Dietrich, L. S. Solubilization and properties of poly(ADP-ribose) polymerases from bovine spleen and Ehrlich ascites cells. *BBA Sect. Nucleic Acids Protein Synth.* **374**, 220–237 (1974).

86. Smulson, M., Henriksen, O. & Rideau, C. Activity of polyadenosine diphosphoribose polymerase during the human cell cycle. *Biochem. Biophys. Res. Commun.* **43**, 1266–1273 (1971).

87. Fujimura, S., Hasegawa, S., Shimizu, Y. & Sugimura, T. Polymerization of the adenosine 5'-diphosphate-ribose moiety of nicotinamide-adenine dinucleotide by nuclear enzyme. I. Enzymatic reactions. *BBA Sect. Nucleic Acids Protein Synth.* **145**, 247–259 (1967).

88. Daniels, C. M., Ong, S. E. & Leung, A. K. L. The Promise of Proteomics for the Study of ADP-Ribosylation. *Molecular Cell* vol. 58 911–924 (2015).

REFERENCES

89.   Rack, J. G. M., Palazzo, L. & Ahel, I. (ADP-ribosyl)hydrolases: Structure, function, and biology. *Genes and Development* vol. 34 263–284 (2020).

90.   Reeder, R. H., Ueda, K., Honjo, T., Nishizuka, Y. & Hayaishi, O. Studies on the polymer of adenosine diphosphate ribose: II. Characterization of the polymer. *J. Biol. Chem.* **242**, 3172–3179 (1967).

91.   Miwa, M., Saikawa, N., Yamaizumi, Z., Nishimura, S. & Sugimura, T. Structure of poly(adenosine diphosphate ribose): Identification of 2'-[1'''-ribosyl-2''-(or 3''-)(1'''-ribosyl)]adenosine-5',5'',5'''-tris(phosphate) as a branch linkage. *Proc. Natl. Acad. Sci. U. S. A.* **76**, 595–599 (1979).

92.   Alemasova, E. E. & Lavrik, O. I. Poly(ADP-ribosyl)ation by PARP1: Reaction mechanism and regulatory proteins. *Nucleic Acids Research* vol. 47 3811–3827 (2019).

93.   Alvarez-Gonzalez, R. & Jacobson, M. K. Characterization of Polymers of Adenosine Diphosphate Ribose Generated in Vitro and in Vivo. *Biochemistry* **26**, 3218–3224 (1987).

94.   Ueda, K., Oka, J., Narumiya, S., Miyakawa, N. & Hayaishi, O. Poly ADP-ribose glycohydrolase from rat liver nuclei, a novel enzyme degrading the polymer. *Biochem. Biophys. Res. Commun.* **46**, 516–523 (1972).

95.   Tsopanakis, C., Leeson, E., Shall, S. & Tsopanakis, A. Purification and Properties of Poly(ADP-ribose) Polymerase from Pig-Thymus Nuclei. *Eur. J. Biochem.* **90**, 337–345 (1978).

96.   Kristensen, T. & Holtlund, J. Purification of Poly(ADP-ribose) Polymerase from Ehrlich Ascites Tumor Cells by Chromatography on DNA-Agarose. *Eur. J. Biochem.* **70**, 441–446 (1976).

97.   Okayama, H., Edson, C. M., Fukushima, M., Ueda, K. & Hayaishi, O. Purification and properties of poly(adenosine diphosphate ribose) synthetase. Role of histone in poly(ADP-ribose) synthesis. *J. Biol. Chem.* **252**, 7000–7005 (1977).

98.   Mandel, P., Okazaki, H. & Niedergang, C. Purification and properties of calf thymus polyadenosine diphosphate ribose polymerase. *FEBS Lett.* **84**, 331–336 (1977).

99.   Shieh, W. M. *et al.* Poly(ADP-ribose) polymerase null mouse cells synthesize ADP-ribose polymers. *J. Biol. Chem.* **273**, 30069–30072 (1998).

100.   Smith, S., Giriat, I., Schmitt, A. & De Lange, T. Tankyrase, a poly(ADP-ribose) polymerase at human telomeres. *Science (80-.).* **282**, 1484–1487 (1998).

101.   Johansson, M. A human poly(ADP-ribose) polymerase gene family (ADPRTL): cDNA cloning of two novel poly(ADP-ribose) polymerase homologues. *Genomics* **57**, 442–445 (1999).

102. Amé, J. C. *et al.* PARP-2, a novel mammalian DNA damage-dependent poly(ADP-ribose) polymerase. *J. Biol. Chem.* **274**, 17860–17868 (1999).

103. Hottiger, M. O., Hassa, P. O., Lüscher, B., Schüler, H. & Koch-Nolte, F. Toward a unified nomenclature for mammalian ADP-ribosyltransferases. *Trends in Biochemical Sciences* vol. 35 208–219 (2010).

104. Martí, J. M. *et al.* The Multifactorial Role of PARP-1 in Tumor Microenvironment. *Cancers (Basel).* **12**, (2020).

105. Ray Chaudhuri, A. & Nussenzweig, A. The multifaceted roles of PARP1 in DNA repair and chromatin remodelling. *Nature Reviews Molecular Cell Biology* vol. 18 610–621 (2017).

106. D'Amours, D., Desnoyers, S., D'Silva, I. & Poirier, G. G. Poly(ADP-ribosyl)ation reactions in the regulation of nuclear functions. *Biochem. J* **342**, 249–268 (1999).

107. Langelier, M. F., Servent, K. M., Rogers, E. E. & Pascal, J. M. A third zinc-binding domain of human poly(ADP-ribose) polymerase-1 coordinates DNA-dependent enzyme activation. *J. Biol. Chem.* **283**, 4105–4114 (2008).

108. Yu, X., Chini, C. C. S., He, M., Mer, G. & Chen, J. The BRCT Domain Is a Phospho-Protein Binding Domain. *Science (80-.).* **302**, 639–642 (2003).

109. Nishizuka, Y., Ueda, K., Honjo, T. & Hayaishi, O. Enzymic adenosine diphosphate ribosylation of histone and poly adenosine diphosphate ribose synthesis in rat liver nuclei. *J. Biol. Chem.* **243**, 3765–3767 (1968).

110. Otake, H., Miwa, M., Fujimura, S. & Sugimura, T. Binding of ADP-Ribose Polymer with Histone. *J. Biochem.* **65**, 145–146 (1969).

111. Nishizuka, Y. *et al.* Enzymic adenosine diphosphoribosylation of nuclear proteins. *Cold Spring Harb. Symp. Quant. Biol.* **34**, 781–786 (1969).

112. Mullins, D. W., Giri, C. P. & Smulson, M. Poly(adenosine diphosphate-ribose) Polymerase: The Distribution of a Chromosome-Associated Enzyme within the Chromatin Substructure. *Biochemistry* **16**, 506–513 (1977).

113. Poirier, G. G., De Murcia, G., Jongstra-Bilent, J., Niedergang, C. & Mandel, P. Poly(ADP-ribosyl)ation of polynucleosomes causes relaxation of chromatin structure. *Proc. Natd Acad. Sci. USA* **79**, 3423–3427 (1982).

114. Aubin, R. J. *et al.* Correlation between endogenous nucleosomal hyper(ADP-ribosyl)ation of histone H1 and the induction of chromatin relaxation. *EMBO J.* **2**, 1685–1693 (1983).

115. Krishnakumar, R. *et al.* Reciprocal binding of PARP-1 and histone H1 at promoters specifies transcriptional outcomes. *Science (80-.).* **319**, 819–821 (2008).

116. Krishnakumar, R. & Kraus, W. L. PARP-1 Regulates Chromatin Structure and

REFERENCES

Transcription through a KDM5B-Dependent Pathway. *Mol. Cell* **39**, 736–749 (2010).

117. De Vos, M. *et al.* Poly(ADP-ribose) polymerase 1 (PARP1) associates with E3 ubiquitin-protein ligase UHRF1 and modulates UHRF1 biological functions. *J. Biol. Chem.* **289**, 16223–16238 (2014).

118. Yu, W. *et al.* Poly(ADP-ribosyl)ation regulates CTCF-dependent chromatin insulation. *Nat. Genet.* **36**, 1105–1110 (2004).

119. Zhao, H. *et al.* PARP1- and CTCF-Mediated Interactions between Active and Repressed Chromatin at the Lamina Promote Oscillating Transcription. *Mol. Cell* **59**, 984–997 (2015).

120. Wright, R. H. G. *et al.* ADP-ribose-derived nuclear ATP synthesis by NUDIX5 is required for chromatin remodeling. *Science (80-.).* **352**, 1221–1225 (2016).

121. Gibson, B. A. *et al.* Chemical genetic discovery of PARP targets reveals a role for PARP-1 in transcription elongation. *Science (80-.).* **353**, 45–50 (2016).

122. Oliver, F. J. *et al.* Resistance to endotoxic shock as a consequence of defective NF-κB activation in poly (ADP-ribose) polymerase-1 deficient mice. *EMBO J.* **18**, 4446–4454 (1999).

123. Hassa, P. O., Buerki, C., Lombardi, C., Imhof, R. & Hottiger, M. O. Transcriptional Coactivation of Nuclear Factor-κB-dependent Gene Expression by p300 Is Regulated by Poly(ADP)-ribose Polymerase-1. *J. Biol. Chem.* **278**, 45145–45153 (2003).

124. Hassa, P. O. *et al.* Acetylation of poly(ADP-ribose) polymerase-1 by p300/CREB-binding protein regulates coactivation of NF-κB-dependent transcription. *J. Biol. Chem.* **280**, 40450–40464 (2005).

125. Hassa, P. O., Covic, M., Bedford, M. T. & Hottiger, M. O. Protein Arginine Methyltransferase 1 Coactivates NF-κB-Dependent Gene Expression Synergistically with CARM1 and PARP1. *J. Mol. Biol.* **377**, 668–678 (2008).

126. Gao, F., Kwon, S. W., Zhao, Y. & Jin, Y. PARP1 poly(ADP-ribosyl)ates Sox2 to control Sox2 protein levels and FGF4 expression during embryonic stem cell differentiation. *J. Biol. Chem.* **284**, 22263–22273 (2009).

127. Lai, Y. S. *et al.* SRY (sex determining region Y)-box2 (Sox2)/poly ADP-ribose polymerase 1 (Parp1) complexes regulate pluripotency. *Proc. Natl. Acad. Sci. U. S. A.* **109**, 3772–3777 (2012).

128. Weber, F. A., Bartolomei, G., Hottiger, M. O. & Cinelli, P. Artd1/Parp1 regulates reprogramming by transcriptional regulation of Fgf4 via Sox2 ADP-ribosylation. *Stem Cells* **31**, 2364–2373 (2013).

129. Elser, M. *et al.* Poly(ADP-ribose) polymerase 1 promotes tumor cell survival by coactivating hypoxia-inducible factor-1-dependent gene expression. *Mol.*

Cancer Res. **6**, 282–290 (2008).

130. Hulse, M. *et al.* Poly(ADP-ribose) polymerase 1 is necessary for coactivating hypoxia-inducible factor-1-dependent gene expression by Epstein-Barr virus latent membrane protein 1. *PLOS Pathog.* **14**, e1007394 (2018).

131. Martí, J. M. *et al.* Selective modulation by PARP-1 of HIF-1α-recruitment to chromatin during hypoxia is required for tumor adaptation to hypoxic conditions. *Redox Biol.* **41**, 101885 (2021).

132. Gonzalez-Flores, A. *et al.* Interaction between PARP-1 and HIF-2 in the hypoxic response. *Oncogene* **33**, 891–898 (2014).

133. Luo, X. *et al.* PARP-1 Controls the Adipogenic Transcriptional Program by PARylating C/EBPβ and Modulating Its Transcriptional Activity. *Mol. Cell* **65**, 260–271 (2017).

134. Miller, E. G. Stimulation of nuclear poly(adenosine diphosphate-ribose) polymerase activity from HeLa cells by endonucleases. *Biochim. Biophys. Acta* **395**, 191–200 (1975).

135. Berger, N. A., Sikorski, G. W., Petzold, S. J. & Kurohara, K. K. Association of poly(adenosine diphosphoribose) synthesis with DNA damage and repair in normal human lymphocytes. *J. Clin. Invest.* **63**, 1164–1171 (1979).

136. Skidmore, C. J. *et al.* The Involvement of Poly(ADP-ribose) Polymerase in the Degradation of NAD Caused by gamma-Radiation and N-Methyl-N-Nitrosourea. *Eur. J. Biochem.* **101**, 135–142 (1979).

137. Durkacz, B. W., Omidiji, O., Gray, D. A. & Shall, S. (ADP-ribose)n participates in DNA excision repair. *Nature* **283**, 593–596 (1980).

138. Benjamin, R. C. & Gill, D. M. Poly(ADP-ribose) synthesis in vitro programmed by damaged DNA. A comparison of DNA molecules containing different types of strand breaks. *J. Biol. Chem.* **255**, 10502–10508 (1980).

139. Gray, D. A., Durkacz, B. W. & Shall, S. Inhibitors of nuclear ADP-ribosyl transferase retard DNA repair after N-methyl-N-nitroso-urea. *FEBS Lett.* **131**, 173–177 (1981).

140. Nduka, N., Skidmore, C. J. & Shall, S. The Enhancement of Cytotoxicity of N-Methyl-N-nitrosourea and of γ-Radiation by Inhibitors of Poly(ADP-ribose) Polymerase. *Eur. J. Biochem.* **105**, 525–530 (1980).

141. Oikawa, A., Tohda, H., Kanai, M., Miwa, M. & Sugimura, T. Inhibitors of poly(adenosine diphosphate ribose) polymerase induce sister chromatid exchanges. *Biochem. Biophys. Res. Commun.* **97**, 1311–1316 (1980).

142. Hori, T. High incidence of sister chromatid exchanges and chromatid interchanges in the conditions of lowered activity of poly(ADP-ribose)polymerase. *Biochem. Biophys. Res. Commun.* **102**, 38–45 (1981).

REFERENCES

143. Ménissier, J. *et al.* Requirement of poly(ADP-ribose) polymerase in recovery from DNA damage in mice and in cells. *Proc. Natl. Acad. Sci. U. S. A.* **94**, 7303–7307 (1997).

144. Bièche, I., de Murcia, G. & Lidereau, R. Poly(ADP-ribose) Polymerase Gene Expression Status and Genomic Instability in Human Breast Cancer. *Clin. Cancer Res.* **2**, 1163–1167 (1996).

145. Simbulan-Rosenthal, C. M. *et al.* Chromosomal aberrations in PARP-/- mice: Genome stabilization in immortalized cells by reintroduction of poly(ADP-ribose) polymerase cDNA. *Proc. Natl. Acad. Sci. U. S. A.* **96**, 13191–13196 (1999).

146. Moschetta, M., George, A., Kaye, S. B. & Banerjee, S. BRCA somatic mutations and epigenetic BRCA modifications in serous ovarian cancer. *Annals of Oncology* vol. 27 1449–1455 (2016).

147. Wooster, R. & Weber, B. L. Breast and Ovarian Cancer. *N. Engl. J. Med.* **348**, 2339–2347 (2003).

148. Bryant, H. E. *et al.* Specific killing of BRCA2-deficient tumours with inhibitors of poly(ADP-ribose) polymerase. *Nature* **434**, 913–917 (2005).

149. Farmer, H. *et al.* Targeting the DNA repair defect in BRCA mutant cells as a therapeutic strategy. *Nature* **434**, 917–921 (2005).

150. McCabe, N. *et al.* Deficiency in the repair of DNA damage by homologous recombination and sensitivity to poly(ADP-ribose) polymerase inhibition. *Cancer Res.* **66**, 8109–8115 (2006).

151. Mateo, J. *et al.* A decade of clinical development of PARP inhibitors in perspective. *Ann. Oncol.* **30**, 1437–1447 (2019).

152. Murai, J. *et al.* Trapping of PARP1 and PARP2 by clinical PARP inhibitors. *Cancer Res.* **72**, 5588–5599 (2012).

153. Kummar, S. *et al.* Phase 0 clinical trial of the poly (ADP-ribose) polymerase inhibitor ABT-888 in patients with advanced malignancies. *J. Clin. Oncol.* **27**, 2705–2711 (2009).

154. Plummer, R. *et al.* Phase I study of the poly(ADP-Ribose) polymerase inhibitor, AG014699, in combination with temozolomide in patients with advanced solid tumors. *Clin. Cancer Res.* **14**, 7917–7923 (2008).

155. Fong, P. C. *et al.* Inhibition of Poly(ADP-Ribose) Polymerase in Tumors from BRCA Mutation Carriers. *N. Engl. J. Med.* **361**, 123–134 (2009).

156. Tutt, A. *et al.* Oral poly(ADP-ribose) polymerase inhibitor olaparib in patients with BRCA1 or BRCA2 mutations and advanced breast cancer: A proof-of-concept trial. *Lancet* **376**, 235–244 (2010).

157. Audeh, M. W. *et al.* Oral poly(ADP-ribose) polymerase inhibitor olaparib in

patients with BRCA1 or BRCA2 mutations and recurrent ovarian cancer: A proof-of-concept trial. *Lancet* **376**, 245–251 (2010).

158. Fong, P. C. *et al.* Poly(ADP)-ribose polymerase inhibition: Frequent durable responses in BRCA carrier ovarian cancer correlating with platinum-free interval. *J. Clin. Oncol.* **28**, 2512–2519 (2010).

159. Galluzzi, L. *et al.* Molecular mechanisms of cisplatin resistance. *Oncogene* vol. 31 1869–1883 (2012).

160. Pettitt, S. J. *et al.* Genome-wide and high-density CRISPR-Cas9 screens identify point mutations in PARP1 causing PARP inhibitor resistance. *Nat. Commun.* **9**, 1–14 (2018).

161. Gogola, E. *et al.* Selective Loss of PARG Restores PARylation and Counteracts PARP Inhibitor-Mediated Synthetic Lethality. (2018) doi:10.1016/j.ccell.2018.05.008.

162. Kaikkonen, M. U. & Adelman, K. Emerging Roles of Non-Coding RNA Transcription. *Trends in Biochemical Sciences* vol. 43 654–667 (2018).

163. Iyer, M. K. *et al.* The landscape of long noncoding RNAs in the human transcriptome. *Nat. Genet.* **47**, 199–208 (2015).

164. Peng, W. X., Koirala, P. & Mo, Y. Y. LncRNA-mediated regulation of cell signaling in cancer. *Oncogene* **36**, 5661–5667 (2017).

165. Long, Y., Wang, X., Youmans, D. T. & Cech, T. R. How do lncRNAs regulate transcription? *Science Advances* vol. 3 (2017).

166. McHugh, C. A. *et al.* The Xist lncRNA interacts directly with SHARP to silence transcription through HDAC3. *Nature* **521**, 232–236 (2015).

167. Ng, S. Y., Bogu, G. K., Soh, B. S. & Stanton, L. W. The long noncoding RNA RMST interacts with SOX2 to regulate neurogenesis. *Mol. Cell* **51**, 349–359 (2013).

168. Wang, P. *et al.* The STAT3-binding long noncoding RNA lnc-DC controls human dendritic cell differentiation. *Science (80-.).* **344**, 310–313 (2014).

169. Singer, R. A. *et al.* The Long Noncoding RNA Paupar Modulates PAX6 Regulatory Activities to Promote Alpha Cell Development and Function. *Cell Metab.* **30**, 1091-1106.e8 (2019).

170. Sanchez Calle, A., Kawamura, Y., Yamamoto, Y., Takeshita, F. & Ochiya, T. Emerging roles of long non-coding RNA in cancer. *Cancer Sci.* **109**, 2093–2100 (2018).

171. Huang, J. *et al.* Linc-RoR promotes c-Myc expression through hnRNP i and AUF1. *Nucleic Acids Res.* **44**, 3059–3069 (2015).

172. Carrieri, C. *et al.* Long non-coding antisense RNA controls Uchl1 translation

through an embedded SINEB2 repeat. *Nature* **491**, 454–457 (2012).

173. Gupta, R. A. *et al.* Long non-coding RNA HOTAIR reprograms chromatin state to promote cancer metastasis. *Nature* **464**, 1071–1076 (2010).

174. Sun, Y. & Ma, L. New Insights into Long Non-Coding RNA MALAT1 in Cancer and Metastasis. *Cancers (Basel).* **11**, 216 (2019).

175. Tripathi, V. *et al.* The nuclear-retained noncoding RNA MALAT1 regulates alternative splicing by modulating SR splicing factor phosphorylation. *Mol. Cell* **39**, 925–938 (2010).

176. Xu, J. *et al.* Exosomal MALAT1 sponges miR-26a/26b to promote the invasion and metastasis of colorectal cancer via FUT4 enhanced fucosylation and PI3K/Akt pathway. *J. Exp. Clin. Cancer Res.* **39**, 54 (2020).

177. Sun, Z. *et al.* YAP1-induced MALAT1 promotes epithelial–mesenchymal transition and angiogenesis by sponging miR-126-5p in colorectal cancer. *Oncogene* **38**, 2627–2644 (2019).

178. YiRen, H. *et al.* Long noncoding RNA MALAT1 regulates autophagy associated chemoresistance via miR-23b-3p sequestration in gastric cancer. *Mol. Cancer* **16**, (2017).

179. Kim, J. *et al.* Long noncoding RNA MALAT1 suppresses breast cancer metastasis. *Nat. Genet.* **50**, 1705–1715 (2018).

180. Schmitt, A. M. *et al.* An inducible long noncoding RNA amplifies DNA damage signaling. *Nat. Genet.* **48**, 1370–1376 (2016).

181. Huarte, M. *et al.* A large intergenic noncoding RNA induced by p53 mediates global gene repression in the p53 response. *Cell* **142**, 409–419 (2010).

182. Diaz-Lagares, A. *et al.* Epigenetic inactivation of the p53-induced long noncoding RNA TP53 target 1 in human cancer. *Proc. Natl. Acad. Sci. U. S. A.* **113**, E7535–E7544 (2016).

183. Rankin, E. B., Nam, J. M. & Giaccia, A. J. Hypoxia: Signaling the Metastatic Cascade. *Trends in Cancer* vol. 2 295–304 (2016).

184. Samanta, D. & Semenza, G. L. Metabolic adaptation of cancer and immune cells mediated by hypoxia-inducible factors. *Biochimica et Biophysica Acta - Reviews on Cancer* vol. 1870 15–22 (2018).

185. Schito, L. & Semenza, G. L. Hypoxia-Inducible Factors: Master Regulators of Cancer Progression. *Trends in Cancer* vol. 2 758–770 (2016).

186. Nakazawa, M. S., Keith, B. & Simon, M. C. Oxygen availability and metabolic adaptations. *Nature Reviews Cancer* vol. 16 663–673 (2016).

187. Jaakkola, P. *et al.* Targeting of HIF-α to the von Hippel-Lindau ubiquitylation complex by O2-regulated prolyl hydroxylation. *Science (80-.).* **292**, 468–472

(2001).

188.   Ivan, M. *et al.* HIFα targeted for VHL-mediated destruction by proline hydroxylation: Implications for O2 sensing. *Science (80-.).* **292**, 464–468 (2001).

189.   Lando, D. *et al.* FIH-1 is an asparaginyl hydroxylase enzyme that regulates the transcriptional activity of hypoxia-inducible factor. *Genes Dev.* **16**, 1466–1471 (2002).

190.   Hewitson, K. S. *et al.* Hypoxia-inducible factor (HIF) asparagine hydroxylase is identical to factor inhibiting HIF (FIH) and is related to the cupin structural family. *J. Biol. Chem.* **277**, 26351–26355 (2002).

191.   Ohh, M. *et al.* Ubiquitination of hypoxia-inducible factor requires direct binding to the β-domain of the von Hippel-Lindau protein. *Nat. Cell Biol.* **2**, 423–427 (2000).

192.   Tanimoto, K., Makino, Y., Pereira, T. & Poellinger, L. Mechanism of regulation of the hypoxia-inducible factor-1α by the von Hippel-Lindau tumor suppressor protein. *EMBO J.* **19**, 4298–4309 (2000).

193.   Cockman, M. E. *et al.* Hypoxia inducible factor-α binding and ubiquitylation by the von Hippel-Lindau tumor suppressor protein. *J. Biol. Chem.* **275**, 25733–25741 (2000).

194.   Yoon, D. *et al.* Hypoxia-inducible factor-1 deficiency results in dysregulated erythropoiesis signaling and iron homeostasis in mouse development. *J. Biol. Chem.* **281**, 25703–25711 (2006).

195.   Iyer, N. V. *et al.* Cellular and developmental control of O2 homeostasis by hypoxia- inducible factor 1α. *Genes Dev.* **12**, 149–162 (1998).

196.   Maltepe, E., Schmidt, J. V., Baunoch, D., Bradfield, C. A. & Simon, M. C. Abnormal angiogenesis and responses to glucose and oxygen deprivation in mice lacking the protein ARNT. *Nature* **386**, 403–407 (1997).

197.   Tian, H., Hammer, R. E., Matsumoto, A. M., Russell, D. W. & McKnight, S. L. The hypoxia-responsive transcription factor EPAS1 is essential for catecholamine homeostasis and protection against heart failure during embryonic development. *Genes Dev.* **12**, 3320–3324 (1998).

198.   Takeda, K. *et al.* Placental but Not Heart Defects Are Associated with Elevated Hypoxia-Inducible Factor α Levels in Mice Lacking Prolyl Hydroxylase Domain Protein 2. *Mol. Cell. Biol.* **26**, 8336–8346 (2006).

199.   Metallo, C. M. *et al.* Reductive glutamine metabolism by IDH1 mediates lipogenesis under hypoxia. *Nature* **481**, 380–384 (2012).

200.   Wise, D. R. *et al.* Hypoxia promotes isocitrate dehydrogenase-dependent carboxylation of α-ketoglutarate to citrate to support cell growth and

viability. *Proc. Natl. Acad. Sci. U. S. A.* **108**, 19611–19616 (2011).

201. Huang, D. *et al.* HIF-1-mediated suppression of acyl-CoA dehydrogenases and fatty acid oxidation is critical for cancer progression. *Cell Rep.* **8**, 1930–1942 (2014).

202. Semenza, G. L. & Wang, G. L. A nuclear factor induced by hypoxia via de novo protein synthesis binds to the human erythropoietin gene enhancer at a site required for transcriptional activation. *Mol. Cell. Biol.* **12**, 5447–5454 (1992).

203. Wong, B. W., Marsch, E., Treps, L., Baes, M. & Carmeliet, P. Endothelial cell metabolism in health and disease: impact of hypoxia. *EMBO J.* **36**, 2187–2203 (2017).

204. Shweiki, D., Itin, A., Soffer, D. & Keshet, E. Vascular endothelial growth factor induced by hypoxia may mediate hypoxia-initiated angiogenesis. *Nature* **359**, 843–845 (1992).

205. Jain, R. K. Antiangiogenesis Strategies Revisited: From Starving Tumors to Alleviating Hypoxia. *Cancer Cell* vol. 26 605–622 (2014).

206. Connolly, D. T. *et al.* Tumor vascular permeability factor stimulates endothelial cell growth and angiogenesis. *J. Clin. Invest.* **84**, 1470–1478 (1989).

207. Potente, M. & Carmeliet, P. The Link between Angiogenesis and Endothelial Metabolism. *Annual Review of Physiology* vol. 79 43–66 (2017).

208. Gerhardt, H. *et al.* VEGF guides angiogenic sprouting utilizing endothelial tip cell filopodia. *J. Cell Biol.* **161**, 1163–1177 (2003).

209. Lobov, I. B. *et al.* Delta-like ligand 4 (DII4) is induced by VEGF as a negative regulator of angiogenic sprouting. *Proc. Natl. Acad. Sci. U. S. A.* **104**, 3219–3224 (2007).

210. Hellström, M. *et al.* Dll4 signalling through Notch1 regulates formation of tip cells during angiogenesis. *Nature* **445**, 776–780 (2007).

211. Suchting, S. *et al.* The Notch ligand Delta-like 4 negatively regulates endothelial tip cell formation and vessel branching. *Proc. Natl. Acad. Sci. U. S. A.* **104**, 3225–3230 (2007).

212. Benedito, R. *et al.* The Notch Ligands Dll4 and Jagged1 Have Opposing Effects on Angiogenesis. *Cell* **137**, 1124–1135 (2009).

213. Jakobsson, L. *et al.* Endothelial cells dynamically compete for the tip cell position during angiogenic sprouting. *Nat. Cell Biol.* **12**, 943–953 (2010).

214. Fantin, A. *et al.* NRP1 acts cell autonomously in endothelium to promote tip cell function during sprouting angiogenesis. *Blood* **121**, 2352–2362 (2013).

215. Fantin, A. *et al.* NRP1 Regulates CDC42 Activation to Promote Filopodia Formation in Endothelial Tip Cells. *Cell Rep.* **11**, 1577–1590 (2015).

216. Marchand, M., Monnot, C., Muller, L. & Germain, S. Extracellular matrix scaffolding in angiogenesis and capillary homeostasis. *Seminars in Cell and Developmental Biology* vol. 89 147–156 (2019).

217. Senger, D. R. *et al.* The α1β1 and α2β1 integrins provide critical support for vascular endothelial growth factor signaling, endothelial cell migration, and tumor angiogenesis. *Am. J. Pathol.* **160**, 195–204 (2002).

218. Stenzel, D. *et al.* Integrin-dependent and -independent functions of astrocytic fibronectin in retinal angiogenesis. *Development* **138**, 4451–4463 (2011).

219. Kim, Y. H. *et al.* A MST1–FOXO1 cascade establishes endothelial tip cell polarity and facilitates sprouting angiogenesis. *Nat. Commun.* **10**, 1–17 (2019).

220. Gerhardt, H. *et al.* Neuropilin-1 is required for endothelial tip cell guidance in the developing central nervous system. *Dev. Dyn.* **231**, 503–509 (2004).

221. Priya, M. K. *et al.* Tipping off endothelial tubes: nitric oxide drives tip cells. *Angiogenesis* **18**, 175–189 (2015).

222. Troyanovsky, B., Levchenko, T., Månsson, G., Matvijenko, O. & Holmgren, L. Angiomotin: An angiostatin binding protein that regulates endothelial cell migration and tube formation. *J. Cell Biol.* **152**, 1247–1254 (2001).

223. Aase, K. *et al.* Angiomotin regulates endothelial cell migration during embryonic angiogenesis. *Genes Dev.* **21**, 2055–2068 (2007).

224. Genet, G. *et al.* Endophilin-A2 dependent VEGFR2 endocytosis promotes sprouting angiogenesis. *Nat. Commun.* **10**, 1–15 (2019).

225. Lu, X. *et al.* The netrin receptor UNC5B mediates guidance events controlling morphogenesis of the vascular system. *Nature* **432**, 179–186 (2004).

226. Larrivée, B. *et al.* Activation of the UNC5B receptor by Netrin-1 inhibits sprouting angiogenesis. *Genes Dev.* **21**, 2433–2447 (2007).

227. Koch, A. W. *et al.* Robo4 Maintains Vessel Integrity and Inhibits Angiogenesis by Interacting with UNC5B. *Dev. Cell* **20**, 33–46 (2011).

228. Costa, G. *et al.* Asymmetric division coordinates collective cell migration in angiogenesis. *Nat. Cell Biol.* **18**, 1292–1301 (2016).

229. Lammert, E. & Axnick, J. Vascular lumen formation. *Cold Spring Harb. Perspect. Med.* **2**, a006619 (2012).

230. Strilić, B. *et al.* The Molecular Basis of Vascular Lumen Formation in the Developing Mouse Aorta. *Dev. Cell* **17**, 505–515 (2009).

231. Strilić, B. *et al.* Electrostatic cell-surface repulsion initiates lumen formation in developing blood vessels. *Curr. Biol.* **20**, 2003–2009 (2010).

232. Phng, L. K. *et al.* Formin-mediated actin polymerization at endothelial junctions is required for vessel lumen formation and stabilization. *Dev. Cell*

REFERENCES

32, 123–132 (2015).

233. Abraham, S. *et al.* A Rac/Cdc42 exchange factor complex promotes formation of lateral filopodia and blood vessel lumen morphogenesis. *Nat. Commun.* **6**, 1–14 (2015).

234. Popson, S. A. *et al.* Interferon-induced transmembrane protein 1 regulates endothelial lumen formation during angiogenesis. *Arterioscler. Thromb. Vasc. Biol.* **34**, 1011–1019 (2014).

235. Gebala, V., Collins, R., Geudens, I., Phng, L. K. & Gerhardt, H. Blood flow drives lumen formation by inverse membrane blebbing during angiogenesis in vivo. *Nat. Cell Biol.* **18**, 443–450 (2016).

236. Herwig, L. *et al.* Distinct cellular mechanisms of blood vessel fusion in the zebrafish embryo. *Curr. Biol.* **21**, 1942–1948 (2011).

237. Lenard, A. *et al.* In vivo analysis reveals a highly stereotypic morphogenetic pathway of vascular anastomosis. *Dev. Cell* **25**, 492–506 (2013).

238. Martin, J. D., Seano, G. & Jain, R. K. Normalizing Function of Tumor Vessels: Progress, Opportunities, and Challenges. *Annu. Rev. Physiol.* **81**, 505–534 (2019).

239. Szymborska, A. & Gerhardt, H. Hold me, but not too tight—endothelial cell–cell junctions in angiogenesis. *Cold Spring Harb. Perspect. Biol.* **10**, a029223 (2018).

240. Lindahl, P., Johansson, B. R., Levéen, P. & Betsholtz, C. Pericyte loss and microaneurysm formation in PDGF-B-deficient mice. *Science (80-.).* **277**, 242–245 (1997).

241. Thurston, G. *et al.* Leakage-resistant blood vessels in mice transgenically overexpressing angiopoietin-1. *Science (80-.).* **286**, 2511–2514 (1999).

242. Gamble, J. R. *et al.* Angiopoietin-1 is an antipermeability and anti-inflammatory agent in vitro and targets cell junctions. *Circ. Res.* **87**, 603–607 (2000).

243. Li, X. *et al.* Basal and angiopoietin-1 mediated endothelial permeability is regulated by sphingosine kinase-1. *Blood* **111**, 3489–3497 (2008).

244. Lee, M. J. *et al.* Vascular endothelial cell adherens junction assembly and morphogenesis induced by sphingosine-1-phosphate. *Cell* **99**, 301–312 (1999).

245. Liu, Y. *et al.* Edg-1, the G protein-coupled receptor for sphingosine-1-phosphate, is essential for vascular maturation. *J. Clin. Invest.* **106**, 951–961 (2000).

246. Saharinen, P. *et al.* Angiopoietins assemble distinct Tie2 signalling complexes in endothelial cell-cell and cell-matrix contacts. *Nat. Cell Biol.* **10**, 527–537 (2008).

247. Fukuhara, S. *et al.* Differential function of Tie2 at cell-cell contacts and cell-substratum contacts regulated by angiopoietin-1. *Nat. Cell Biol.* **10**, 513–526 (2008).

248. Shen, J. *et al.* Targeting VE-PTP activates TIE2 and stabilizes the ocular vasculature. *J. Clin. Invest.* **124**, 4564–4576 (2014).

249. Maisonpierre, P. C. *et al.* Angiopoietin-2, a natural antagonist for Tie2 that disrupts in vivo angiogenesis. *Science (80-.).* **277**, 55–60 (1997).

250. Davies, P. F., Robotewskyj, A. & Griem, M. L. Quantitative studies of endothelial cell adhesion: Directional remodeling of focal adhesion sites in response to flow forces. *J. Clin. Invest.* **93**, 2031–2038 (1994).

251. Tzima, E., Del Pozo, M. A., Shattil, S. J., Chien, S. & Schwartz, M. A. Activation of integrins in endothelial cells by fluid shear stress mediates Rho-dependent cytoskeletal alignment. *EMBO J.* **20**, 4639–4647 (2001).

252. Tzima, E. *et al.* A mechanosensory complex that mediates the endothelial cell response to fluid shear stress. *Nature* **437**, 426–431 (2005).

253. Osawa, M., Masuda, M., Kusano, K. I. & Fujiwara, K. Evidence for a role of platelet endothelial cell adhesion molecule-1 in endothelial cell mechanosignal transduction: Is it a mechanoresponsive molecule? *J. Cell Biol.* **158**, 773–785 (2002).

254. Shay-Salit, A. *et al. VEGF receptor 2 and the adherens junction as a mechanical transducer in vascular endothelial cells.* vol. 99 www.pnas.orgcgidoi10.1073pnas.142224299 (2002).

255. Di Russo, J. *et al.* Endothelial basement membrane laminin 511 is essential for shear stress response. *EMBO J.* **36**, 183–201 (2017).

256. Chen, Q. *et al.* Haemodynamics-Driven Developmental Pruning of Brain Vasculature in Zebrafish. *PLoS Biol.* **10**, e1001374 (2012).

257. Franco, C. A. *et al.* Dynamic Endothelial Cell Rearrangements Drive Developmental Vessel Regression. *PLOS Biol.* **13**, e1002125 (2015).

258. Davis, G. E., Pintar, K. A., Salazar, A. R. & Maxwell, S. A. Matrix metalloproteinase-1 and -9 activation by plasmin regulates a novel endothelial cell-mediated mechanism of collagen gel contraction and capillary tube regression in three-dimensional collagen matrices. *J. Cell Sci.* **114**, 917–930 (2001).

259. Saunders, W. B., Bayless, K. J. & Davis, G. E. MMP-1 activation by serine proteases and MMP-10 induces human capillary tubular network collapse and regression in 3D collagen matrices. *J. Cell Sci.* **118**, 2325–2340 (2005).

260. Mason, D. P. *et al.* Matrix metalloproteinase-9 overexpression enhances vascular smooth muscle cell migration and alters remodeling in the injured rat

carotid artery. *Circ. Res.* **85**, 1179–1185 (1999).

261. Sluijter, J. P. G., De Kleijn, D. P. V. & Pasterkamp, G. Vascular remodeling and protease inhibition - Bench to bedside. *Cardiovascular Research* vol. 69 595–603 (2006).

262. Lobov, I. B. *et al.* The DII4/notch pathway controls postangiogenic blood vessel remodeling and regression by modulating vasoconstriction and blood flow. *Blood* **117**, 6728–6737 (2011).

263. Phng, L. K. *et al.* Nrarp Coordinates Endothelial Notch and Wnt Signaling to Control Vessel Density in Angiogenesis. *Dev. Cell* **16**, 70–82 (2009).

264. Korn, C. *et al.* Endothelial cell-derived non-canonical Wnt ligands control vascular pruning in angiogenesis. *Dev.* **141**, 1757–1766 (2014).

265. Folkman, J. Tumor Angiogenesis: Therapeutic Implications. *N. Engl. J. Med.* **285**, 1182–1186 (1971).

266. Jayson, G. C., Kerbel, R., Ellis, L. M. & Harris, A. L. Antiangiogenic therapy in oncology: current status and future directions. *The Lancet* vol. 388 518–529 (2016).

267. Holash, J. *et al.* VEGF-Trap: A VEGF blocker with potent antitumor effects. *Proc. Natl. Acad. Sci. U. S. A.* **99**, 11393–11398 (2002).

268. Casanovas, O., Hicklin, D. J., Bergers, G. & Hanahan, D. Drug resistance by evasion of antiangiogenic targeting of VEGF signaling in late-stage pancreatic islet tumors. *Cancer Cell* **8**, 299–309 (2005).

269. Rigamonti, N. *et al.* Role of angiopoietin-2 in adaptive tumor resistance to VEGF signaling blockade. *Cell Rep.* **8**, 696–706 (2014).

270. Ceradini, D. J. *et al.* Progenitor cell trafficking is regulated by hypoxic gradients through HIF-1 induction of SDF-1. *Nat. Med.* **10**, 858–864 (2004).

271. Aghi, M., Cohen, K. S., Klein, R. J., Scadden, D. T. & Chiocca, E. A. Tumor stromal-derived factor-1 recruits vascular progenitors to mitotic neovasculature, where microenvironment influences their differentiated phenotypes. *Cancer Res.* **66**, 9054–9064 (2006).

272. Rubenstein, J. L. *et al.* Anti-VEGF antibody treatment of glioblastoma prolongs survival but results in increased vascular cooption. *Neoplasia* **2**, 306–314 (2000).

273. Schnegg, C. I., Yang, M. H., Ghosh, S. K. & Hsu, M. Y. Induction of vasculogenic mimicry overrides VEGF-A silencing and enriches stem-like cancer cells in melanoma. *Cancer Res.* **75**, 1682–1690 (2015).

274. Kuczynski, E. A., Vermeulen, P. B., Pezzella, F., Kerbel, R. S. & Reynolds, A. R. Vessel co-option in cancer. *Nature Reviews Clinical Oncology* vol. 16 469–493 (2019).

275. Stylianopoulos, T., Munn, L. L. & Jain, R. K. Reengineering the Physical Microenvironment of Tumors to Improve Drug Delivery and Efficacy: From Mathematical Modeling to Bench to Bedside. *Trends in Cancer* vol. 4 292–319 (2018).

276. Burrage, K., Hellmann, K. & Salsbury, A. J. Inhibition of metastatic spread by I.C.R.F. 159: Selective deletion of a malignant characteristic. *British Medical Journal* vol. 4 344–346 (1970).

277. Le Serve, A. W. & Hellmann, K. Metastases and the Normalization of Tumour Blood Vessels by ICRF 159: A New Type of Drug Action. *Br. Med. J.* **1**, 597–601 (1972).

278. Speyer, J. L. *et al.* Protective Effect of the Bispiperazinedione ICRF-187 against Doxorubicin-Induced Cardiac Toxicity in Women with Advanced Breast Cancer. *N. Engl. J. Med.* **319**, 745–752 (1988).

279. Jain, R. K. Normalizing tumor vasculature with anti-angiogenic therapy: A new paradigm for combination therapy. *Nature Medicine* vol. 7 987–989 (2001).

280. Winkler, F. *et al.* Kinetics of vascular normalization by VEGFR2 blockade governs brain tumor response to radiation: Role of oxygenation, angiopoietin-1, and matrix metalloproteinases. *Cancer Cell* **6**, 553–563 (2004).

281. Tong, R. T. *et al.* Vascular normalization by vascular endothelial growth factor receptor 2 blockade induces a pressure gradient across the vasculature and improves drug penetration in tumors. *Cancer Res.* **64**, 3731–3736 (2004).

282. Sorensen, A. G. *et al.* A 'vascular normalization index' as potential mechanistic biomarker to predict survival after a single dose of cediranib in recurrent glioblastoma patients. *Cancer Res.* **69**, 5296–5300 (2009).

283. Sorensen, A. G. *et al.* Increased survival of glioblastoma patients who respond to antiangiogenic therapy with elevated blood perfusion. *Cancer Res.* **72**, 402–407 (2012).

284. Emblem, K. E. *et al.* Vessel architectural imaging identifies cancer patient responders to anti-angiogenic therapy. *Nat. Med.* **19**, 1178–1183 (2013).

285. Falcón, B. L. *et al.* Contrasting actions of selective inhibitors of angiopoietin-1 and angiopoietin-2 on the normalization of tumor blood vessels. *Am. J. Pathol.* **175**, 2159–2170 (2009).

286. Park, J. S. *et al.* Normalization of Tumor Vessels by Tie2 Activation and Ang2 Inhibition Enhances Drug Delivery and Produces a Favorable Tumor Microenvironment. *Cancer Cell* **30**, 953–967 (2016).

287. Goel, S. *et al.* Effects of Vascular-Endothelial Protein Tyrosine Phosphatase Inhibition on Breast Cancer Vasculature and Metastatic Progression. *JNCI J.*

REFERENCES

Natl. Cancer Inst. **105**, 1188–1201 (2013).

288. Peterson, T. E. *et al.* Dual inhibition of Ang-2 and VEGF receptors normalizes tumor vasculature and prolongs survival in glioblastoma by altering macrophages. *Proc. Natl. Acad. Sci. U. S. A.* **113**, 4470–4475 (2016).

289. Kloepper, J. *et al.* Ang-2/VEGF bispecific antibody reprograms macrophages and resident microglia to anti-tumor phenotype and prolongs glioblastoma survival. *Proc. Natl. Acad. Sci. U. S. A.* **113**, 4476–4481 (2016).

290. Fagiani, E. & Christofori, G. Angiopoietins in angiogenesis. *Cancer Letters* vol. 328 18–26 (2013).

291. La Porta, S. L. *et al.* Endothelial Tie1–mediated angiogenesis and vascular abnormalization promote tumor progression and metastasis. *J. Clin. Invest.* **128**, 834–845 (2018).

292. Niland, S. & Eble, J. A. Neuropilins in the context of tumor vasculature. *International Journal of Molecular Sciences* vol. 20 639 (2019).

293. Maione, F. *et al.* Semaphorin 3A is an endogenous angiogenesis inhibitor that blocks tumor growth and normalizes tumor vasculature in transgenic mouse models. *J. Clin. Invest.* **119**, 3356–3372 (2009).

294. Gioelli, N. *et al.* A rationally designed NRP1-independent superagonist SEMA3A mutant is an effective anticancer agent. *Sci. Transl. Med.* **10**, 4807 (2018).

295. Reis, M. *et al.* Endothelial Wnt/β-catenin signaling inhibits glioma angiogenesis and normalizes tumor blood vessels by inducing PDGF-B expression. *J. Exp. Med.* **209**, 1611–1627 (2012).

296. Maes, H. *et al.* Tumor vessel normalization by chloroquine independent of autophagy. *Cancer Cell* **26**, 190–206 (2014).

297. Mazzone, M. *et al.* Heterozygous Deficiency of PHD2 Restores Tumor Oxygenation and Inhibits Metastasis via Endothelial Normalization. *Cell* **136**, 839–851 (2009).

298. Gutknecht, M. F. *et al.* Identification of the S100 fused-type protein hornerin as a regulator of tumor vascularity. *Nat. Commun.* **8**, 1–14 (2017).

299. Delgado-Bellido, D., Serrano-Saenz, S., Fernández-Cortés, M. & Oliver, F. J. Vasculogenic mimicry signaling revisited: Focus on non-vascular VE-cadherin. *Molecular Cancer* vol. 16 (2017).

300. Maniotis, A. J. *et al.* Vascular channel formation by human melanoma cells in vivo and in vitro: Vasculogenic mimicry. *Am. J. Pathol.* **155**, 739–752 (1999).

301. McDonald, D. M., Munn, L. & Jain, R. K. Vasculogenic mimicry: How convincing, how novel, and how significant? *American Journal of Pathology* vol. 156 383–388 (2000).

302. Shirakawa, K. *et al.* Hemodynamics in Vasculogenic Mimicry and Angiogenesis of Inflammatory Breast Cancer Xenograft. *Cancer Res.* **62**, 560–566 (2002).

303. Van Der Schaft, D. W. J. *et al.* Tumor cell plasticity in Ewing sarcoma, an alternative circulatory system stimulated by hypoxia. *Cancer Res.* **65**, 11520–11528 (2005).

304. Scavelli, C. *et al.* Vasculogenic mimicry by bone marrow macrophages in patients with multiple myeloma. *Oncogene* **27**, 663–674 (2008).

305. Sun, T. *et al.* Expression and functional significance of Twist1 in hepatocellular carcinoma: Its role in vasculogenic mimicry. *Hepatology* **51**, 545–556 (2010).

306. El Hallani, S. *et al.* A new alternative mechanism in glioblastoma vascularization: tubular vasculogenic mimicry. *Brain* **133**, 973–982 (2010).

307. Yang, J. P. *et al.* Tumor vasculogenic mimicry predicts poor prognosis in cancer patients: a meta-analysis. *Angiogenesis* **19**, 191–200 (2016).

308. Hendrix, M. J. C. *et al.* Expression and functional significance of VE-cadherin in aggressive human melanoma cells: Role in vasculogenic mimicry. *Proc. Natl. Acad. Sci. U. S. A.* **98**, 8018–8023 (2001).

309. Liu, Z. *et al.* Zinc finger E-box binding homeobox 1 promotes vasculogenic mimicry in colorectal cancer through induction of epithelial-to-mesenchymal transition. *Cancer Sci.* **103**, 813–820 (2012).

310. Liu, T. *et al.* HER2/neu expression correlates with vasculogenic mimicry in invasive breast carcinoma. *J. Cell. Mol. Med.* **17**, 116–122 (2013).

311. Mao, X. -g. *et al.* CDH5 is specifically activated in glioblastoma stemlike cells and contributes to vasculogenic mimicry induced by hypoxia. *Neuro. Oncol.* **15**, 865–879 (2013).

312. Du, J. *et al.* Hypoxia promotes vasculogenic mimicry formation by inducing epithelial-mesenchymal transition in ovarian carcinoma. *Gynecol. Oncol.* **133**, 575–583 (2014).

313. Topczewska, J. M. *et al.* Embryonic and tumorigenic pathways converge via Nodal signaling: Role in melanoma aggressiveness. *Nat. Med.* **12**, 925–932 (2006).

314. Liu, Y. *et al.* IGFBP2 promotes vasculogenic mimicry formation via regulating CD144 and MMP2 expression in glioma. *Oncogene* **38**, 1815–1831 (2019).

315. Sun, T. *et al.* Promotion of tumor cell metastasis and vasculogenic mimicry by way of transcription coactivation by Bcl-2 and Twist1: A study of hepatocellular carcinoma. *Hepatology* **54**, 1690–1706 (2011).

316. Schatton, T. *et al.* Identification of cells initiating human melanomas. *Nature*

REFERENCES

451, 345–349 (2008).

317. Frank, N. Y. *et al.* VEGFR-1 expressed by malignant melanoma-initiating cells is required for tumor growth. *Cancer Res.* **71**, 1474–1485 (2011).

318. Lai, C. Y., Schwartz, B. E. & Hsu, M. Y. CD133+ melanoma subpopulations contribute to perivascular niche morphogenesis and tumorigenicity through vasculogenic mimicry. *Cancer Res.* **72**, 5111–5118 (2012).

319. Peris-Torres, C. *et al.* Extracellular Protease ADAMTS1 Is Required at Early Stages of Human Uveal Melanoma Development by Inducing Stemness and Endothelial-Like Features on Tumor Cells. *Cancers (Basel).* **12**, 801 (2020).

320. Gavard, J. & Gutkind, J. S. VEGF Controls endothelial-cell permeability promoting β-arrestin-dependent Endocytosis VE-cadherin. *Nat. Cell Biol.* **8**, 1223–1234 (2006).

321. Orsenigo, F. *et al.* Phosphorylation of VE-cadherin is modulated by haemodynamic forces and contributes to the regulation of vascular permeability in vivo. *Nat. Commun.* **3**, 1–15 (2012).

322. Allingham, M. J., van Buul, J. D. & Burridge, K. ICAM-1-Mediated, Src- and Pyk2-Dependent Vascular Endothelial Cadherin Tyrosine Phosphorylation Is Required for Leukocyte Transendothelial Migration. *J. Immunol.* **179**, 4053–4064 (2007).

323. Lampugnani, M. G., Dejana, E. & Giampietro, C. Vascular endothelial (VE)-cadherin, endothelial adherens junctions, and vascular disease. *Cold Spring Harb. Perspect. Biol.* **10**, a029322 (2018).

324. Delgado-Bellido, D. *et al.* VE-cadherin promotes vasculogenic mimicry by modulating kaiso-dependent gene expression. *Cell Death Differ.* **26**, 348–361 (2019).

325. Hess, A. R. *et al.* Focal Adhesion Kinase Promotes the Aggressive Melanoma Phenotype. *Cancer Res.* **65**, 9851–9860 (2005).

326. Jean, C. *et al.* Inhibition of endothelial FAK activity prevents tumor metastasis by enhancing barrier function. *J. Cell Biol.* **204**, 247–263 (2014).

327. Rodríguez, M. I. *et al.* PARP-1 Regulates Metastatic Melanoma through Modulation of Vimentin-induced Malignant Transformation. *PLoS Genet.* **9**, e1003531 (2013).

328. Delgado-Bellido, D., Bueno-Galera, C., López-Jiménez, L., Garcia-Diaz, A. & Oliver, F. J. Endothelial Phosphatase VE-PTP Participates in Vasculogenic Mimicry by Preventing Autophagic Degradation of VE-Cadherin. *Front. Oncol.* **10**, 18 (2020).

329. Liu, S. *et al.* S1PR1 regulates the switch of two angiogenic modes by VE-cadherin phosphorylation in breast cancer. *Cell Death Dis.* **10**, 1–15 (2019).

330. Wessel, F. *et al.* Leukocyte extravasation and vascular permeability are each controlled in vivo by different tyrosine residues of VE-cadherin. *Nat. Immunol.* **15**, 223–230 (2014).

331. Hess, A. R. *et al.* Molecular Regulation of Tumor Cell Vasculogenic Mimicry by Tyrosine Phosphorylation: Role of Epithelial Cell Kinase (Eck/EphA2) . *Cancer Res.* **61**, 3250–3255 (2001).

332. Hess, A. R., Seftor, E. A., Seftor, R. E. B. & Hendrix, M. J. C. Phosphoinositide 3-Kinase Regulates Membrane Type 1-Matrix Metalloproteinase (MMP) and MMP-2 Activity during Melanoma Cell Vasculogenic Mimicry. *Cancer Res.* **63**, 4757–4762 (2003).

333. Seftor, R. E. B. *et al.* Cooperative Interactions of Laminin 5γ2 Chain, Matrix Metalloproteinase-2, and Membrane Type-1-Matrix/Metalloproteinase Are Required for Mimicry of Embryonic Vasculogenesis by Aggressive Melanoma. *Cancer Res.* **61**, 6322–6327 (2001).

334. Biondani, G. *et al.* Extracellular matrix composition modulates PDAC parenchymal and stem cell plasticity and behavior through the secretome. *FEBS J.* **285**, 2104–2124 (2018).

335. Bedal, K. B., Grässel, S., Spanier, G., Reichert, T. E. & Bauer, R. J. The NC11 domain of human collagen XVI induces vasculogenic mimicry in oral squamous cell carcinoma cells. *Carcinogenesis* **36**, 1429–1439 (2015).

336. Velez, D. O. *et al.* 3D collagen architecture induces a conserved migratory and transcriptional response linked to vasculogenic mimicry. *Nat. Commun.* **8**, 1–12 (2017).

337. Wang, M. *et al.* HIF-1α promoted vasculogenic mimicry formation in hepatocellular carcinoma through LOXL2 up-regulation in hypoxic tumor microenvironment. *J. Exp. Clin. Cancer Res.* **36**, 60 (2017).

338. Maes, H. *et al.* BNIP3 supports melanoma cell migration and vasculogenic mimicry by orchestrating the actin cytoskeleton. *Cell Death Dis.* **5**, e1127–e1127 (2014).

339. Hardy, K. M. *et al.* Regulation of the embryonic morphogen nodal by Notch4 facilitates manifestation of the aggressive melanoma phenotype. *Cancer Res.* **70**, 10340–10350 (2010).

340. Qi, L. *et al.* Wnt3a Promotes the Vasculogenic Mimicry Formation of Colon Cancer via Wnt/β-Catenin Signaling. *Int. J. Mol. Sci.* **16**, 18564–18579 (2015).

341. Dunleavey, J. M. *et al.* Vascular channels formed by subpopulations of PECAM1+ melanoma cells. *Nat. Commun.* **5**, 1–16 (2014).

342. Thijssen, V. L. *et al.* Targeting PDGF-mediated recruitment of pericytes blocks vascular mimicry and tumor growth. *J. Pathol.* **246**, 447–458 (2018).

REFERENCES

343.   Li, Y. *et al.* Long non-coding RNA MALAT1 promotes gastric cancer tumorigenicity and metastasis by regulating vasculogenic mimicry and angiogenesis. *Cancer Lett.* **395**, 31–44 (2017).

344.   Yu, W. *et al.* Estrogen receptor β promotes the vasculogenic mimicry (VM) and cell invasion via altering the lncRNA-MALAT1/miR-145-5p/NEDD9 signals in lung cancer. *Oncogene* **38**, 1225–1238 (2019).

345.   You, B. *et al.* Androgen receptor promotes renal cell carcinoma (RCC) vasculogenic mimicry (VM) via altering TWIST1 nonsense-mediated decay through lncRNA-TANAR. *Oncogene* **40**, 1674–1689 (2021).

346.   Shi, D. *et al.* LncRNA AFAP1-AS1 promotes tumorigenesis and epithelial-mesenchymal transition of osteosarcoma through RhoC/ROCK1/p38MAPK/Twist1 signaling pathway. *J. Exp. Clin. Cancer Res.* **38**, 375 (2019).

347.   Hendrix, M. J. C. *et al.* Tumor cell vascular mimicry: Novel targeting opportunity in melanoma. *Pharmacology and Therapeutics* vol. 159 83–92 (2016).

348.   Andrés-León, E., Núñez-Torres, R. & Rojas, A. M. miARma-Seq: A comprehensive tool for miRNA, mRNA and circRNA analysis. *Sci. Rep.* **6**, 1–8 (2016).

349.   Andrews, S. Babraham Bioinformatics - FastQC A Quality Control tool for High Throughput Sequence Data. https://www.bioinformatics.babraham.ac.uk/projects/fastqc/ (2010).

350.   Li, H. Seqtk: Toolkit for processing sequences in FASTA/Q formats. https://github.com/lh3/seqtk (2013).

351.   Kim, D., Langmead, B. & Salzberg, S. L. HISAT: A fast spliced aligner with low memory requirements. *Nat. Methods* **12**, 357–360 (2015).

352.   Liao, Y., Smyth, G. K. & Shi, W. FeatureCounts: An efficient general purpose program for assigning sequence reads to genomic features. *Bioinformatics* **30**, 923–930 (2014).

353.   Nikolayeva, O. & Robinson, M. D. edgeR for differential RNA-seq and ChIP-seq analysis: An application to stem cell biology. *Methods Mol. Biol.* **1150**, 45–79 (2014).

354.   Robinson, M. D. & Oshlack, A. A scaling normalization method for differential expression analysis of RNA-seq data. *Genome Biol.* **11**, 1–9 (2010).

355.   Reeb, P. D., Bramardi, S. J. & Steibel, J. P. Assessing dissimilarity measures for sample-based hierarchical clustering of RNA sequencing data using plasmode datasets. *PLoS One* **10**, 132310 (2015).

356.   Ritchie, M. E. *et al.* Limma powers differential expression analyses for RNA-

sequencing and microarray studies. *Nucleic Acids Res.* **43**, e47 (2015).

357. Yu, G., Wang, L. G., Han, Y. & He, Q. Y. ClusterProfiler: An R package for comparing biological themes among gene clusters. *Omi. A J. Integr. Biol.* **16**, 284–287 (2012).

358. Subramanian, A. *et al.* Gene set enrichment analysis: A knowledge-based approach for interpreting genome-wide expression profiles. *Proc. Natl. Acad. Sci. U. S. A.* **102**, 15545–15550 (2005).

359. Shabalin, A. A. Matrix eQTL: Ultra fast eQTL analysis via large matrix operations. *Bioinformatics* **28**, 1353–1358 (2012).

360. Cerami, E. *et al.* The cBio Cancer Genomics Portal: An open platform for exploring multidimensional cancer genomics data. *Cancer Discov.* **2**, 401–404 (2012).

361. Fornes, O. *et al.* JASPAR 2020: Update of the open-Access database of transcription factor binding profiles. *Nucleic Acids Res.* **48**, D87–D92 (2020).

362. Li, Y. *et al.* LncMAP: Pan-cancer Atlas of long noncoding RNA-mediated transcriptional network perturbations. *Nucleic Acids Res.* **46**, 1113–1123 (2018).

363. Gaynor, R. *et al.* S100 protein: a marker for human malignant melanomas? *Lancet* **317**, 869–871 (1981).

364. Schlingemann, R. O. *et al. Differential Expression of Markers for Endothelial Cells, Pericytes, and Basal Lamina in the Microvasculature of Tumors and Granulation Tissue. American Journal of Pathology* vol. 138 (1991).

365. Gil, N. & Ulitsky, I. Regulation of gene expression by cis-acting long non-coding RNAs. *Nature Reviews Genetics* vol. 21 102–117 (2020).

366. Seftor, E. A. *et al.* Expression of multiple molecular phenotypes by aggressive melanoma tumor cells: Role in vasculogenic mimicry. *Critical Reviews in Oncology/Hematology* vol. 44 17–27 (2002).

367. Sulzmaier, F. J., Jean, C. & Schlaepfer, D. D. FAK in cancer: Mechanistic findings and clinical applications. *Nature Reviews Cancer* vol. 14 598–610 (2014).

368. Poullet, P. *et al.* Ezrin Interacts with Focal Adhesion Kinase and Induces its Activation Independently of Cell-matrix Adhesion. *J. Biol. Chem.* **276**, 37686–37691 (2001).

369. Nawroth, R. *et al.* VE-PTP and VE-cadherin ectodomains interact to facilitate regulation of phosphorylation and cell contacts. *EMBO J.* **21**, 4885–4895 (2002).

370. Zlot, C. *et al.* Stanniocalcin 1 Is an Autocrine Modulator of Endothelial Angiogenic Responses to Hepatocyte Growth Factor. *J. Biol. Chem.* **278**,

REFERENCES

47654–47659 (2003).

371.   Legrand, A. J. *et al.* The Level of Ets-1 Protein Is Regulated by Poly(ADP-Ribose) Polymerase-1 (PARP-1) in Cancer Cells to Prevent DNA Damage. *PLoS One* **8**, e55883 (2013).

372.   Choulli, S., Legrand, A. J., Vicogne, D., Villeret, V. & Aumercier, M. Ets-1 interacts through a similar binding interface with Ku70 and poly (ADP-Ribose) polymerase-1. *Biosci. Biotechnol. Biochem.* **82**, 1753–1759 (2018).

373.   Fang, E. *et al.* Therapeutic Targeting of MZF1-AS1/PARP1/E2F1 Axis Inhibits Proline Synthesis and Neuroblastoma Progression. *Adv. Sci.* **6**, 1900581 (2019).

374.   Oda, N., Abe, Ma. & Sato, Y. ETS-1 converts endothelial cells to the angiogenic phenotype by inducing the expression of matrix metalloproteinases and integrin β3. *J. Cell. Physiol.* **178**, 121–132 (1999).

375.   Wei, G. *et al.* Ets1 and Ets2 are required for endothelial cell survival during embryonic angiogenesis. *Blood* **114**, 1123–1130 (2009).

376.   Chen, J. *et al.* VEGF amplifies transcription through ETS1 acetylation to enable angiogenesis. *Nat. Commun.* **8**, 1–13 (2017).

377.   Kumari, A. *et al.* Regulation of E2F1-induced apoptosis by poly(ADP-ribosyl)ation. *Cell Death Differ.* **22**, 311–322 (2015).

378.   Feng, L., Houck, J. R., Lohavanichbutr, P. & Chen, C. Transcriptome analysis reveals differentially expressed lncRNAs between oral squamous cell carcinoma and healthy oral mucosa. *Oncotarget* **8**, 31521–31531 (2017).

379.   Chaudhary, R. *et al.* Prosurvival long noncoding RNA PINCR regulates a subset of p53 targets in human colorectal cancer cells by binding to Matrin 3. *Elife* **6**, (2017).

380.   Zimta, A. A. *et al.* An Emerging Class of Long Non-coding RNA With Oncogenic Role Arises From the snoRNA Host Genes. *Frontiers in Oncology* vol. 10 (2020).

381.   Li, H. *et al.* SNHG1 promotes malignant biological behaviors of glioma cells via microRNA-154-5p/miR-376b-3p- FOXP2- KDM5B participating positive feedback loop. *J. Exp. Clin. Cancer Res.* **38**, (2019).

382.   Bai, J., Xu, J., Zhao, J. & Zhang, R. lncRNA SNHG1 cooperated with miR-497/miR-195-5p to modify epithelial–mesenchymal transition underlying colorectal cancer exacerbation. *J. Cell. Physiol.* **235**, 1453–1468 (2020).

383.   Jiang, H. *et al.* Long non-coding RNA SNHG15 interacts with and stabilizes transcription factor Slug and promotes colon cancer progression. *Cancer Lett.* **425**, 78–87 (2018).

384.   Saeinasab, M. *et al.* SNHG15 is a bifunctional MYC-regulated noncoding locus

encoding a lncRNA that promotes cell proliferation, invasion and drug resistance in colorectal cancer by interacting with AIF. *J. Exp. Clin. Cancer Res.* **38**, (2019).

385. Wang, Z. Y., Duan, Y. & Wang, P. SP1-mediated upregulation of lncRNA SNHG4 functions as a ceRNA for miR-377 to facilitate prostate cancer progression through regulation of ZIC5. *J. Cell. Physiol.* **235**, 3916–3927 (2020).

386. Li, P. *et al.* Long noncoding RNA RGMB-AS1 indicates a poor prognosis and modulates cell proliferation, migration and invasion in lung adenocarcinoma. *PLoS One* **11**, (2016).

387. Xu, J. *et al.* Long noncoding RNA MIR17HG promotes colorectal cancer progression via miR-17-5p. *Cancer Res.* **79**, 4882–4895 (2019).

388. Cao, S. *et al.* FXR1 promotes the malignant biological behavior of glioma cells via stabilizing MIR17HG. *J. Exp. Clin. Cancer Res.* **38**, (2019).

389. Gossage, L., Eisen, T. & Maher, E. R. VHL, the story of a tumour suppressor gene. *Nature Reviews Cancer* vol. 15 55–64 (2015).

390. Wu, J., Liu, T., Sun, L., Zhang, S. & Dong, G. Long noncoding RNA SNHG4 promotes renal cell carcinoma tumorigenesis and invasion by acting as ceRNA to sponge miR-204-5p and upregulate RUNX2. *Cancer Cell Int.* **20**, 1–14 (2020).

391. Bhatia, V. & Ateeq, B. Molecular Underpinnings Governing Genetic Complexity of ETS-Fusion-Negative Prostate Cancer. *Trends in Molecular Medicine* vol. 25 1024–1038 (2019).

392. Mendes-Pereira, A. M. *et al.* Synthetic lethal targeting of PTEN mutant cells with PARP inhibitors. *EMBO Mol. Med.* **1**, 315–322 (2009).

393. Dedes, K. J. *et al.* PTEN deficiency in endometrioid endometrial adenocarcinomas predicts sensitivity to PARP inhibitors. *Sci. Transl. Med.* **2**, 53ra75-53ra75 (2010).

394. Sulkowski, P. L. *et al.* 2-Hydroxyglutarate produced by neomorphic IDH mutations suppresses homologous recombination and induces PARP inhibitor sensitivity. *Sci. Transl. Med.* **9**, (2017).

395. Molenaar, R. J. *et al.* IDH1/2 mutations sensitize acute myeloid leukemia to parp inhibition and this is reversed by idh1/2-mutant inhibitors. *Clin. Cancer Res.* **24**, 1705–1715 (2018).

396. Boysen, G. *et al.* SPOP mutation leads to genomic instability in prostate cancer. *Elife* **4**, (2015).

397. Soker, S., Takashima, S., Miao, H. Q., Neufeld, G. & Klagsbrun, M. Neuropilin-1 is expressed by endothelial and tumor cells as an isoform- specific receptor

REFERENCES

REFERENCES

for vascular endothelial growth factor. *Cell* **92**, 735–745 (1998).

398. Kawasaki, T. *et al.* A requirement for neuropilin-1 in embryonic vessel formation. *Development* **126**, 4895–4902 (1999).

399. Yamada, Y. *et al.* Exogenous clustered neuropilin 1 enhances vasculogenesis and angiogenesis. *Blood* **97**, 1671–1678 (2001).

400. Uniewicz, K. A., Cross, M. J. & Fernig, D. G. Exogenous recombinant dimeric neuropilin-1 is sufficient to drive angiogenesis. *J. Biol. Chem.* **286**, 12–23 (2011).

401. Wang, L., Zeng, H., Wang, P., Soker, S. & Mukhopadhyay, D. Neuropilin-1-mediated vascular permeability factor/vascular endothelial growth factor-dependent endothelial cell migration. *J. Biol. Chem.* **278**, 48848–48860 (2003).

402. Aspalter, I. M. *et al.* Alk1 and Alk5 inhibition by Nrp1 controls vascular sprouting downstream of Notch. *Nat. Commun.* **6**, 1–13 (2015).

403. Kitsukawa, T., Shimono, A., Kawakami, A., Kondoh, H. & Fujisawa, H. Overexpression of a membrane protein, neuropilin, in chimeric mice causes anomalies in the cardiovascular system, nervous system and limbs. *Development* **121**, 4309–4318 (1995).

404. Xu, M. *et al.* LECT2, a Ligand for Tie1, Plays a Crucial Role in Liver Fibrogenesis. *Cell* **178**, 1478-1492.e20 (2019).

405. Yuan, H. T. *et al.* Activation of the orphan endothelial receptor Tie1 modifies Tie2-mediated intracellular signaling and cell survival. *FASEB J.* **21**, 3171–3183 (2007).

406. Seegar, T. C. M. *et al.* Tie1-Tie2 Interactions Mediate Functional Differences between Angiopoietin Ligands. *Mol. Cell* **37**, 643–655 (2010).

407. Savant, S. *et al.* The Orphan Receptor Tie1 Controls Angiogenesis and Vascular Remodeling by Differentially Regulating Tie2 in Tip and Stalk Cells. *Cell Rep.* **12**, 1761–1773 (2015).

408. Korhonen, E. A. *et al.* Tie1 controls angiopoietin function in vascular remodeling and inflammation. *J. Clin. Invest.* **126**, 3495–3510 (2016).

409. D'Amico, G. *et al.* Tie1 deletion inhibits tumor growth and improves angiopoietin antagonist therapy. *J. Clin. Invest.* **124**, 824–834 (2014).

410. Singhal, M. *et al.* Preclinical validation of a novel metastasis-inhibiting Tie1 function-blocking antibody. *EMBO Mol. Med.* **12**, e11164 (2020).

411. Sato, T. N. *et al.* Distinct roles of the receptor tyrosine kinases Tie-1 and Tie-2 in blood vessel formation. *Nature* vol. 376 70–74 (1995).

412. Garcia, J. *et al.* Tie1 deficiency induces endothelial-mesenchymal transition. *EMBO Rep.* **13**, 431–439 (2012).

413. Piera-Velazquez, S. & Jimenez, S. A. Endothelial to mesenchymal transition: Role in physiology and in the pathogenesis of human diseases. *Physiol. Rev.* **99**, 1281–1324 (2019).

414. Zeniou, M., Nguekeu-Zebaze, L. & Dantzer, F. Therapeutic considerations of PARP in stem cell biology: Relevance in cancer and beyond. *Biochemical Pharmacology* vol. 167 107–115 (2019).

ABBREVIATIONS

ABBREVIATIONS

αSMA	α-smooth muscle actin
ADP	adenosine diphosphate
ANGPT	angiopoietin
AM	acral melanoma
ARE	AU-rich elements
ARTD	diphteria toxin-like ADP-ribosyl transferases
ATP	adenosine triphosphate
BAP1	BRCA1-associated protein 1
BRAFi	BRAF inhibitors
BRCA	breast cancer susceptibility protein
BRCT	BRCA C-terminus
C/EBP	CCAAT/enhancer-binding protein
CCCH	Cys–Cys–Cys–His
CDK	cyclin-dependent kinase
CDKN2A	cyclin-dependent kinase inhibitor 2A
cDNA	complementary DNA
ceRNA	competing endogenous RNA
CHD2	chromodomain helicase DNA-binding protein 2
CM	cutaneous melanoma
CNV	copy number variations
CPM	counts per million
CTCF	CCCTC-binding factor
CYSLTR2	cysteinyl leukotriene receptor 2
DAG	diacylglycerol
DDR	DNA damage response
DEG	differently expressed genes
DINO	damage-induced non-coding
Dll4	delta-like 4
DMSO	dimethyl sulfoxide
DNA	deoxyribonucleic acid
DNA-PKcs	DNA-dependent protein kinase catalytic subunit
DOCK4	dedicator of cytokinesis 4
DSB	double strand break
E	glutamic acid
EC	endothelial cell

EIF1AX	eukaryotic translation initiation factor 1A X-linked
EMA	European Medicines Agency
EMT	epithelial–mesenchymal transition
EndoMT	endothelial–mesenchymal transition
EphA2	ephrin type-A receptor 2
FAK	focal adhesion kinase
FDA	Food and Drug Administration
FDR	false discovery rate
FGF	fibroblast growth factor
FIH1	factor inhibiting HIF 1
FR	FR900359
G protein	guanine nucleotide-binding protein
GAP	GTPase activating protein
GDP	guanosine diphosphate
GFP	green fluorescent protein
ggNER	global genome nucleotide excision repair
GLUT	glucose transporter
GNA11	G protein α-subunit 11
GNAQ	G protein α-subunit q
GO	gene ontology
GO-BP	gene ontology- biological process
GPCR	G-protein-coupled receptor
GSEA	gene set enrichment analysis
GTP	guanosine triphosphate
H	histidine
H3K4me3	histone H3 K4 trimethylation
H3K27me3	histone H3 K27 trimethylation
HER2	human epidermal growth factor receptor 2
HGF	hepatocyte growth factor
HIF	hypoxia-inducible factors
HOTAIR	HOX transcript antisense RNA
HR	homologous recombination
HRE	hypoxia response elements
HRP	horseradish peroxidase
IFITM1	interferon-induced transmembrane protein 1
IGFBP2	insulin-like growth factor–binding protein 2
IP$_3$	inositol-1,4,5-trisphosphate
K	lysine

ABBREVIATIONS

KDM5B	K demethylase 5B
KO	knockout
LDHA	lactate dehydrogenase A
LECT2	leukocyte cell-derived chemotaxin 2
lncRNA	long non-coding RNA
MALAT1	metastasis-associated lung adenocarcinoma transcript 1
MAPK	mitogen-activated protein kinase
MAR	mono-ADP-ribose
MEKi	MEK inhibitors
miRNA	microRNA
MITF	microphthalmia-associated transcription factor
MMP	matrix metalloproteinase
MRE11	meiotic recombination 11
MRN	MRE11-RAD50-NBS1
mRNA	messenger RNA
MST1	mammalian sterile 20-like kinase 1
MZF1	myeloid zinc finger 1
NAD+	nicotinamide adenine dinucleotide
NBS1	Nijmegen breakage syndrome protein 1
NELF	negative elongation factor
NF1	neurofibromin 1
NHEJ	non-homologous end-joining
NM	nodular melanoma
NO	nitric oxide
Nrarp	Notch-regulated ankyrin repeat protein
NRP	neuropilin
NUDIX	nucleoside diphosphate–linked moiety X
PAR	poly-(ADP-ribose)
PARG	poly-(ADP-ribose) glycohydrolase
PARP	poly-(ADP-ribose) polymerase
PARPi	PARP inhibitor
PAS	periodic acid-Schiff
PBS	phosphate-buffered saline
PDGFβ	platelet-derived growth factor β
PDGFRβ	PDGFβ receptor β
PDH	pyruvate dehydrogenase
PDK1	PDH kinase 1
PDL1	programmed death-ligand 1

PECAM1	platelet endothelial cell adhesion molecule 1
PHD	prolyl hydroxylases
PI3K	phosphoinositide 3-kinase
PKC	protein kinase C
PLC	phospholipase C
PODXL	podocalyxin
poly-A	poly-adenosine monophosphate
PRC2	polycomb repressive complex 2
PTEN	phosphatase and tensin homolog
PVDF	polyvinylidene difluoride
pVHL	von Hippel-Lindau tumor suppressor
pY658	phospho-Y658
Q	glutamine
R	arginine
RFP	red fluorescent protein
RMST	rhabdomyosarcoma 2-associated transcript
RNA	ribonucleic acid
RNAseq	RNA sequencing
Robo4	roundabout 4
RPKM	reads per kilobase per million mapped reads
S	serine
S1PR1	sphingosine-1-phosphate receptor 1
SCE	sister chromatid exchange
SDF1	stromal cell–derived factor-1
Sema	semaphorin
SDS	sodium dodecyl sulfate
SEM	standard error of the mean
SF3B1	splicing factor 3B subunit 1
siRNA	small interfering RNA
SOX2	sex determining region Y-box 2
SRSF	serine- and arginine-rich splicing factor
SSB	single strand break
SSM	superficial spreading melanoma
STAT	signal transducer and activator of transcription
STC1	stanniocalin 1
TARG1	terminal ADP-ribose protein glycohydrolase 1
TBS	Tris-buffered saline
TCGA	The Cancer Genome Atlas

TDP1	tyrosyl-DNA phosphodiesterase 1
TERT	telomerase reverse transcriptase
TKI	tyrosine kinase inhibitors
TNB	Tris-NaCl-blocking buttfer
TNT	Tris-NaCl-Tween
UM	uveal melanoma
UNC	uncoordinated
UV	ultraviolet
V	valine
VE-cadherin	vascular endothelial cadherin
VEGF	vascular endothelial growth factor
VEGFR	VEGF receptor
VE-PTP	vascular endothelial-protein tyrosine phosphatase
VM	vasculogenic mimicry
W	tryptophan
WHO	World Health Organization
Xist	X-inactive specific transcript
XRCC	X-ray repair cross-complementing protein
Y	tyrosine
YAP	yes-associated protein
ZEB1	zinc finger E-box binding homeobox 1
ZnF	zinc finger motif
ZO1	zonula occludens-1